

**EVALUATION OF PYROLYZED ARECA HUSK  
FOR THE REMOVAL OF FERROUS IONS FROM  
AQUEOUS SOLUTION**

*Thesis*

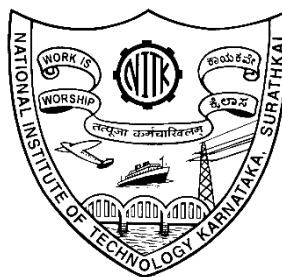
*Submitted in partial fulfilment of the requirements for the  
degree of*

**DOCTOR OF PHILOSOPHY**

**by**

**SHEEKA SUBRAMANI B**

**155096CV15F09**



**DEPARTMENT OF CIVIL ENGINEERING  
NATIONAL INSTITUTE OF TECHNOLOGY KARNATAKA  
SURATHKAL, MANGALORE – 575025,  
AUGUST, 2021**



**EVALUATION OF PYROLYZED ARECA HUSK  
FOR THE REMOVAL OF FERROUS IONS FROM  
AQUEOUS SOLUTION**

*Thesis*

*Submitted in partial fulfilment of the requirements for the  
degree of*

**DOCTOR OF PHILOSOPHY**

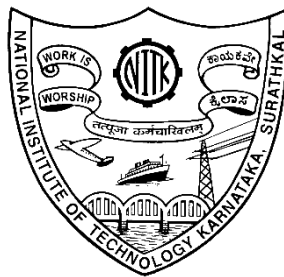
by

**SHEEKA SUBRAMANI B**

**155096CV15F09**

Under the guidance of

**Dr. S SHRIHARI & Dr. MANU B**



**DEPARTMENT OF CIVIL ENGINEERING  
NATIONAL INSTITUTE OF TECHNOLOGY KARNATAKA  
SURATHKAL, MANGALORE – 575025,**

**AUGUST, 2021**



# DECLARATION

By the Ph.D. Scholar

I hereby declare that the Research Thesis entitled “**Evaluation of pyrolyzed areca husk for the removal of ferrous ions from aqueous solution**” which is being submitted to the **National Institute of Technology Karnataka, Surathkal** in partial fulfilment of the requirements for the award of the Degree of **Doctor of Philosophy in Civil Engineering** is a bonafide report of the research work carried out by me. The material contained in this Research Synopsis has not been submitted to any University or Institution for the award of any degree.



**(SHEEKA SUBRAMANI B)**

Register No.**155096CV15F09**,

Department of Civil Engineering

Place: NITK-Surathkal

Date: 10/08/2021



# CERTIFICATE

This is to certify that the Research Thesis entitled "Evaluation of pyrolyzed areca husk for the removal of ferrous ions from aqueous solution" submitted by Ms. SHEEKA SUBRAMANI B (155096CV15F09) as the record of the research work carried out by her, is accepted as the Research Thesis submission in partial fulfilment of the requirements for the award of degree of Doctor of Philosophy.



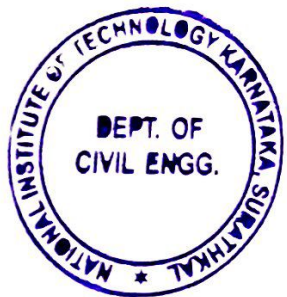
Dr. Shrihari S  
Research Guide

(Signature with date and seal)



Dr. Manu B  
Research Guide

(Signature with date and seal)



Jayalekh M  
20/09/2024  
Chairman - DRPC  
Chairman (DRPC)  
Department of Civil Engineering  
National Institute of Technology Karnataka, Surathkal  
Mangalore - 575 025, Karnataka, INDIA  
(Signature with date and seal)





## ACKNOWLEDGEMENT

You go through life wondering what is it all about, but at the end of the day it's all about family. I am blessed to have the most supportive family, my husband **Dr Dyan Chinnappa A** and my adorable son **Veer**

**“It is the supreme art of the teacher to awaken joy in creative expression and knowledge.”**

**- Albert Einstein**

What a teacher is, is more important than what he teaches. A teacher can affect you eternally and **Dr Babu Narayan K S** has influenced and been inspirational all throughout my course of work.

Do not give them a candle to light the way, teach them how to make fire instead. That is the meaning of true guidance. My guide **Dr S. Srihari** and co-guide **Dr Basavaraj Manu** were the best that a research scholar can have.

I would like to thank my research committee, **Dr. A S Balu**, Associate Professor, Dept. of Civil Engg. and **Dr. Amba Shetty**, Professor, Dept. of Applied Mechanics for their insightful comments and encouragement which helped me to widen my research from various perspectives

I would like to express my thank to **Dr. B R Jayalekshmi**, Head, Department of Civil Engineering for her kindly intime support. I extend my gratitude to **Dr B M Sunil**, Dept of Civil Engg for his encouragement and support.

I also extend my deep sense of gratitude to **Mr. Manohar Shanbouge** and **Mr Dheeraj**, Environmental Lab, Dept. of Civil Engg, National Institute of Technology Karnataka (NITK), Surathkal.

I thank **Mr Naveen Thimmaiah**, Rainbow pipe fittings, Manipal; **Mr Narasimha Shenoy** and M/s **Tuff Coats**, Yeyadi, Mangalore for solving design issues and fabricating my column apparatus.

My heartfelt gratitude to **Mr Niranjan Gachimath & Mr A Manoj** for helping me in conducting experiments during the late hours.

I thank my fellow lab-mates without whom my PhD wouldn't have been successful. I want to name and offer my deepest gratitude to each of them for helping me in the way they have **Dr. Sanjeev Sangami, Dr Manu D, Dr Amrutha, Ms Anupama, Ms Poorani, Mrs Divya, Mr Vinod T, Dr Bhaskar M, Dr. Mahesh G B, Mrs. Anjali, Dr. Krishnamurthy M P, Dr Prachi.**

If there is one thing that I think that God has given me the best in the world, it is my family. My parents **Subramani & Shwetha**, parents-in-law **Dr Ganapathi & Indira**, uncle & aunt **Roy & Savitha**, siblings **Swekritha & Bopanna**, cousins **Keerthana and Smaran**. I thank each of them for being with me through thick and thin.

My heartfelt gratitude to my strongest support system, **Mrs Rajeevi S** who has looked after my son like her own and has always stood by me in times of need.

Last but not the least, I thank **God Almighty** for blessing me with good health and zeal to pursue my research in the right direction and accomplish my dream.

**SHEEKA SUBRAMANI B**

## **All reality is Water!**

Formless and fearless, like an open mind  
Spelling harmony, thou dispel none  
You create and you provide, oh mother so kind  
Thy grace so boundless, none you shun

Cascade or gurgle, intrinsic is your freedom  
We tamper you with disdain, yet thou don't frown  
Mizzle on us mortals, abundant wisdom  
I vow to thee, will not let you down

This work is dedicated to my mother deity who spawns  
spirituality.

In the human form, she has a clear identity of a woman.

All bestowing, grand in her stride, depicting style, splendor and  
spirit.

**~ Mother Kaveri~**



## ABSTRACT

The hurdle of valorisation of Arecanut husk on one side and the pollution of aquatic bodies by heavy metals like Iron on the other end are contemplated together in this study. The areca husk is pyrolyzed at 450°C for two hours to obtain Biochar. Batch adsorption studies were employed to investigate the effect of adsorbent dosage (2-10 g/L), initial concentration of adsorbate (1-5 mg/L) and contact time (30 -360 min) at temperature of 28±2 °C & pH 4.0±0.2 for the removal of Iron from pyrolyzed areca husk. The adsorption capacity was found to increase with increase in initial Iron concentration and contact time, but decreases with the adsorbent dosage. Langmuir, Freundlich, Temkin and Dubinin-Radushkevich Isotherms was used to analyse the equilibrium data. Langmuir and Dubinin-Radushkevich model best described the uptake of Iron ions implying a monolayer adsorption with physisorption. Pseudo second order exhibited the best fit for the effectiveness of Iron adsorption indicating the maximum limit of chemisorption. Thermodynamic studies indicated that the adsorption was spontaneous and exothermic in nature. The mechanisms responsible for adsorption of Iron on pyrolysed areca husk was conducted by SEM-EDAX, XRD and FTIR indicating oxidation and precipitation of Iron into complex compounds of jarosite and ferrous hydroxy sulphates. The results of the column studies suggest that the adsorption process is cost effective and can be scaled up to for continuous treatment of water. It was found that treatment efficiency improved with reduced flow rate and an increase in the height of adsorbent bed of the column. Maximum biosorption capacity of ferrous ions was observed as 0.487mg/g at bed depth of 3 cm; flow rate of 2 mL/min and initial concentration of 2 mg/L. PCA was also employed to predict the performance of the fixed bed column. It also indicated the same as the dynamic models. In conclusion, pyrolyzed areca husk can be technically & economically feasible alternative adsorbent material.



# TABLE OF CONTENTS

<b>ABSTRACT.....</b>	<b>I</b>
<b>LIST OF TABLES.....</b>	<b>VIII</b>
<b>LIST OF FIGURES.....</b>	<b>X</b>
<b>NOMENCLATURE .....</b>	<b>XIII</b>
<b>1. CHAPTER 1 .....</b>	<b>1</b>
<b>1.1. BACKGROUND .....</b>	<b>1</b>
<b>1.2. RESEARCH MOTIVATION.....</b>	<b>3</b>
<b>1.3. STRUCTURE OF THE THESIS .....</b>	<b>4</b>
<b>2. CHAPTER 2 .....</b>	<b>7</b>
<b>2.1. GENERAL.....</b>	<b>7</b>
<b>2.2. RESEARCH PERSPECTIVE.....</b>	<b>7</b>
<b>2.3. ADSORPTION.....</b>	<b>7</b>
<b>2.3.1. Factors influencing Adsorption .....</b>	<b>8</b>
<b>2.3.2. Adsorption Isotherms .....</b>	<b>11</b>
<b>2.3.3. Adsorption Kinetics.....</b>	<b>13</b>
<b>2.3.4. Adsorption Contact Systems .....</b>	<b>14</b>
<b>2.3.5. Empirical Models.....</b>	<b>17</b>
<b>2.4. BASIC TYPE OF ADSORBENTS.....</b>	<b>18</b>

<b>2.5. CARBON ADSORBENTS FROM AGRO-WASTES .....</b>	<b>20</b>
<b>2.6. ARECAHUSK .....</b>	<b>24</b>
2.6.1. <i>Demography and Primary Uses of Arecanut</i> .....	24
2.6.2. <i>Finding Alternate Uses</i> .....	26
2.6.3. <i>Properties of Areca Husk fiber</i> .....	27
2.6.4. <i>Use of Areca Husk for Carbon</i> .....	28
<b>2.7. IRON CONTAMINATION.....</b>	<b>29</b>
2.7.1. <i>Magnitude of Iron Contamination</i> .....	29
2.7.2. <i>Occurrence of Iron in water</i> .....	31
2.7.3. <i>Health Hazards</i> .....	32
2.7.4. <i>Treatment Techniques for removal of Iron</i> .....	33
<b>2.8. LITERATURE SUMMARY .....</b>	<b>36</b>
<b>2.9. OBJECTIVES .....</b>	<b>37</b>
<b>3. CHAPTER 3.....</b>	<b>39</b>
<b>3.1. CHEMICALS AND REAGENTS. ....</b>	<b>39</b>
<b>3.2. PREPARATION OF ARECA HUSK ADSORBENT. ....</b>	<b>39</b>
<b>3.3. CHARACTERISATION OF ADSORBENT.....</b>	<b>40</b>
<b>3.4. BATCH ADSORPTION EXPERIMENTS.....</b>	<b>40</b>
<b>3.5. CONTINUOUS FLOW ADSORPTION STUDIES.....</b>	<b>42</b>
<b>4. CHAPTER 4.....</b>	<b>47</b>



<b>4.1. CHARACTERISATION OF ADSORBENT .....</b>	<b>47</b>
<b>4.2. PERFORMANCE APPRAISAL OF PYROLYZED ARECANUT HUSK FOR IRON REMOVAL BY BATCH PROCESS .....</b>	<b>49</b>
4.2.1. <i>Effect of adsorbent dose on Iron adsorption.....</i>	49
4.2.2. <i>Effect of initial concentration and contact time.....</i>	50
<b>4.3. ADSORPTION ISOTHERMS .....</b>	<b>53</b>
<b>4.4. ADSORPTION KINETICS.....</b>	<b>59</b>
<b>4.5. DESORPTION STUDIES.....</b>	<b>63</b>
<b>4.6. ADSORPTION MECHANISM FOR THE ADSORPTION OF IRON ON CARBONISED ARECA HUSK .....</b>	<b>65</b>
4.6.1. <i>Thermodynamic studies .....</i>	65
4.6.2. <i>Precipitation with minerals.....</i>	67
4.6.3. <i>Complexation with functional groups.....</i>	68
<b>4.7. PERFORMANCE APPRAISAL OF PYROLYZED ARECANUT HUSK FOR IRON REMOVAL IN CONTINUOUS MODE.....</b>	<b>69</b>
4.7.1. <i>Effect of initial concentration of adsorbate .....</i>	70
4.7.2. <i>Effect of Flow Rate of adsorbate solution.....</i>	71
4.7.3. <i>Effect of bed height of adsorbent on Iron adsorption.....</i>	72
<b>4.8. DYNAMIC ADSORPTION COLUMN MODELLING.....</b>	<b>73</b>
4.8.1. <i>Yoon Nelson Model.....</i>	73
4.8.2. <i>Thomas Model.....</i>	81

4.8.3. Bohart–Adam’s Model.....	89
<b>4.9. PCA FOR COLUMN ADSORPTION DATA .....</b>	<b>96</b>
4.9.1. Prediction of $\eta$ from experimental variables using multi-variable linear regression .....	98
4.9.2. Illustrative Example .....	100
<b>CHAPTER 5 .....</b>	<b>101</b>
<b>CONCLUSION.....</b>	<b>101</b>
<b>APPENDIX I .....</b>	<b>117</b>
<b>COST ESTIMATION.....</b>	<b>117</b>
<b>APPENDIX II.....</b>	<b>119</b>
<b>EXPERIMENTAL PHOTOGRAPHS.....</b>	<b>119</b>



## LIST OF TABLES

Table 2.1 Various Adsorption Contact Systems (Patel 2019). .....	15
Table 2.2 Various type of Adsorbents .....	19
Table 2.3 Preparation of Activated Carbon from Agricultural Biomass to remove heavy metal in water.....	21
Table 2.4 Various forms of Iron in water (Khatri et al. 2017).....	32
Table 3.1 Proximate analysis of Arecanut husk.....	39
Table 4.1 Langmiur, Freundlich, Temkin and Dubinin-Radushkevich Isotherm Parameters .....	58
Table 4.2 Lagergren's first-order and Pseudo-second-order kinetic parameters for the adsorption of Iron on Carbonised areca husk. ....	61
Table 4.3 Intra-particle diffusion model parameters for the adsorption of Iron on Carbonised areca husk. ....	63
Table 4.4 Thermodynamic parameters for the adsorption of Iron on Carbonised areca husk.....	66
Table 4.5 Yoon-Nelson model parameters using linear regression analysis for Fe <sup>2+</sup> adsorption under various operating conditions.....	79
Table 4.6 Thomas model parameters using linear regression analysis for Fe <sup>2+</sup> adsorption under various operating conditions.....	82
Table 4.7 Bohart-Adam's model parameters using linear regression analysis for Fe <sup>2+</sup> adsorption under various operating conditions.....	95



## LIST OF FIGURES

Figure 2.1 Well Cultivated Arecanut Grove .....	25
Figure 2.2 Areca Cultivation Worldwide.....	26
Figure 2.3 Iron contamination in India (The CGWB, Ministry of Water Resources, 2015).....	31
Figure 3.1 Schematic representation of Packed Bed Column Adsorption.....	43
Figure 4.1 SEM image of pyrolysed areca husk .....	47
Figure 4.2 $pH_{zpc}$ of pyrolyzed areca husk. ....	48
Figure 4.3 Effect of adsorbent dosage on the adsorption of Iron on pyrolyzed areca husk (Contact Time = 5 hours and Initial Concentration $C_o = 1, 2, 3, 4$ & $5\text{mg/L}$ ). .....	50
Figure 4.4(a-e) Effect of initial concentration and contact time on Fe adsorption ( $W =$ $2, 4, 6, 8$ & $10\text{ g}$ ; $V = 1\text{ L}$ ) .....	53
Figure 4.5 Plots for Langmiur (a), Freundlich (b), Temkin (c) and Dubinin- Radushkevich (d) isotherms for Iron on pyrolyzed arecanut husk ( $C_o = 4\text{mg/L}$ , Adsorbent = $2, 4, 6, 8$ & $10\text{ mg/L}$ ) .....	57
Figure 4.6 Plots for Lagergren's pseudo-first order and pseudo-second-order models for Iron on carbonized arecanut husk .....	62
Figure 4.7 Plot for intra-particle diffusion model for Iron on carbonized arecanut husk .....	63
Figure 4.8 Comparison of eluents at the concentration of $0.1\text{ M}$ on metal loaded pyrolyzed areca husk. ....	64

Figure 4.9 Plot for $\ln K_c$ versus $1/T$ for the estimation of thermodynamic parameters for the adsorption of Iron on carbonized arecanut husk .....	67
Figure 4.10 XRD results of Pyrolyzed areca husk pre and post adsorption of $Fe^{2+}$ ....	68
Figure 4.11 SEM results of Pyrolyzed areca husk post adsorption of $Fe^{2+}$ .....	68
Figure 4.12 FTIR results of Pyrolyzed areca husk before and after adsorption of $Fe^{2+}$ . .....	69
Figure 4.13 Adsorption breakthrough curves of $Fe^{2+}$ ions at different concentrations (Bed ht - 3cm, Flowrate - 1mL/min) .....	70
Figure 4.14 Adsorption breakthrough curves of $Fe^{2+}$ ions at different flowrate (Bed height – 3cm, Initial concentration – 5mg/L) .....	71
Figure 4.15 Adsorption breakthrough curves of $Fe^{2+}$ ions at different Bed height (initial concentration – 5mg/L, Flow rate –1mL/min).....	72
Figure 4.16(a-i) Linear plot of Yoon-Nelson model with experimental data at different bed heights, flow rate and initial concentration.....	78
Figure 4.17(a-i) Linear plot of Thomas model with experimental data at different bed heights, flow rate and initial concentration .....	88
Figure 4.18(a-i) Linear plot of Bohart Adam’s Model with experimental data at different bed heights, flow rate and initial concentration.....	94
Figure 4.19 Plot of first two principal axes.....	97
Figure 4.20 PCA results for different flowrate (30, 60 & 120 mL/hr) datasets.....	98





## **NOMENCLATURE**

PAH	:	Pyrolyzed Areca Husk
WHO	:	World Health Organisation
MCF	:	Mangalore Chemicals & Fertilizers
KIOCL	:	Karnataka Iron Ore Corporation Ltd
NMPT	:	New Mangalore Port Trust
MRPL	:	Mangalore Refineries & Petrochemicals Ltd
MTZ	:	Mass Transfer Zone
FR	:	Flow Rate
BH	:	Bed Height



# CHAPTER 1

## INTRODUCTION

### 1.1. BACKGROUND

Environmental pollution is the biggest threat to our society and the world at large. Pollution causes innumerable effects to human health and nature as such. It destroys the living environment and endangers human existence on Earth. Agricultural waste contributes highly to this pollution. These agricultural wastes refer to waste produced from various agricultural activities. In the facet of development, agriculture too has been a major source of environmental pollution and waste generation. The valorisation of these agricultural wastes to form important products, will help in reducing its accumulation & further pollution. These agricultural wastes end up as animal fodder, briquetting, biogas or composting, precursor for activated carbon production and so on (Tsai et al. 2012).

Activated carbon finds its use in filtration and purification for its proven adsorption capacity. This is because of its high porosity. Stringent Environmental legislations have increased the demand for activated carbon in recent years. Abounding research has been undertaken to find materials that can be used as an adsorbent which are inexpensive, easy to access and needs less processing.(Kadirvelu and Namasivayam 2003). Carbons can be developed from agricultural wastes such as peanut hull, baggage pith, tea dust leaves, paddy straw, wood products, coir pith, parthenium plant etc. Each of these has its own shortcomings and leverages (Kadirvelu et al. 2002). Such alternative sources for activated carbon would decrease the treatment costs (Dias et al. 2007).

Activated Carbon is manufactured in two stages, carbonization and activation. In the first stage the raw material is dried and then heated to separate by-products as well as to drive off any gases generated. This process is accomplished by heating the material over 400 °C in an oxygen-free atmosphere that cannot support combustion. The

process of activation is achieved by exposing the carbonised particles to an oxidising agent usually carbon dioxide or steam at high temperature.

Adsorption is a surface phenomenon in which the contaminant molecules adheres to the “adsorbent” solid surface by physical attractive forces, chemical binding and ion exchange. Various adsorbents are used to remove different kind of dyes and heavy metal ions from wastewater, that are harmful (Thomas and Crittenden 1998). The high capacity required for the purification process and separation is provided by the high internal surface area of the adsorbent (Goud et al. 2005). The range of internal surface required for practical applications is between 300-1200 m<sup>2</sup>/gram. However, adsorbents with internal surface area ranging from 100 to 300 m<sup>2</sup>/gram can also be produced to be used. The pores in the material are the determinant of internal surface area in an adsorbent. Both, batch and continuous flow configurations are considered in the treatment of waste water to bring about adequate contact between the adsorbent and the fluid containing the contaminant (the adsorbate).

Areca catechu (*Areceaceae*), commonly called Arecanut, is a widely grown commercial crop. Also known as has betel nut, it is mainly grown in south & south east Asian countries with an annual estimated production of 1.2 million tonnes of fruits & provides sustenance to more than 10 million farmers (Peng et al. 2015). Production of arecanut fruit in India was 833,000 tonnes from an area of 497,000 ha in 2017–18. Arecanut has agro-financial, religious, political & medicinal significance in producer nations. It is mainly used as a masticating agent. Approximately 40% of the fruit consists of husk, that means 333,200 tonnes of husk is generated as agricultural biomass in our country alone. The lignin & cellulose composition in the husk makes it difficult for its rapid decomposition. Arecanut husk has found its use as a raw material in production of industrial chemicals (ethanol, xylose, furfural), enzyme's, mushroom cultivation and its fibre for making of composites, fabrics, thick boards, fluffy cushions, non-woven, paperboards, thermal insulators. But most of the time, the husk is simply dumped in the backyards of the farms or processing units. This goes on to be an environmental hazard by converting into decaying mass and in turn a breeding ground for pathogenic organisms. Since areca husk has the advantages

of being cheap and widely available, its usage needs characterisation from process point of view (Gogoi et al. 2017).

The earth's crust mainly consists of Iron. Iron is also an integral part of the many different enzymes of the human body and helps in its proper functioning. Iron is abundantly found in rock layers and soil. Contamination of water bodies by Iron is mainly due to the careless disposing of domestic and industrial effluents and geogenic sources. Surface water pollution of iron is mainly from industries related to mining and Iron & steel and also Corrosion. Water seeping through the many layers of the earth causes contamination of Iron in Ground water (Khatri et al. 2017). Iron in ground water can turn indissoluble when exposed to air, giving it a brown red color. Water containing Iron may have altered taste, odour, colour and turbidity. These problems could be of aesthetic nature, or causing indirect health concerns and in-turn economic problems (Jusoh et al. 2005). Apart from this, according to WHO, the permissible limit for Iron in water is below 0.3 mg/L.

## **1.2. RESEARCH MOTIVATION**

Surathkal, Mangalore is situated in the southern part of India on the coastal side of Karnataka. It is a fast-growing city and has been urbanized and industrialized rapidly during the past 15 years. It harbors the mega industries like MCF, KIOCL, NMPT, MRPL and several small and medium scale industries in and around. Since all these industrial establishments have triggered the growth of urban population, transport facilities etc., abatement of pollution of water, air and soil have become a challenging problem. Adding to the pollution woes, this region is mainly made up of laterite soil and rock formations whose main constituent are oxides of Iron. During monsoon run offs, the Iron gradually seeps into the ground and also surface water causing pollution and makes it unfit for use in domestic as well as industrial establishments. Iron in its ferrous ( $\text{Fe}^{2+}$ ) form, at concentrations of several milligrams per liter can remain without discoloration or turbidity in the water when directly pumped from a well. Although turbidity and colour may develop in piped systems at Iron levels above 0.05–0.1 mg/L. In drinking-water supplies, Iron ( $\text{Fe}^{2+}$ ) salts are unstable and are precipitated as insoluble Iron ( $\text{Fe}^{3+}$ ) hydroxide, which settles out as a rust-colored silt.

The state of Karnataka stands first in the cultivation of Arecanut in India. Arecanut consists of the quid, which is mainly used for masticating and the fibrous outer cover called the husk, which accounts to a large portion of the volume & weight is of no much use. This husk is simply strewn around and is a major source of pollution. Contemplating on utilizing the husk as a precursor for the preparation of adsorbent, thereby achieving 'Waste to Wealth' is the focus of this study.

Although extensive progress is carried out in the field of adsorption, the process provides for a wide range of studies in relation to precursor material used for adsorbent preparation, adsorption mechanism and contaminant recovery. Reaching to this gap, the current study focuses mainly on two aspects namely the usage of areca husk as precursor to prepare activated carbon and removal of Iron from waste water by adsorption.

### **1.3. STRUCTURE OF THE THESIS**

This section explains the main components of thesis written,

Chapter 1 of the thesis introduces the reader to the present study with brief and conceptualized note. This chapter covers the background for the research, means and motivation for conducting research.

Chapter 2 provides a brief literature survey carried out and deals with the study of process and mechanism of adsorption with insight to various factors affecting it, adsorbents and its availability, biochar as an adsorbent and its benefits to the environment, properties of Arecahusk and its pyrolysis to be used as an adsorbent and removal of iron from water. This encompasses the studies that has already been carried out in relevance to the present study and brief research outcome of the previous works. The chapter highlights the need for current study.

Chapter 3 gives the plan and methodology adopted to accomplish the objectives framed. Chemicals, reagents used for experimental investigation is addressed with the grade. The methods are explained in detail.

Chapter 4 presents before the outcome of the research in detail. Experimental and graphical representation of the analysed data is presented in this section along with the discussion in detail. Discussion of the result obtained in the present work to that of previous research and its relevancy has been presented.

Chapter 5 concludes the research objectives based on the obtained results and interpretations. This section concludes the research accomplishments and contribution.





## **CHAPTER 2**

### **LITERATURE REVIEW**

#### **2.1. GENERAL**

Published literature, pertaining to similar interests, conducted around the world is compiled from various sources to determine the feasibility and scope of work. Similar studies undertaken on the preparation of Carbon from agricultural waste for the adsorption of contaminants from water are reviewed and mentioned below

#### **2.2. RESEARCH PERSPECTIVE**

Work carried on characterization of the potential adsorbent, adsorption as a concept, the performance analysis of the novel adsorbent and analysis of the data acquired is the perspective of the research undertaken.

#### **2.3. ADSORPTION**

Adsorption is a general expression for the process of accumulation of contaminant concentration at the surface. Adsorption is the result of the interactive forces between the porous solid surface and contaminant molecules being removed from the bulk phase. Adsorption is a surface phenomenon, where any solute lowering the surface tension of the liquid in which it is dissolved will be adsorbed at the boundary of the solid phase. (Thomas and Crittenden 1998).

The adsorption of solute to the internal surface of the adsorbent in a reactor can be broken down into four steps

- Bulk transport
- Film transport
- Intra-particle transport
- Adsorption of solute into active sites

In the first step, the contaminant molecules are transported to the boundary layer of the liquid surrounding the adsorbent from the stock solution. This diffusion or advective transport of the adsorbate in the liquid phase occurs faster than other steps. In the second stage, contaminants are transferred by molecular diffusion onto the surface within the film layer surrounding the adsorbent. This is controlled by the physical properties of the liquid phase, hydraulics etc. The rate of flow is the determining factor for the time taken to diffuse into the hydrodynamic boundary of the adsorbent. In the third step, there is intra particle diffusion where the contaminant moves through the adsorbent pores to the available adsorption sites. Intra particle diffusion involves both, pore diffusion where the adsorptive gets attached to the pores and Surface diffusion onto the adjacent adsorptive surface. In the final step, an attachment is developed between the adsorbate and adsorbent. This occurs rapidly and the process is reversible (Ibrahim and Hassan 2008). Based on the bond between the adsorbate and Adsorbent molecules, adsorption can be broadly classified as (i) Physical Adsorption and (ii) Chemical Adsorption. Physical Adsorption is very simple and involves the attachment of adsorptive molecules onto the surface of the adsorbent through weak bonds such as Van der Waals, hydrogen bonding, hydrophobic or dipole – dipole interactions. Physical adsorption is accompanied by a decrease in entropy and free energy of the adsorption system and, hence the process is exothermic. In Chemical adsorption or Chemisorption, the type of bonding forces is similar to that found in chemical reactions characteristic of ionic bond, covalent bond etc. It is an irreversible process where in the desorbed compounds are diverse from the adsorbed one's. it is differentiated on the basis of high activation energy involved and higher heat of adsorption. (Králík 2014).

### **2.3.1. Factors influencing Adsorption**

The important factors affecting adsorption are Point of zero charge, Surface area, Pore Volume, Nature of Adsorbate & Adsorbent and Temperature

#### i] $\text{pH}_{\text{zpc}}$

Point of Zero charge ( $\text{pH}_{\text{zpc}}$ ) or Iso electric point is defined as the pH at which the surface of the adsorbent is neutral or zero i.e. if it contains equal amount of positive and negative sites. This is of fundamental importance in surface technology specially in the field of environmental engineering where contaminant molecules are easily adsorbed by the substrate. At pH values below the  $\text{pH}_{\text{zpc}}$  value, the material surface is positively charged and above it, the surface is negatively charged.

#### ii] Surface Area & Pore Volume

As adsorption is a surface phenomenon, specific surface area becomes the critical factor in deciding the adsorption capacity of the adsorbent and to a certain extent, the rate at which the adsorbate is up taken. Specific Surface area is defined as the total surface area available for adsorption. The amount of adsorption is greater in adsorbents if the solid particles is finely divided and more porous in nature. The disintegration of larger porous activated carbon into smaller ones opens up the tiny, sealed channels in the carbon surface which becomes accessible for adsorption. The size and shape of the particles are contributing factors to reach equilibrium during the adsorption process.

Pore Volume is defined as the ratio of the porous activated Carbon's air volume to its total volume. The total volume is described by the amount of space contained within an imaginary film that has been largely decreased around the outside of the porous activated carbon's exterior geometry. Activated carbons exhibit different porous structures namely ultra-micropores with diameter below 0.4nm, micropores with dia 0.4 – 2nm, transport mesopores with dia 2 – 50nm and macropores of dia above 50nm. The porous carbonaceous phase of the activated carbon demonstrates hydrophobic properties, which are responsible for the adsorption of organic compounds. Since the specific surface of macropores is low (0.5 - 2  $\text{m}^2/\text{g}$ ), the scope for adsorption is trivial. All the same these macropores help in the transit of contaminants, facilitating the diffusion of adsorbed substances to the small, precarious

pores. The intermediate or the mesopores display similar function as their specific surface in the range of 10 - 400 m<sup>2</sup>/g. (Drag et al. 2002)

### iii] Nature of the Adsorbate

The extent of adsorption depends on the solubility and the molecular structure of the adsorbate. In case of a stronger solute-solvent bond, the degree of adsorption is lesser. Adsorption decreases with increasing solubility of the contaminants in water and increases if the contaminants are hydrophobic. The empirical Lundelius rule states that the extent of adsorption of a solute is inversely proportional to its solubility in the solvent from which adsorption occurs.

### iv] Nature of the Adsorbent

The structural composition and surface functional groups of the activated carbon has propounded effect on the capacity and rate of adsorption. Activated Carbon is mainly composed of Carbonyl and Carboxyl functional groups. Adsorbents that are hydrophobic in nature adsorb hydrophobic adsorptive's and vice versa. Water has a polar nature which is induced by the covalent bonds between hydrogen and oxygen atoms along with the fact that these bonds are at an angle, resulting in a net dipole from the more O-rich pole to the more H-rich pole of the molecule. Hydrophobic adsorbents can be oxidized to produce -OH<sup>-</sup> and -COO<sup>-</sup> groups on their surface, in turn forming hydrogen bonds in water and making it hydrophilic. This enhances the dispersibility of the adsorbent and helps in contaminant adsorption to the adsorbative molecules.

### v] Temperature

Adsorption process is exothermic in nature. According to Le Chatelier's principle, adsorption is favorable at low temperature. Therefore, the extent of adsorption, especially physical adsorption would increase on decreasing the temperature. Even though chemical adsorption is an exothermic process, due to high kinetic energy barrier, it does not occur slowly at lower temperature. Hence, like most chemical

changes, the extent of chemisorption increases with increase in temperature up to certain limit and after that it starts decreasing.

### 2.3.2. Adsorption Isotherms

Adsorption isotherms are vital graphs that relates the variation in the amount of material adsorbed by the adsorbent with concentration, at constant temperature. The interaction of contaminated water with activated carbon that is, the uptake of adsorbate is called the adsorption capacity and this is characterized by Adsorption Isotherms. These Adsorption Isotherms are empirical models that best describe the behavior of material at equilibrium. Adsorption Isotherms play a significant role in defining how pollutants interact with activated carbon and also elucidates pollutant pathway mechanism. It sheds info on the adsorbent surface coverage, adsorption capacity and effective system design for specific contaminant removal (Gregg et al. 1967). Langmuir, Freundlich, Temkin, and Dubinin-Radushkevich isotherm models are the most often used isotherms to describe the adsorption data for contaminant concentration.

According to Langmuir adsorption isotherm, there is only monolayer adsorption on the adsorbent. The equilibrium distribution of the contaminant between the solid and liquid phases is given by a single layer. There is no adsorption occurring after this monolayer is formed atop the adsorbent. This kind of single layer adsorption takes place on the adsorbent surface which has a restricted number of similar sites. This model used in bio-sorption processes is given by the equation:

$$q_e = \frac{q_m C_e}{1 + k_l C_e} \quad \dots (2.1)$$

The linearized form of the isotherm is

$$\frac{1}{q_e} = \frac{1}{q_m} + \frac{1}{(k_l q_m)} \frac{1}{C_e} \quad \dots (2.2)$$

where,  $C_e$  – equilibrium Iron ion concentration (mg/L) &  $q_e$  – amount of Iron adsorbed at equilibrium (mg/g).  $k_l$  (L/mg) and  $q_m$  (mg/g) are Langmuir constants related to energy of adsorption and adsorption capacity respectively.

The Freundlich isotherm model is based on the heterogeneous distribution of active sites accompanied by interactions between molecules adsorbed. The following equation expresses this model:

$$q_e = C_e^{1/n} k_f \quad \dots (2.3)$$

The linearized form of the isotherm is

$$\ln q_e = \ln k_f + \frac{1}{n} \ln C_e \quad \dots (2.4)$$

where,  $k_f$  (mg/g) and  $1/n$  are Freundlich constants related to relative adsorption capacity of activated carbon and intensity of adsorption & indicate the tendency of the adsorbate to be adsorbed. (Goher et al. 2015)

The Temkin isotherm assumes the heat of adsorption increases linearly with decreasing coverage. The following equation expresses this model:

$$Q_e = B \ln A + B \ln C_e \quad \dots (2.5)$$

where,  $B = RT/b$ , is the Temkin constant related to heat of sorption (J/mol),  $A$  is the Temkin isotherm constant (L/g),  $R$  is the gas constant (8.314 J/mol K),  $b$  is Temkin isotherm constant, and  $T$  is the absolute temperature (K) (Hameed 2009)

The Dubinin-Radushkevich (D-R) (Girods et al. 2009) equation sheds detail on the type of adsorption as in whether it is physisorption or chemisorption and expressed as

$$\ln q_e = X_m - \beta \varepsilon^2 \quad \dots (2.6)$$

where  $\varepsilon$  (Polanyi potential) =  $RT \ln(1+1/C_e)$ ,  $X_m = \ln q_m$ ,  $q_m$  is the maximum adsorption capacity (mg/g),  $\beta$  is related to mean free energy,  $E$  (E in kJ/mol) as:

$$E = \frac{1}{\sqrt{-2\beta}} \quad \dots (2.7)$$

### 2.3.3. Adsorption Kinetics

Adsorption Kinetics describes the rate of release or retention of the contaminant from an aqueous environment to solid-phase interface at a given adsorbent dose, temperature, flow rate and pH. It gives the time taken to reach equilibrium and is the rate determining state

The most common models used to fit the kinetic sorption experiments were Lagergren's pseudo-first-order model and pseudo-second-order model (Liang et al. 2010)

$$\log(q_e - q_t) = \log q_e - \frac{K_1 t}{2.303} \quad \dots (2.8)$$

$$\frac{t}{q_t} = \frac{1}{K_s q_e^2} + \frac{1}{q_e} t \quad \dots (2.9)$$

where  $q_e$  (mg/g) and  $q_t$  (mg/g) are the amount of adsorbate adsorbed at equilibrium and at time  $t$ , respectively.  $K_1$  ( $\text{min}^{-1}$ ) and  $K_s$  ( $\text{g mg}^{-1} \text{min}$ ) are the pseudo-first-order and pseudo-second order adsorption rate constants, respectively.

To investigate the mechanism of contaminant adsorption onto activated carbon, intraparticle diffusion-based mechanism was studied. The most commonly used technique for identifying the mechanism involved in the adsorption process is by fitting an intra particle diffusion plot. It is an empirically formulated functional relationship, familiar to most adsorption processes, where the uptake varies almost proportionally with  $t^{1/2}$ . According to the theory proposed by Weber and Morris

$$q_t = k_{id} t^{1/2} + C_i \quad \dots (2.10)$$

where  $k_{id}$  ( $\text{mg g}^{-1} \text{min}^{1/2}$ ), the rate parameter of stage  $i$ , is obtained from the slope of the straight line of  $q_t$  versus  $t^{1/2}$ .  $C$  is the intercept (Wu et al. 2009).

#### **2.3.4. Adsorption Contact Systems**

The various types of techniques by which the contact between adsorbate and adsorbent is achieved are Batch and Continuous process. The continuous flow systems are further classified into moving bed, fixed bed (up-flow or downflow), fluidized bed and pulsed bed. Each method has its own merits and demerits which is described in Table 2.1.

In adsorption batch process, the adsorption capacity is defined as the amount of solute adsorbed on the surface of the solid at equilibrium per mass of adsorbent. Whereas, in fixed bed sorption, adsorption capacity corresponds to the mass of pollutants retained in the column when exhaustion is reached per mass of adsorbent (Dichiara et al. 2015). Adsorption Isotherms and material balance equations are used to design batch process. Alternatively, breakthrough curves are used to describe fixed bed adsorption. The fixed bed adsorption can be described with the help of breakthrough curves which is expressed using adsorption zone or mass transfer zone (MTZ).

If we consider a up flow fixed bed adsorber, the wastewater containing pollutants is progressively adsorbed by the adsorbent in the first few layers of the fresh adsorbent initially. The length of the bed where most contaminants is removed is called the mass transfer zone. The length of the bed is keeps changing as it is dependent on the adsorbate concentration on its lower boundary. The rest of the contaminants gets adsorbed as the wastewater traverses the rest of the fixed bed above the adsorption zone. As more wastewater enters the column, the bottom portion of the fixed bed gets saturated with pollutants and the MTZ moves upwards. Finally, when the upper edge of the MTZ reaches the top of the column, the effluent concentration starts to rise and the fixed adsorbent bed reaches saturation. Usually breakthrough curves display a characteristic 'S' shape, but with varying degree of steepness.



**Table 2.1 Various Adsorption Contact Systems (Patel 2019).**

Particulars	Batch Process	Continuous fixed bed	Continuous moving bed	Continuous fluidised bed	Pulsed bed
Definition	In Batch process, the adsorbent and adsorbate are completely mixed in diluted solution at constant volume	In Fixed-bed system, the adsorbate is continuously flowing through the fixed bed of adsorbent at constant flow rate	In Continuous moving bed sorption system, both the adsorbent and adsorbate are in motion, and the bed of adsorbent remains at constant volume, but not similar in concentration	In Continuous fluidised bed sorption, adsorbate is contacted with fluidized bed of adsorbent with sufficient or insufficient flow	In pulsed bed sorption, the adsorbate is in contact with same adsorbent in bed, until desired results are achieved

---

Features	<p>This technique is to mainly analyse feasibility of adsorbent — adsorbate system and can be used to treat small volume of wastewater</p>	<p>Used for large volumes of wastewater having higher contamination. Also, widely used for industrial purpose, because the adsorbate is continuously in contact with fresh adsorbent in fixed-bed column system</p>	<p>In this process, the adsorbent is continuously replaced and the raw adsorbent is in constant contact with adsorbate</p>	<p>It is mainly applicable for industries &amp; factories because of rapid mixing of adsorbent—adsorbate. The adsorbate is in continuous flow with controlled flow of adsorbent.</p>	<p>It is easily controlled and an automatically operated system. This type has an advantage of better utilization of adsorbent because the adsorbents are immediately regenerated after it reaches saturation.</p>
----------	--	---	--	--	--

---

### 2.3.5. Empirical Models

These models describe the performance of packed bed columns giving information on breakthrough curves, adsorption curves and rates.

#### 2.3.5.1 Yoon and Nelson model

This model is based on the assumption that the probability of adsorption for each adsorbate molecule is proportional to the rate of decrease of adsorbate adsorption and the chances of adsorbate breakthrough on the adsorbent. The Yoon and Nelson equation regarding to a single component system is expressed as (Nwabanne and Igbokwe 2012)

$$\frac{Ct}{C_0} = \frac{1}{1 + \exp[k(\tau - t)]} \quad \dots (2.11)$$

where  $k$  is the rate constant (1/min),  $\tau$  is the time required for 50% adsorbate breakthrough (min) and  $t$  is the breakthrough (sampling) time (min).

The linearized form of the Yoon and Nelson model is as follows:

$$\ln \frac{Ct}{C_0 - Ct} = kt - \tau k \quad \dots (2.12)$$

#### 2.3.5.2 Thomas model

The Thomas model is widely used in column performance study and follows Langmuir isotherm of adsorption and plug flow behaviour in the column bed. The model is suitable for adsorption processes where there is no axial dispersion and the rate of reaction follows second-order reversible reaction. The Thomas model is expressed as (Suksabye et al. 2008)

$$\frac{Ct}{C_0} = \frac{1}{1 + \exp \left( k_{Th} / Q(q_0x - C_0V_{eff}) \right)} \quad \dots (2.13)$$

where  $k_{Th}$  is the rate constant (mL/min mg),  $q_0$  is the equilibrium uptake of the adsorbent (mg/g),  $x$  is the amount of adsorbent in the column(g),  $V_{eff}$  is effluent,  $C_0$  is the influent concentration (mg/L),  $Q$  is flow rate (ml/min),  $C_t$  is the effluent concentration and  $t$  is the time (min,  $t=V_{eff}/Q$ ).

The linearized form of Thomas model is as follows:

$$\ln\left(\frac{C_t}{C_0} - 1\right) = \frac{k_{Th}q_0x}{Q} - k_{Th}C_0t \quad \dots (2.14)$$

### 2.3.5.3 Bohart Adam's Model

Bohart Adam's Model assumes the equation that gives the relationship between  $C_t/C_0$  and time in continuous system. It is used to describe the initial part of the breakthrough curve. The Bohart Adam's model is expressed as (Ahmad and Hameed 2010)

$$\frac{C_t}{C_0} = \exp(k_{AB}C_0t - k_{AB}N_0\frac{Z}{F}) \quad \dots (2.15)$$

where  $k_{AB}$  is the rate constant (L/min mg),  $Z$  is the bed depth in the column(cm),  $N_0$  is the saturation concentration (mg/L),  $F$  is the linear velocity calculated by dividing the flow rate by the column section area (cm/min),  $C_0$  is the influent concentration (mg/L),  $C_t$  is the effluent concentration and  $t$  is the time (min,  $t=V_{eff}/Q$ ).

The linearized form of Bohart Adam's model is as follows:

$$\ln\frac{C_t}{C_0} = k_{AB}C_0t - k_{AB}N_0\frac{Z}{F} \quad \dots (2.16)$$

## 2.4. BASIC TYPE OF ADSORBENTS

Over a period of time, different type of adsorbents has been developed which also led to the usage of different adsorption techniques (Table 2.2). To a large extent, Charcoal, a carbon-based adsorbent has been used and its usage has been reported as early as 3750 BC in an ancient Egyptian papyrus.(Dabrowski 2001)

**Table 2.2 Various type of Adsorbents**

<b>Mineral Adsorbents</b>	<b>Carbon Adsorbents</b>	<b>Synthetic Adsorbents</b>
Zeolites, Bauxite, Silica gels, Metal Oxides, Metal hydroxides, Alumina, Clay Minerals, Pillared Clays, Porous clay hetero-structures (PCHs), Inorganic nanomaterials	Charcoal, Activated Carbons, Active carbon fibers, Molecular carbon sieves, Meso-carbon microbeads, Fullerenes, Hetero-fullerenes, Carbonaceous nanomaterials	Polymers, Composites such as complex mineral-carbons, X-elutrilithe where X= Zn, Ca Mixed sorbents

Charcoal brought about the practice of applying adsorbents in industrial use. Carbon later came into common parlance to be used in food industries such as refining sugar, oils, fats and waxes. Activated charcoal was the next to be employed for recovery of solvents, eliminating odors and purifying air and industrial gases. When it came to water treatment, base exchanging silicates were used, while some other chars were capable of recovering precious metals. (Thomas and Crittenden 1998). Overtime, activated carbon gained momentum in medical applications to eliminate bacteria and toxins.

Activated carbon has a large adsorption capacity due to its high porosity. Its use in filtration and purification are widespread. The two methods to prepare activated carbon are physical activation and chemical activation. The former technique uses gaseous activating agents such as steam or CO<sub>2</sub> to carbonize a precursor and the latter adopts a technique wherein the precursor is mixed with a chemical activating agent phosphoric acid (H<sub>3</sub>PO<sub>4</sub>), zinc chloride (ZnCl<sub>2</sub>) or alkali hydroxides (NaOH and KOH) and is then heated with inert gas (Liou and Wu 2009). The characteristics of activated carbon are largely dependent on the activation methods, as well as the properties of the precursor. Chemical activation scores over physical activation because it can be performed in a single step and a relatively low temperature. Moreover, the outturn is much higher and it also leads to reduction in the contaminant (Duman et al. 2009). The process of producing activated carbon can be broken down

into Carbonization and Activation, while carbonization enriches the carbon content and creates an initial porosity on the char, the activation further develops the porosity and creates the ordering of the structure there by generating a highly porous solid.

With fast paced development in technology which uses activated carbon in a wide range of applications involving adsorption, the want for locally available carbonaceous material has seen an uptrend for producing activated carbons. The abundance and low economic value of agro-wastes and also the problem of its deposition have created environmental issues. Conversion of agro biomass into activated carbon is a good alternative to solve the problem of its disposition and also to reduce the manufacturing costs of activated carbon. All agro-wastes with an average carbon content of 85% or more have drawn the interest of researchers who are in search of substitute sources for less expensive carbon (Verla et al. 2012). Lignin and cellulose are the major components of these agro-wastes along with polar functional groups of lignin namely aldehydes, alcohols, ketones, phenolic, carboxylic and ether groups. These functional groups have the ability to bind with metal elements by accepting or donating electron pair to form complexes in the metal pollutant solution.

## **2.5. CARBON ADSORBENTS FROM AGRO-WASTES**

A large number of studies has been conducted on the usage of agro-wastes for the production of activated carbon. The focus is on biomass which is considerably rigid such as shells, husk or/and stones of fruits like nuts, peanuts, olives, dates, almonds, apricots and cherries; however, wastes resulting from the production of cereals such as rice, coffee, soybean, maize and corn as well as olive cakes, sugar cane and sugar beet bagasse, coir pith, oil-palm shell (from oil-palm processing mills) and various seed wastes are also used. These adsorbents prepared are used to remove both organic and inorganic pollutants from aqueous phase along with heavy metals. Adsorption of heavy metals from wastewater is comparatively a new process that has proven to be favourable for the removal of pollutants from effluents. Table 2.3 gives a list of agro-wastes used for the removal of heavy metals.

**Table 2.3 Preparation of Activated Carbon from Agricultural Biomass to remove heavy metal in water**

<b>Wastewater Pollutants</b>	<b>Raw Material</b>	<b>Relevant Adsorption Procedure</b>	<b>Reference</b>
Copper (II)	<i>Turbinaria ornata</i> , a brown marine alga	Batch tests were conducted at pH 6 with reported adsorption capacity of 147.06 mg/g. Column test reported 68 mg/g copper uptake irrespective of the bed height but decreased with high flow rate.	Vijayaraghavan et al. 2005
Lead	<i>Pinus Sylvestris</i> (Scot Pine) Sawdust	The results obtained with the pilot plant show that the process can decontaminate 1200 l of effluent containing 1mg/L of lead (II) with only 1 kg of sawdust.	Taty-Costodes et al. 2005
	Oil Palm fibre (OPF)	Column studies indicated adsorption efficiency increased with increase in the inlet concentration and bed height and decreased with increase in flow rate.	Nwabanne and Igbokwe 2012
	Rubber wood sawdust	Maximum removal of lead ion in column process was found as 38.56mg/g	Biswas and Mishra 2015

	Coconut Coir Pith	The Column studies reported that at the highest bed depth of 60 cm and lowest flow rate of 10 ml/min, the maximum adsorption reached 201.47mg/g.	Suksabye et al. 2008
Chromium (VI)	Acorn of <i>Quercus ithaburensis</i> (Mount Tabor oak)	The fixed-bed column results elucidate that the adsorption capacity is strongly dependent on the flow rate, pH of solution and particle size.	Malkoc and Nuhoglu 2006
	Peanut shell	Maximum adsorption capacity of 16.26mg/g was observed on oxidized peanutshell carbon.	AL-Othman et al. 2012
Zinc (II)	Coconut shell carbon modified with chitosan	Batch study results described Langmuir isotherm displayed a better fitting model indicating the applicability of monolayer coverage of the zinc (II)	Amuda et al. 2007
	Tea factory waste	The maximum adsorption capacity of Zn(II) per gram of Tea Waste was calculated as 8.9±0.08 mg.	Wasewar et al. 2009



Nickel (II)	Marine algae <i>Sargassum filipendula</i>	At temperature = 30 °C and pH 3.0, biosorption of nickel was predicted based on the least square statistical method. The developed model can be useful tool for optimization and design of columns using biomass of <i>S. filipendula</i> as a sorbent.	Borba et al. 2006
	Parthenium	Batch process indicated the Adsorption Capacity is 54.5mg/g of Nickel.	Kadirvelu et al. 2002
Iron (II)	Sugarcane Bagasse	The adsorbent showed high affinity for the removal of Fe(II), where uptake values of 7.01mg/g were reported, at 25°C.	Elwakeel et al. 2014
	Pomegranate peel carbon	The maximum adsorption potential of pomegranate peel adsorbent for Fe (II) removal was 18.5 mg/g	Moghadam et al. 2013
	Calabrian pine bark wastes ( <i>Pinus brutia Ten</i> )	The amount of Fe (II) ions removed by the bark increases slightly from 1.225 mg/g to 1.408 mg/g when changing temperature from 30 to 50°C.	Acemio 2004

## 2.6. ARECAHUSK

### 2.6.1. Demography and Primary Uses of Arecanut

Areca catechu are palm species, botanically it belongs to the Kingdom *Plantae*, Order *Arecales*, Family *Arecaceae*. It is popularly known as betel nut tree, as its fruit is combinedly chewed along with betel leaf. It is exactly not known how Arecanut got its name, but is theorized that it is derived from the Kanarese "adeke" or the Malayalam "adakka" and catechu may be from the Malay name, "caccu". It is speculated that the areca nut has its origins in Malaysia or Philippines and then traveled to the rest of Asia where it is cultivated as a commercial crop. (Raghavan, V., & Baruah 1958). There are references made to the areca nut in ancient Greek, Sanskrit, and Chinese literature as early as 1<sup>st</sup> century BC. Historians have reported its use in Ceylon and Persia around 600 AD and parts of the Arab world in the 8<sup>th</sup> and 9<sup>th</sup> centuries. It is of the opinion that the areca nut was brought to Europe from the travels of Marco Polo around 1300AD. (Ahuja and Ahuja 2011).

Areca catechu palms are upright tall and can attain a height of up to 20 to 30 meters and a diameter of about 30-45 cm. Alike other palms, Areca palms break off in a crown crowded with long graceful pinnate leaves, which are generally bright green but turn golden yellow and finally brown, on aging. The roots of the areca palms are primarily fibrous, each measuring a dia of 0.6 to 1.25 cm. These dense adventitious roots appear from the bottom of the stem about 30 to 45 cm advancing as fine branches below the soil base. The areca flowers are golden yellow in color hermaphroditic in nature and crowded in inflorescences. The inflorescences are branched with muscular rachis. The fruits are characterized as hard, shiny with ovoid or ellipsoid achenes of 3 to 5 mm length. The fruits are green in color when they are young and turn golden yellow to orange as they ripen, which roughly takes about six to eight months (Figure 2.1).

As earlier mentioned Arecanut quids are mainly used as a chewable item, combined popularly with beetle leaf and lime for its CNS stimulating effects in a manner similar to use of tobacco or caffeine. Arecoline, found in arecanut is believed to be

responsible for effects such as alertness, euphoria, increased appetite and digestion. Arecanut has its use in indigenous medicine as an excellent diuretic, digestion aiding and anti-parasitic compound. Its antiparasitic properties had made it the numero uno medication to treat tapeworm, pin worm etc. (Peng et al. 2015).



**Figure 2.1 Well Cultivated Arecanut Grove**

Wide distribution of cultivation of *Areca catechu* is observed mainly in Southeast Asia and other parts of Southern Asia. Countries accounting to major growers & consumers include China, India, Indonesia, Malaysia, Philippines, New Guinea, etc. Over 400 million people are believed to be daily users of Arecanut in Tropical & Subtropical countries (Figure 2.2).

Statistical data obtained in the official portal of information about Arecanut in India reports production of over 7 lakh tones during 2013-14. An overall area of 445,000 hectares & production of 729,000 tonnes has also been mentioned. Karnataka stands first in the list of Arecanut producing states in India with an estimated production of 457,000 tonnes from an area of 218,000 hectares. But consumption of the nut is a pan India habit mainly in rural & semi-urban areas.



**Figure 2.2 Areca Cultivation Worldwide**

### **2.6.2. Finding Alternate Uses**

Owing to increased reports of health hazards due to Arecanut use and growing outcry to ban arecanut in the chewing form has inspired Researchers and Progressive growers to find alternative uses for arecanut. Polyphenols, fat polysaccharides, fiber and protein are the main components besides which alkaloids i.e. Arecoline (0.1 to 0.7%) and Arecadine, Guvacoline and Guvacine are all found in trace amounts.

While tannin, a byproduct from the processing finds its use in leather industry, dyeing & as a food color, the fat is used in confectionaries. The fat when refined is used for blending food. Other isolates like flavones, triterpenes & fatty acids have found pharmacological uses. A wide range of diseases were tried to be treated with areca extracts namely as an anti-parasitic, antioxidant, anti-inflammatory and promote digestive functions.

The fibrous outer cover of the betel nut which accounts to a large portion of the volume & weight of the fruit called the husk has found some use as raw material for hardboards, plastic & packaging material. However, in most cases, the growers consider it a waste byproduct & use it as an inferior fuel and mulch. Here is a list of other uses of husk; for the most part it remains only for academic purpose.

- Gasification
- Substrate for the cultivation of mushroom
- Reinforcement of plastic sheets
- Use in resins and paints

More often than not, especially in rural areas, it is left in piles to dry and is considered a nuisance. It is predominantly composed of lignocellulose fibers.

### **2.6.3. Properties of Areca Husk fiber**

Areca husk fibers are generally lignocelluloses, consisting of helically wound cellulose microfibrils in an amorphous matrix of lignin and hemicellulose. It consists of varying proportions of  $\alpha$ -cellulose, hemicellulose, lignin, pectin, wax, and moisture. Desai et al. (2016) explains that areca fibers consist of 53.2% of  $\alpha$  cellulose, 30-64.8% hemicellulose, 7-24.8% lignin, 4.4-4.8% of ash, 11.7% of moisture, and very negligible percentage of the pectin and wax.

Generally, the cellulose constituent is a polysaccharide comprising of linear combination of d-glucose units bound to each other by  $\beta(1\rightarrow4)$  glucosidic bonds. Cellulose has strong inclination to form inter and intramolecular hydrogen bonds, and the assemblage of the linear chains of molecules within microfibrils creates a highly crystalline structure. A lot of crystalline structures of cellulose are familiar, with distinct placement of hydrogen bonds within and between the strands. Hemicellulose is again a complex polysaccharide consisting of pentose sugars (xylose and arabinose) and hexose sugars (mannose, galactose, glucose, rhamnose or glucuronic acid). In comparison to cellulose, hemicelluloses are amorphous in nature. The hemicellulose found in hardwoods are made of acetyl glucuronoxylan in relation with other components such as galactose, arabinose, rhamnose, glucuronic acid and acetyl groups whereas softwoods comprise primarily of galacto-glucomannan and glucomannan. Pectin is another component present in lignocellulosic biomass. Pectin is also a polymer of elements of galacturonic acid with scattered components of rhamnose, galactose or arabinose. Lignin is a randomly linked, amorphous, high-molecular dense phenolic compound. The primary components in lignin are p-

coumaryl, coniferyl and sinapyl alcohol units. Lignin is less polymeric and ample in hardwoods than in softwoods.

The process of pyrolysis has high potential in converting biomass to produce liquid bio-oil (complex mixture of volatiles) and a solid residue, called biochar. The biochar resulting from pyrolysis reaction is highly porous and carbonaceous in nature. The final pyrolysis temperature and initial nature of the biomass material is the deciding factor for the composition of the bio char. The increase in the pyrolysis temperature results in higher carbon content. The inorganic components present in the biomass determines the ash content of the biochar. In the course of pyrolysis, a decrease in oxygen-containing functional groups and an increase in aromatic compounds occur. At temperature higher than 400°C, there is a significant increase in the surface area. As pyrolysis progresses, the biomass becomes hydrophobic as the energy density increases.(Anca-couce 2020)

Gokul et al. (2019) reported the chemical composition that is hemicellulose, cellulose, lignin and other extractives of areca husk determined by the modified Van Soest method as 35.22%, 28.89%, 19.08% and 16.81%. The Ultimate analysis results revealed C, H, N, S, and O content in areca husk to be 44.11, 6.28, 0.64, 0.06, and 48.91 wt%, respectively. The gross calorific value of areca husk was 16.52 MJ/kg. The pyrolysis behavior of areca nut husk was described using thermogravimetric analysis divulging a major mass loss (44.4 wt%) to be in the temperature range of 220–370°C wherein rapid decomposition took place. The variation in activation energy (62.35–591.972 kJ/mol) values with increase in conversion indicates the presence of a complex multi-step process that occurs during the thermal decay leading to conclude that arecahusk has the potential to be pyrolyzed.

#### **2.6.4. Use of Areca Husk for Carbon**

Pyrolysis can convert arecanut husk to Carbon. The use of Carbon to remove contaminants has been an intense topic of research interest in the last decade. The properties of the Carbon derived from pyrolysis vary depending on the type of feed

stock, its process and pyrolytic conditions and those bio-char properties influence the environment and agronomic impacts. (Ippolito et al. 2012)

Areca husk was chemically activated with 0.2M H<sub>2</sub>SO<sub>4</sub> to adsorb Cd<sup>2+</sup> and Cu<sup>2+</sup> ions from wastewater. The results showed 97.75% and 96.46% adsorption potential for Cd<sup>2+</sup> and Cu<sup>2+</sup> respectively.(Wei Zheng et al, 2008). Areca husk was torrefied to biochar to be used as an adsorbent in the removal of As (V) from aqueous solution. The torrefied Areca husk biochar showed 40% removal within 10 min and almost complete removal within 70 min (Gogoi et al. 2017). These results show that areca husk can be used for adsorbent treatment of polluted waters.

## **2.7. IRON CONTAMINATION**

Iron is the most common elements found in the earth's crust. Ground water which in turn has filtered down through rock and soil can dissolve these minerals and hold them in solution. Iron pipes could corrode and source iron into the water transmitting through them. Water containing the above elements may have altered taste, odor, color and turbidity. Iron in ground water can turn indissoluble when exposed to air, giving it a brown red color. These problems could be of aesthetic nature, or causing indirect health concerns and in-turn economic problems (Jusoh et al. 2005).

Ground water is an important source of drinking water. Iron present as divalent ions (Fe<sup>2+</sup>) in water are considered as contaminants because of its organoleptic properties. Worldbank.org states that India is the largest consumer of ground water in the world. Over 85% of drinking water sources & 60% of irrigated agriculture are dependent on ground water (Ellis et al. 2000).

### **2.7.1. Magnitude of Iron Contamination**

Iron has been repeatedly quoted to be a major contaminant in drinking water supplies. Altered taste can be notified at iron concentrations above 40µg/L. In well water, Iron concentrations below 0.3 mg/L were notified as permissible, above which staining of laundry & plumbing issues may occur. Rust colored silt seen in ground water is often an insoluble precipitate of Iron Hydroxide. Anaerobic conditions in ground water may

contain iron (II) at concentrations of up to several milligrams per liter without discoloration or turbidity in the water when directly pumped from a well, although turbidity and color may develop in piped systems at iron levels above 0.05–0.1 mg/L. A commonly noted slimy coating on the piping's of water distribution systems is actually an undesirable bacterial growth promoted by the iron contents.

Iron Contamination of concentrations of 1 to 3 mg/L are also accepted by some individuals but often, many refuses to consume water containing high Iron due to discoloration & bad taste. In India, of the 21,428 water samples test carried out on hand bore wells in the Ganga-Brahmaputra River Basin, Iron concentrations above 0.3, 3, and 20 mg/L were recorded in 92.6%, 50.6%, and 6.3% of samples, respectively. Concentrations as high as 80 mg/L was also reported. It was also noted that the depth of these wells had no influence with the level of pollution. As many as 20 out of 33 districts in Rajasthan have groundwater polluted with high concentrations of Iron (Chakraborti et al. 2011). In an exercise conducted by Central Water Commission (<http://cwc.gov.in/publications> 2018), 2400 water samples from 414 water quality monitoring stations along the major Indian rivers were tested. Iron concentration exceeding permissible limits were noted in 524 samples of the 137 waterways during this study period. Concentration as high as 14.55 mg/L was observed at Chenimari on Buridehing River.

Karnataka has also reported higher levels of Iron pollution in ground water in many of its districts. Test results analyzed on borewells by the Karnataka Rural Water Supply and Sanitation Department in late 2010 disclosed 24,948 of the 1,45,860 water samples tested are polluted with total hardness, chloride, fluoride, nitrate, Iron. (Figure 2.3)



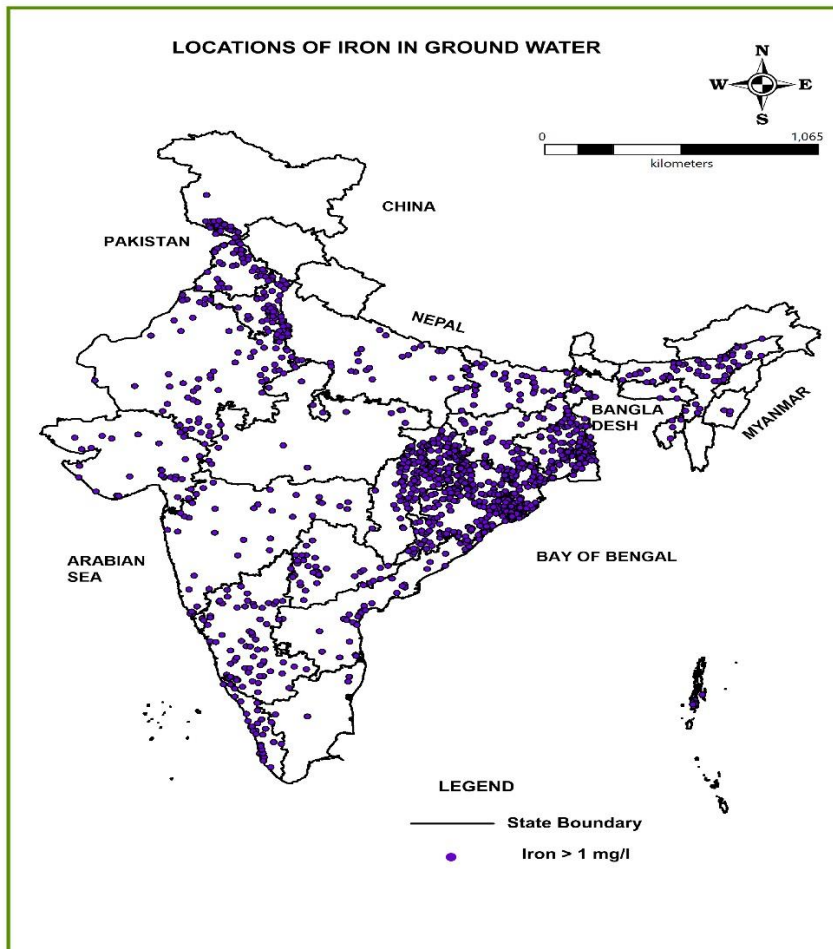


**Figure 2.3 Iron contamination in India (The CGWB, Ministry of Water Resources, 2015)**

### **2.7.2. Occurrence of Iron in water**

Iron in water can be found in many diverse forms. Table 2.4 gives the list of the same. The soluble  $\text{Fe}^{2+}$  ions are found both in surface and ground water. Its presence in water remains clear and colorless and does not cause any physical change unless oxidized to its trivalent form ( $\text{Fe}^{3+}$ ) which appears as brownish red in color and precipitates. This divalent form of Iron in water when exceeds the limit can cause health hazards.

**Table 2.4 Various forms of Iron in water (Khatri et al. 2017)**

Based on Mineral form	Based on Solubility	Based on Chemical nature
Oxides such as Hematite (Fe <sub>2</sub> O <sub>3</sub> ), Magnetite (Fe <sub>3</sub> O <sub>4</sub> ), Limonite FeO(OH)·nH <sub>2</sub> O	Soluble (Fe <sup>2+</sup> )	Organic
Silicates such as Pyroxene, Amphibole, Biotite, Olivine	Insoluble (Fe <sup>3+</sup> )	Inorganic
Sulphides such as Pyrite	Bacterial	

### 2.7.3. Health Hazards

Higher concentration of Iron in water does not cause acute health emergency, but overtime, causes adverse effects. Iron imparts bad odour and colour to water and the taste is “astringent”, which can alter the taste of other beverages such as coffee, tea etc. Excessive Iron intake give rise to a disorder called Iron overload, caused by the mutation of HFE gene responsible for Iron digestion, which can lead to hemochromatosis. Iron Overload causes weight loss, fatigue and joint pain initially and later can damage liver, heart and pancreas.(Papanikolaou and Pantopoulos 2005). Higher concentration of iron in water when consumed can damage skin cells, with an early onset of wrinkles.

There is no threat to human life from Iron bacteria, but these bacteria feed on the dissolved ferrous ions to produce slimy layers around plumbing systems, reducing the flowrate of water. These iron bacteria can also form a substrate to other microbes and help them metabolize to form acidic by-products and hydrogen sulphide (Cullimore and McCANN 1977). Grazuleviciene et al. (2009) discussed the effects of chronic

exposure to elevated levels of Iron through drinking water was linked with higher risk of delivering low baby weight baby.

#### **2.7.4. Treatment Techniques for removal of Iron**

A lot of treatment techniques has been envisaged for the removal of Iron from water over the decades. Some of the strategies such as oxidation/aeration–precipitation, filtration, electrocoagulation, removal by using calcium carbonate-based materials, supercritical fluid or sequestering agents and the in situ vyredox technology, ion exchange, wetland, biological methods, membrane technology and adsorption have been found effective in iron remediation from water.

As most of the Iron found in water is in its soluble ferrous form, it is predominantly oxidized to ferric salts resulting in precipitation. The precipitated ferric compounds can easily be filtered rendering the water free from Iron. This is one of the oldest and traditional technique for iron removal and is widely used. The oxidization of ferrous ions to ferric compounds is an easy procedure, entailing the use of oxidants or aeration.

Oxidants namely hydrogen peroxide, hypochlorite, potassium permanganate ( $\text{KMnO}_4$ ), ozone, chlorine and chlorine dioxide are most commonly used in the treatment of Iron. The optimal dose to be added is decided by conducting the jar test in the lab. Oxidant is selected based on its cost and quantity of water to be treated.  $\text{Fe}^{3+}$  ions are formed by the transfer of electrons from  $\text{Fe}^{2+}$  to the oxidant. These  $\text{Fe}^{3+}$  ions upon transformation easily precipitates into complex ferrous compounds and can be filtered. The method of aeration is an alternative to adding oxidants, where Oxygen is directly introduced to the water systems. This reduces the cost and accumulation of chemicals. Sometimes specific microbes are also introduced along with aeration to increase its efficiency.

The mechanism involved in the process of electrocoagulation is the application of electric current to undermine or break the dissolved pollutants in the water. Aluminum electrodes are chiefly used to destabilize  $\text{Fe}^{2+}$  ions to  $\text{Fe}^{3+}$  followed by

removal of  $\text{Fe}^{3+}$  by the complexes of aluminum hydroxide through adsorption and precipitation. Magnesium as anode and galvanized iron as cathode is also utilised for iron remediation. The advantages of this technique include no use of chemicals, no sludge and less operating cost.

Calcium Carbonate based materials have been employed to remove iron pollution from water. Limestone is the frequently used, for its availability and low cost. Calcium Carbonate based materials adsorb or precipitate the ferrous ions on its surface to form calcium siderite,  $\text{CaFe}(\text{CO}_3)_2$ . Existing cations, pH and organic matter play a vital role in the performance of these materials.

Another low-cost technique for removing iron from ground water is by utilizing chemicals called sequestering agents. In this technique, metal ions are complexed when a ligand or an electron donor from the sequestering agents bind to a metal ion. The most commonly used sequestering agents are sodium hexa metaphosphate, sodium silicates and tri sodium phosphate. This process is primarily used for remediation of groundwater having low concentrations of Iron (less than 1 mg/L); existing in the form of ions ( $\text{Fe}^{2+}$  or  $\text{Fe}^{3+}$ ) or as carbonates. (Volpe 2012)

Supercritical fluids are also found efficient in the removal of Iron. These fluids are defined as those which are heated and compressed above the critical pressure and temperature. Supercritical carbon dioxide ( $\text{scCO}_2$ ) is one such fluid which has garnered a lot of attention in the treatment of wastewater due to its non-toxicity and low cost. This technique is more like an extraction process where the metal ions (the extractant) are separated from liquid (the matrix) using supercritical fluids as the extracting solvent. (Boukouvalas et al. 2011)

Vyredox technology involves the oxidation of ferrous ions to ferric compounds. The oxidation is achieved in situ by injecting the supply wells with highly aerated or oxygenated water for about 6 to 14 hours, which helps the iron bacteria's growth in turn converting  $\text{Fe}^{2+}$  to insoluble  $\text{Fe}^{3+}$  naturally. (Braester and Martinell 1988)

Ion exchange is usually used to describe a process to treat water in which dissolved unwanted contaminants are exchanged with similar charge ions. Ion exchange is best used when iron is in its divalent form, that is completely dissolved in water otherwise the ferric ions can precipitate on the resin and it becomes difficult for regeneration. (Korngold 1994). Research on different resins for remediation of iron shows around 65 to 85% efficiency.

Wetland systems have been implemented in mining industry to treat acid mine drainage and also has a co-treatment for secondary effluents from many industries. Wetland increase the aesthetic value as it blends in with the natural environment (Sudarsan et al. 2016). A synergy exists in the various process of removal of iron by these wetlands. Initially precipitation of iron could be seen in the proximal parts of the wetland and biotic remediation was observed in the distal areas.(Lesley et al. 2015)

Iron bacteria namely *Leptothrix sp.*, *Flavobacterium sp.*, *Gallionella sp.*, *Sphaerotilus sp.*, *Siderocapsa sp.* naturally metabolize Iron for their nutrient intake. The mechanism is believed to be similar to that of oxidation of iron. These bacteria when employed in biofilters or trickling filters results in bio-remediation of iron without the addition of any chemicals, reducing operational costs. Bioremediation of iron is sensitive to process variations of temperature, flowrate, concentration of oxygen etc. Major drawback of utilizing these bacteria is its adverse effects on the population health.(Sharma et al. 2005)

Availing membrane technology for the remediation of iron from water is found to be promising. The ferrous ions need to be pre-treated with oxidising agents, surfactants or polymers to precipitate and/or increase its size, depending on which various techniques such as ultrafiltration, microfiltration, reverse osmosis or the advanced nano technology can be envisaged. Membrane technology can be alternatively used over conventional systems, however disadvantages such as membrane fouling and cake deposits decrease the efficiency. With advances in membrane material and design improvisation, membrane technology can be wisely used to treat polluted water.(Jimbo and Goto 2001). Nanotechnology entails fabricating materials smaller than 100 nm dimension either by building atom on atom or self-assembly. These

materials are called nano particles or nano materials and has found use to solve a lot of environmental problems. Carbon nano tube (CNT) is one such nanotube which has gained a lot of attention in water treatment. The basic mechanism involved is the adsorption of iron on the surface of these CNT rendering the water clean.

Adsorption is a surface phenomenon used for the treatment water. It adsorbs the contaminant on its surface making the water clean. it is the most widely used method to treat heavy metals in water. Numerous adsorbents namely activated carbon, clay, ash, char, etc. have been exploited by researchers to treat wastewater and have been successful. These adsorbents are naturally available or can be prepared and modified to suit our needs and increase removal efficiency. A lot of studies are being carried out to use agricultural waste as a precursor to produce activated carbon thereby valorising it and reducing solid waste.

## **2.8. LITERATURE SUMMARY**

According to the various literature reviewed, it is observed that Arecanut is a widely grown crop primarily used as betel nut which is chewed mostly in rural and semi urban India. The husk or the outer cover of the nut is discarded without any productive utilization. As most of the agro-waste contains more than 85% carbon, it ignites interest in being converted into activated carbon to be used as adsorbent.

It is deduced that activated carbon has a high surface area and is highly porous in nature which makes it an excellent material for the treatment of water. Iron is a common metallic contaminant which causes taste, odor, color and aesthetic issues. Apart from this, it also causes severe health hazards in the long run. Adsorption is one of the treatment processes that has been studied and shown success in water purification to standards acceptable even in developed countries. In this regard, the study is aimed at testing the efficacy of activated carbon derived from areca husk as a potential adsorbent to treat water to permissible limits.

A thorough literature survey indicated that Arecanut husk waste has not been converted into Carbon for adsorbent use in the removal of Iron thus far. In fact, the studies conducted earlier concentrated on other agro-wastes as precursor for the

preparation of adsorbent. Water contamination due to Iron needs a low-cost process for the treatment of water. Researches on the models to identify the efficiency of the adsorbent have been developed from case to case. In this regard, a model to find the capacity of the carbon prepared from Arecanut husk needs to be developed. To fill these gaps, the following objectives are considered

## **2.9. OBJECTIVES**

- i. Study the properties of Bio Char from Areca husk.
- ii. Analysis of the Removal efficiency of Iron by batch process and Isotherm studies
- iii. Design a Column to remove Iron from water and understanding experimental results with existing dynamic models.
- iv. To develop a statistical model





## CHAPTER 3

### METHODOLOGY

#### 3.1. CHEMICALS AND REAGENTS.

The adsorbate Ferrous Sulphate Heptahydrate ( $\text{Fe}_2\text{SO}_4 \cdot 7\text{H}_2\text{O}$ ) was purchased from Merck. The stock solution of 1000mg/L was prepared with 4.978 g of  $\text{Fe}_2\text{SO}_4 \cdot 7\text{H}_2\text{O}$  in 1000ml deionised water. Concentration of Iron was measured using UV-VIS Double Beam Spectrophotometer (Systronics Make, AU-2701 Model) at 510nm. 1,10 Phenanthroline method was used to determine the concentration which reacts with ferrous ions forming reddish orange colour. (Harvey et al. 1955)

#### 3.2. PREPARATION OF ARECA HUSK ADSORBENT.

The Arecanut husk is obtained from a plantation in Thirthalli town of Karnataka. The husk is washed repeatedly for removal of dirt and other impurities with water & deionized water. The husk rendered ready was oven dried at 378K (105°C) for 24 hours until the residual moisture was completely evaporated. Results of proximate analysis of the husk adsorbate carried out as per ASTM standards are presented in Table 3.1.

**Table 3.1 Proximate analysis of Arecanut husk**

Parameter	Weight % (on dry basis)
Moisture	8.23
Volatile matter	57.01
Ash	3.16
Fixed carbon	31.6

It is seen that the high fixed carbon and low ash content justify suitability of Arecanut husk as an activated carbon precursor.

Pyrolysis of arecanut husk was carried out in a muffle furnace at 450°C for 2 hours. The pyrolyzed sample was then ground with the help of ball mill to obtain particle size range to 40-80 mesh. The ground pyrolyzed areca husk was suspended and agitated for 2 hours on ultrasound bath. The suspension was filtered and dried in the oven (Indhumathi et al. 2014) The resulting sample was carefully stored in desiccators for characterization and adsorption experiments.

### **3.3. CHARACTERISATION OF ADSORBENT**

The surface morphology of pyrolyzed areca husk was examined using scanning electron microscopy (SEM) attached with energy dispersive X-ray (EDAX) analyzer (Zeiss EVO MA18 with Oxford EDS (X-act)). The surface area, total pore volume, and pore size distribution of all samples were determined by N<sub>2</sub> adsorption at -196 °C using Autosorb (Quantachrome Corp.). The surface area and pore volume were obtained by applying the Brunauer-Emmett-Teller (BET) equation to the adsorption data.

X-ray diffraction (XRD) patterns of pyrolyzed areca husk is obtained with an automated Rigaku 600 instrument using Cu K $\alpha$  radiation at 40 kV and 30 mA over the range ( $2\theta$ ) of 10° to 90°, with a scanning speed at 2° per minute. Fourier transfer infrared (FT-IR) spectra were collected on a Shimadzu with a resolution of 4 cm<sup>-1</sup> by using the KBr technique. The spectrum was scanned from (400 to 4000 cm<sup>-1</sup>). The pH<sub>zpc</sub> of pyrolyzed areca husk was experimentally found by pH drift method.

### **3.4. BATCH ADSORPTION EXPERIMENTS**

Data Acquisition – Different amounts of pyrolyzed areca husk (2, 4, 6, 8 and 10g) were added into 300-ml stoppered glass bottles containing a fixed volume (100ml in each flask) of varied initial concentration (1, 2, 3, 4 and 5 mg/L) of synthetic Iron solution at pH between 4.0±0.2, at an ambient temperature of 28 ± 2°C. The bottles were placed in a shaker (Rotek, India) and agitation was provided at 150 rpm for 6 hours and the Iron concentrations were measured at 1hour interval.

Data Analysis – From the experimental data, adsorbent performing characteristics were obtained. Concentration reduction of Iron at various time intervals were computed and from plots of adsorption amount versus contact time for various adsorbent dosages for different initial concentrations were understood and appraised. All experiments were conducted in duplicate to minimise any errors.

Available popular and recognised Isotherm models like Langmuir, Freundlich, Temkin and the Dubinin-Radushkevich (D-R) (Goher et al. 2015);(Hameed 2009);(Girods et al. 2009) were considered to describe how adsorbents interact with solutes. The linearized forms of the four isotherms are

$$\frac{1}{q_e} = \frac{1}{q_m} + \frac{1}{(k_1 q_m)} \frac{1}{C_e} \quad \dots (3.1)$$

$$\ln q_e = \ln K_f + \frac{1}{n} \ln C_e \quad \dots (3.2)$$

$$q_e = B \ln A + B \ln C_e \quad \dots (3.3)$$

$$\ln qe = X_m - \beta \varepsilon^2 \quad \dots (3.4)$$

The Langmuir constants  $q_m$  (mg/g) and  $k_1$  (l/mg) are related to adsorption capacity and energy of adsorption, respectively. The constants  $q_m$  and  $k_1$  can be determined from the plot  $1/q_e$  versus  $1/C_e$  (eq. (3.1)).  $C_e$  (mg/L) and  $q_e$  (mg/g) are the equilibrium concentration and the amount of Iron adsorbed at equilibrium, respectively. Similarly, the Freundlich Isotherm constants  $K_f$  and  $1/n$  can be calculated from the plot of  $\ln(q_e)$  versus  $\ln(C_e)$  (eq. (3.2)).  $K_f$  and  $n$  are the Freundlich constants, which are indicators of adsorption capacity and adsorption intensity, respectively. The Temkin isotherm has generally been applied in the form given by eq. (3.3). Therefore, plotting  $q_e$  versus  $\ln C_e$ , enables the determination of the constants  $A$  and  $B$ .  $B$  is the Temkin constant related to heat of sorption (J/mol),  $A$  is the Temkin isotherm constant (l/g). The Dubinin-Radushkevich (D-R) equation sheds detail on the type of adsorption as in whether it is physisorption or chemisorption.  $\varepsilon$  (Polanyi potential) =  $RT \ln(1+1/C_e)$ ,  $X_m = \ln q_m$ ,  $q_m$  is the maximum adsorption capacity (mg/g),  $\beta$  is related to mean free energy,  $E$  ( $E$  in kJ/mol) as:

$$E = \frac{1}{\sqrt{-2\beta}}$$

The most common models used to fit the kinetic sorption experiments were Lagergren's pseudo-first-order model (Eq. (3.5)) and pseudo-second-order model (Eq. (3.6)): (Liang et al. 2010)

$$\log(q_e - q_t) = \log q_e - \frac{K_1 t}{2.303} \quad \dots (3.5)$$

$$\frac{t}{q_t} = \frac{1}{K_s q_e^2} + \frac{1}{q_e} t \quad \dots (3.6)$$

where  $q_e$  (mg/g) and  $q_t$  (mg/g) are the amount of adsorbate adsorbed at equilibrium and at time  $t$ , respectively.  $K_1$  ( $\text{min}^{-1}$ ) and  $K_s$  ( $\text{g mg}^{-1} \text{min}$ ) are the pseudo-first-order and pseudo-second order adsorption rate constants, respectively.

To further understand the mechanism of Iron adsorption onto pyrolyzed areca husk, a commonly used technique named intraparticle diffusion-based plot was studied. It is an empirically formulated functional relationship, familiar to most adsorption processes, where the uptake varies almost proportionally with  $t^{1/2}$ . According to the theory proposed by Weber and Morris

$$q_t = k_{id} t^{1/2} + C_i \quad \dots (3.7)$$

where  $k_{id}$  ( $\text{mg g}^{-1} \text{min}^{1/2}$ ), the rate parameter of stage  $i$ , is obtained from the slope of the straight line of  $q_t$  versus  $t^{1/2}$ .  $C$  is the intercept (Wu et al. 2009).

### 3.5. CONTINUOUS FLOW ADSORPTION STUDIES.

For practical application of the adsorption process, column studies in continuous operation mode seems to be more useful. It is possible to reach high removal efficiency and it can be easily scaled up from a laboratory to an industrial application.

Experimental Setup – Packed bed column experiments is conducted in a fabricated aluminum column of 2 cm diameter and 30 cm height. At the top of the column, an

adjustable porous plunger of Teflon is used to change the effective depth of the column. The adsorption experiments will be carried at effective depth of 3, 5 and 9 cm. The column packed with pyrolyzed Arecanut husk is operated in up flow mode using peristaltic pump. All experiments are carried out at room temperature. The initial pH of the ferrous ion's solution was kept in the range of 4 to 4.2 which is the optimum pH value determined by  $pH_{zpc}$  test. The treated water samples are collected at the exit at regular time intervals and measured using UV spectrophotometer for the remaining contaminants to identify the bed exhausting time. (Figure 3.1)

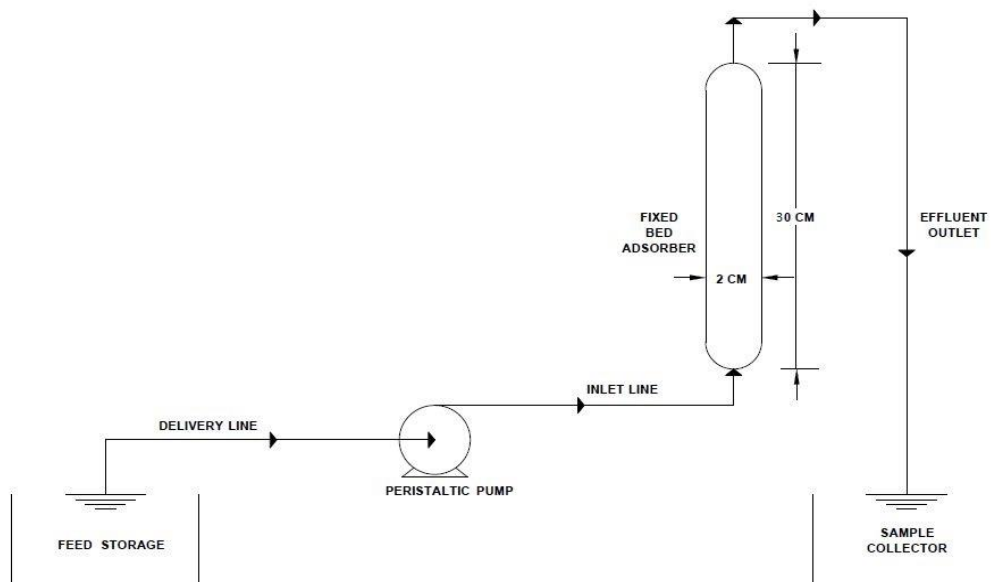


**Figure 3.1 Schematic representation of Packed Bed Column Adsorption**

#### Data Analysis of Column – Breakthrough curves and Design parameters

The breakthrough curve expresses the ratio of effluent iron concentration to the inlet iron concentration ( $C_t/C_0$ ) as a function of time. The experimental data is analyzed to determine the design parameters of breakthrough curves for packed bed column. The total adsorbed quantity ( $q_{total}$ , mg) of iron ions can be calculated by using the area ( $A$ ) under the plot of adsorbed concentration of iron ions versus time. Hence  $A$  is obtained by taking definite integral of the adsorbed concentration of iron ion with respect to time. The concentration of iron ions adsorbed on pyrolyzed arecanut husk is

determined from the difference of the concentration of iron ions at the inlet and outlet. The area was calculated using the trapezoid method to find the definite integral. The equation for calculating the  $q_{total}$  is given by

$$q_{total} = 0.06QA = 0.06Q \int_{t=0}^{t=te} C_{ad} dt \quad \dots (3.8)$$

The total metal uptake capacity of the packed bed column can be calculated by dividing the total amount of metal adsorbed by the mass of the bio-sorbent packed inside the column

$$q_{exp} = \frac{q_{total}}{m} \quad \dots (3.9)$$

The length of mass transfer zone (MTZ) is determined for all the operating conditions using the relationship

$$MTZ = Z \left( \frac{te - tb}{te} \right) \quad \dots (3.10)$$

For this analysis, breakthrough time ( $t_b$ ) was selected as the time when the effluent concentration of ferrous ions reaches 30% of the influent concentration. The exhaustion time ( $t_e$ ) was taken as the time when effluent concentration of  $Fe^{2+}$  ions reached 70% of the influent concentration. (Ahmad and Haydar 2016)

Column studies are described by dynamic models. The most common models used to describe the performance of packed bed columns are Yoon and Nelson model, Thomas model and Bohart Adam's model and their linearized equations respectively are as follows:

$$\ln \frac{C_t}{C_0 - C_t} = kt - \tau k \quad \dots (3.11)$$

$$\ln \left( \frac{C_t}{C_0} - 1 \right) = \frac{k_{Th} q_0 x}{Q} - k_{Th} C_0 t \quad \dots (3.12)$$

$$\ln \frac{C_t}{C_0} = k_{AB} C_0 t - k_{AB} N_0 \frac{Z}{F} \quad \dots (3.13)$$

The Yoon–Nelson model explains the rate of decrease in the probable adsorption for each adsorbate molecule which is proportional to the probable adsorbate adsorption and the probable adsorbate breakthrough on the adsorbent. The values of  $k$  (a rate constant) and  $\tau$  (the time required for 50% sorbate breakthrough) are determined from plots of  $\ln[C_t/(C_0 - C_t)]$  versus  $t$ . Presuming plug-flow operation of the column bed and using Langmuir isotherm for equilibrium and second-order reversible reaction kinetics, the Thomas model gives the maximum adsorption capacity of the adsorbent and this helps in designing the column. A linear plot of  $\ln[(C_t/C_0) - 1]$  versus  $t$  enables the determination of the kinetic coefficient,  $k_{Th}$ , and the sorption capacity of the bed,  $q_0$ . Bohart Adam's model focuses on the estimation of characteristic parameters such as maximum adsorption capacity ( $N_0$ ) and kinetic constant ( $k_{AB}$ ) and it explains the initial part of the breakthrough curve. (Han et al. 2009)





## CHAPTER 4

### RESULTS AND DISCUSSION

The results of the current investigation are presented and discussed in this section.

#### 4.1. CHARACTERISATION OF ADSORBENT

The SEM image detected the structure of the pyrolyzed areca husk as porous and amorphous which is supported by XRD results (Figure 4.1). As the areca husk is mainly composed of lignin and cellulose composites bonded together, it degraded to create a corrugated sheet like structure creating active adsorption sites (Supriadi et al. 2017). EDAX measurement carried out ascertained the elemental composition in the prepared pyrolyzed areca husk. The raw areca husk had 31.6% fixed carbon which enriched to more than 75% after the pyrolysis process as observed from EDX result and this may be attributed to areca husk not being volatilized and the higher level of carbon content in the areca husk feedstock.

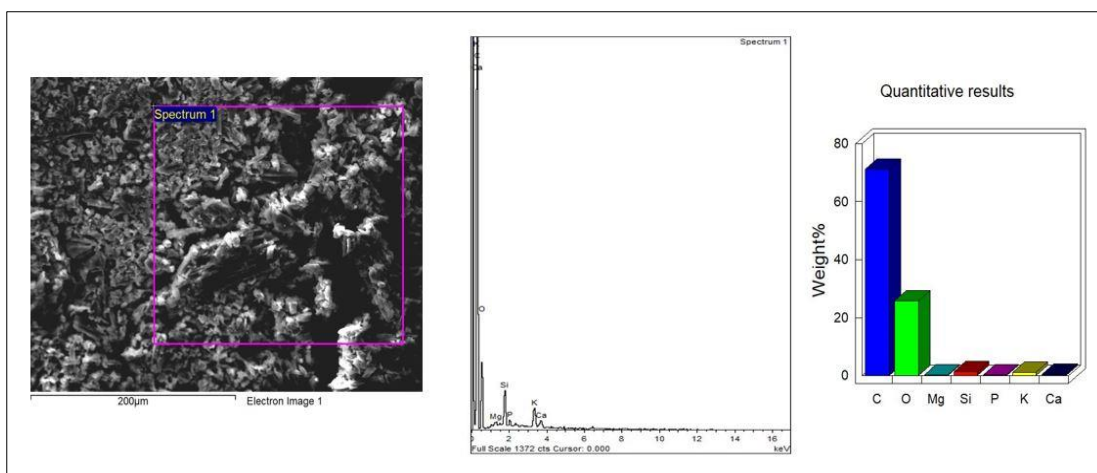


**Figure 4.1 SEM image of pyrolysed areca husk**

The XRD result consisted of distinct, broad peaks ranging from  $2\theta \sim 20^\circ$  to  $28^\circ$ , and a weak peak at  $\sim 43^\circ$ . These peaks are assigned as (002) and (001) graphite planes, respectively. The broad initial peaks at (002) graphite plane were centred at  $\sim 25^\circ$  which is attributed to the lower reflection than graphite at around  $27^\circ$ , thus displaying

a significant level of interlayer d spacing ( $3.67\text{\AA}$ ) which was similar to the observations of coir-pith by Supriadi et al. (2017).

The peaks obtained in the FTIR spectrum decide the participation of surface functional groups in adsorption interaction. The IR spectra exhibited broad peaks at  $3382\text{ cm}^{-1}$  indicating O-H stretching vibration of hydroxyl functional groups. The presence of peaks at  $2920\text{ cm}^{-1}$  and  $2851\text{ cm}^{-1}$  is related to methyl C-H stretching. At  $2360\text{ cm}^{-1}$  peak, C=O stretching was indicated. The band at  $1590\text{ cm}^{-1}$  is attributed to the presence of highly conjugated C-O in carbonyl structure. The overlapping bands at  $400\text{ cm}^{-1}$  to  $500\text{ cm}^{-1}$  is due to the stretching vibration of S-S of Polysulphides and Aryl disulphide (Kavitha and Namasivayam 2008). The results from FTIR analysis indicate that the surface contains acidic functional groups, which increases metal ion adsorptions.

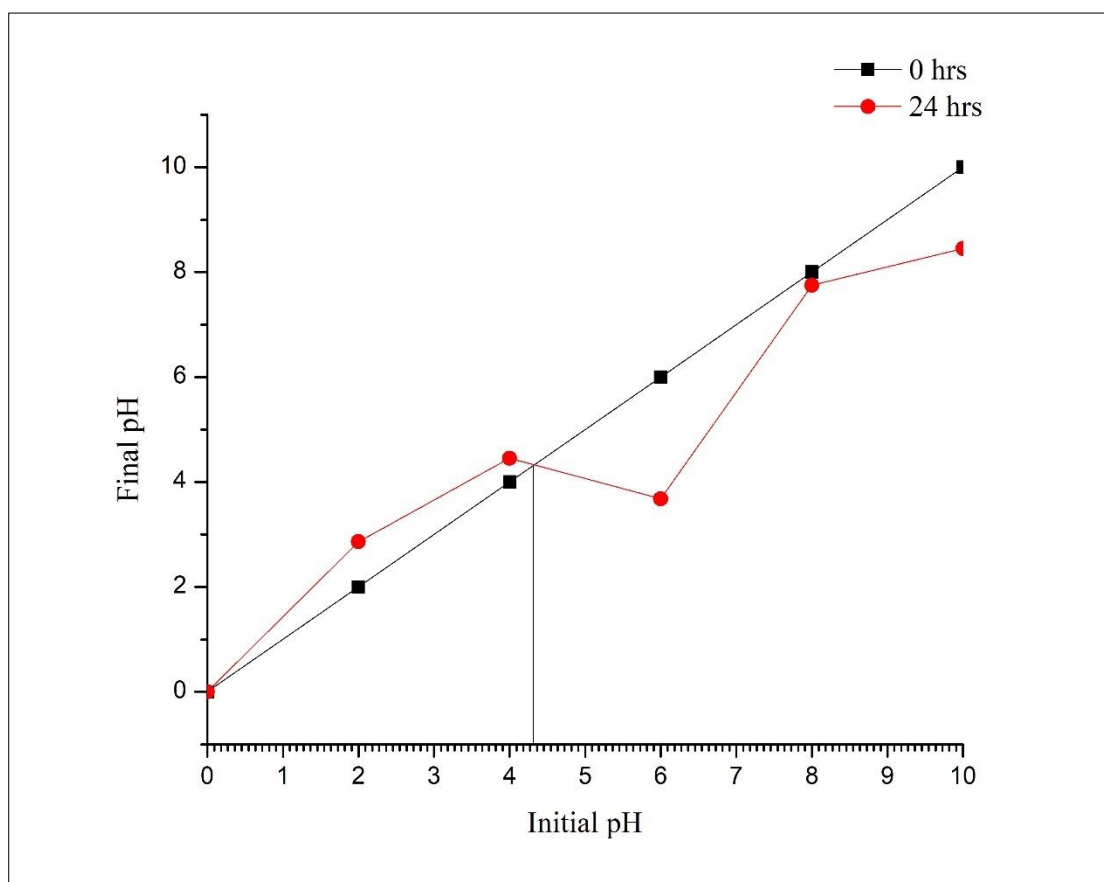


**Figure 4.2**  $\text{pH}_{\text{zpc}}$  of pyrolyzed areca husk.

The surface area, using N<sub>2</sub> as adsorbate at 196°C measured the specific surface area as 54.5 m<sup>2</sup>/g and the volume of the pore as 0.0142 cm<sup>3</sup>/g. The surface charge of the biochar in the aqueous media conducted and analyzed experimentally by pH drift method to finalize the optimum pH<sub>zpc</sub> or pH point of zero charge of the adsorbent material (Figure 4.2) The point of zero charge (pH<sub>zpc</sub>) on pyrolyzed areca husk is 4.2 meq·g<sup>-1</sup> indicating acidic functional groups which are confirmed by the FTIR results. This suggests that the pyrolyzed areca husk surface releases hydroxide groups into the solution, hence the adsorbent surface is positively charged attracting anions (Rahman et al. 2014).

The newly produced carbonised areca husk is cost effective and is estimated at around 0.09 INR/kg. From the internet search results, the cost of commercially available activated charcoal varies from USD 2.2 to 5 (Selvaraju and Bakar 2017). Hence, this carbonised areca husk can be used as an alternative which is more promising and a cleaner adsorbent. The rates were estimated based on the price rate in India. The details are presented in APPENDIX I. (Liew et al. 2018).

## **4.2. PERFORMANCE APPRAISAL OF PYROLYZED ARECANUT HUSK FOR IRON REMOVAL BY BATCH PROCESS**

The experimental setup and methodology for the parametric studies made in this investigation is elaborated in these sections.

### **4.2.1. Effect of adsorbent dose on Iron adsorption**

The maximum removal efficiency of about 80% Iron is obtained at 10 g/l of pyrolyzed arecanut husk dosage. As observed from Figure 4.3, with the increase in adsorbent quantity (w = 2, 4, 6, 8 & 10 g/l) for the same initial Iron concentration (1 to 5 mg/L), the amount of Iron adsorbed by pyrolyzed arecanut husk for Iron removal reduced gradually. This is attributed to the aggregation of adsorbent at a higher dosage and subsequent reduction of adsorption sites. A similar response is reported in the experimental investigation for the adsorption of Iron on commercially available granular activated carbon by Jusoh et al. (2005)

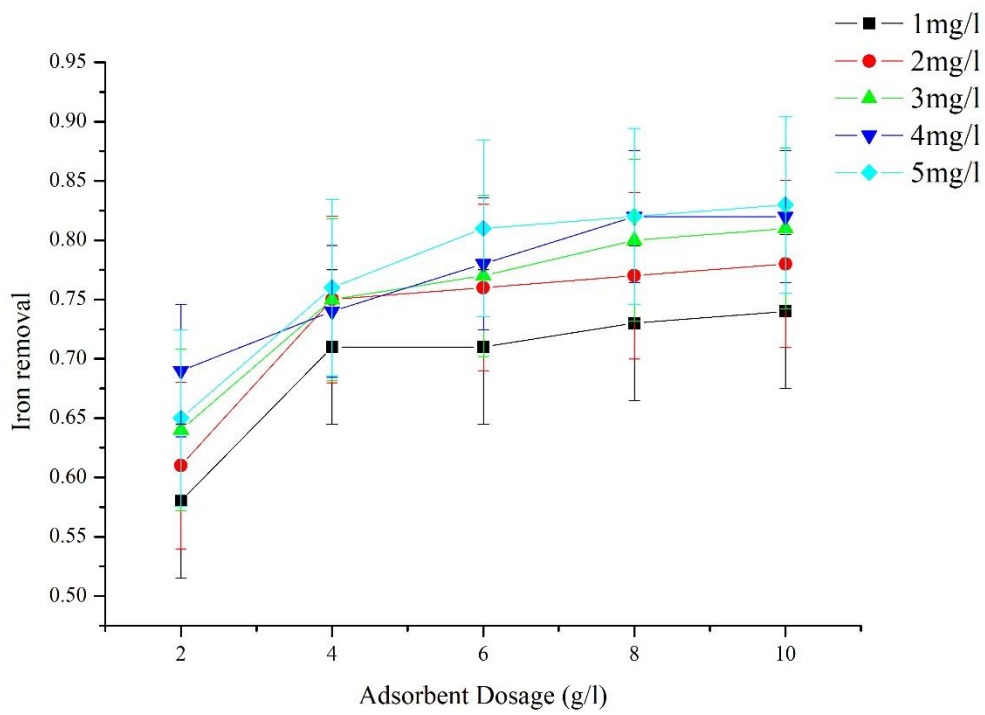


**Figure 4.3 Effect of adsorbent dosage on the adsorption of Iron on pyrolyzed areca husk (Contact Time = 5 hours and Initial Concentration  $C_0 = 1, 2, 3, 4$  &  $5 \text{ mg/L}$ ).**

#### 4.2.2. Effect of initial concentration and contact time

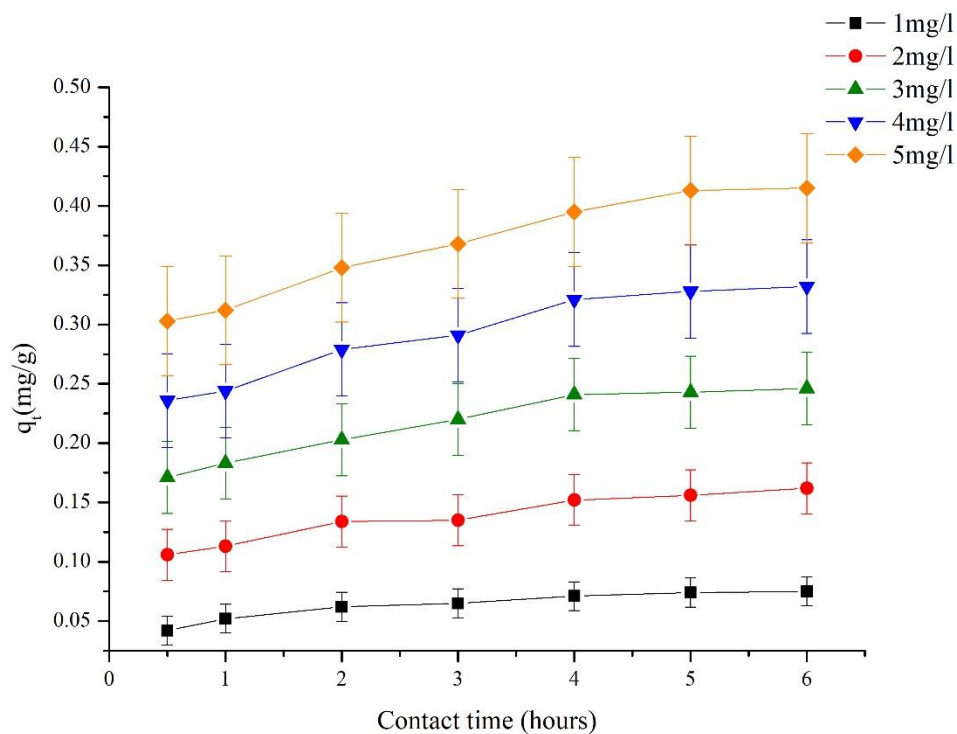
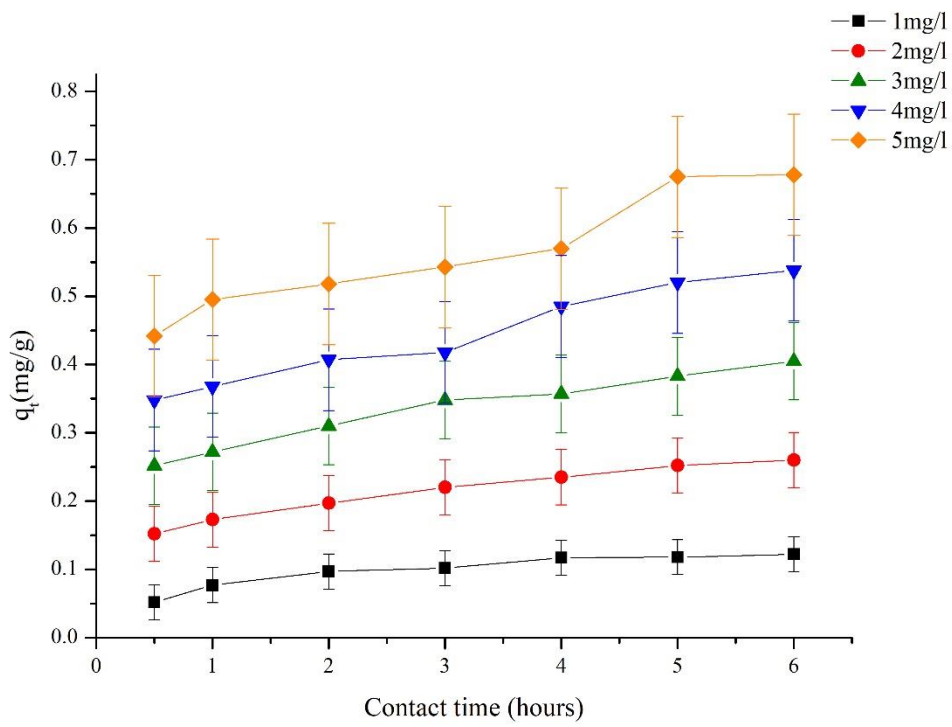
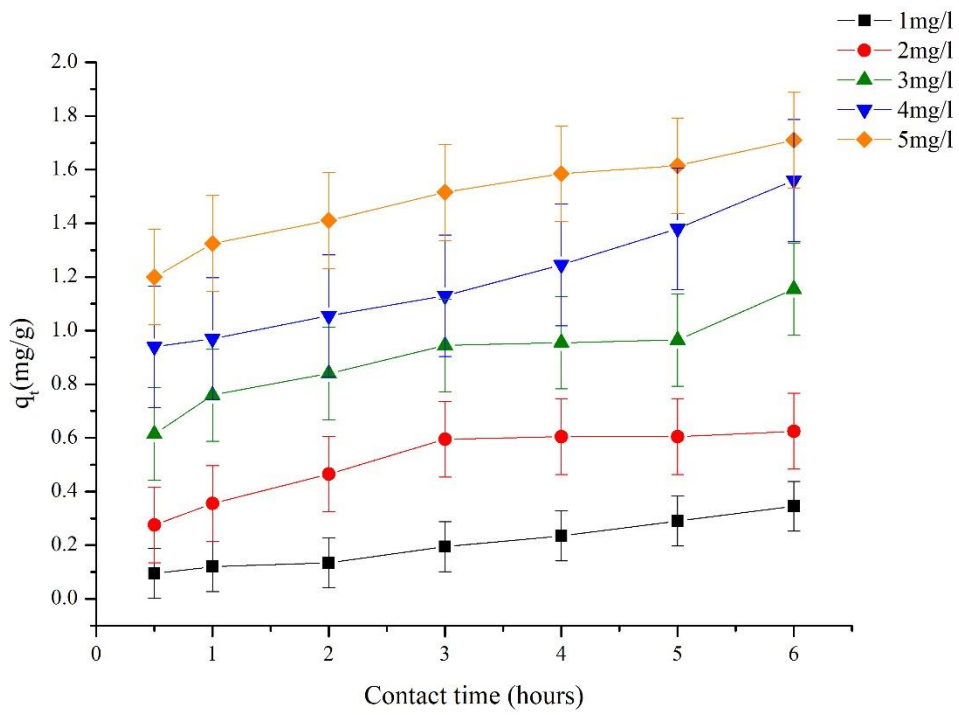
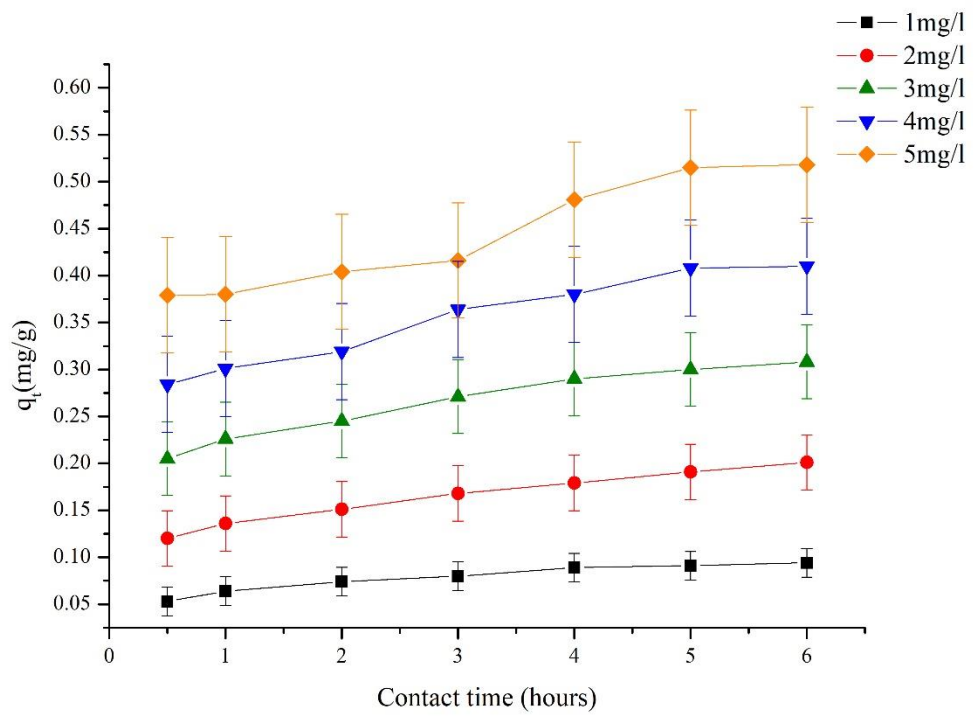
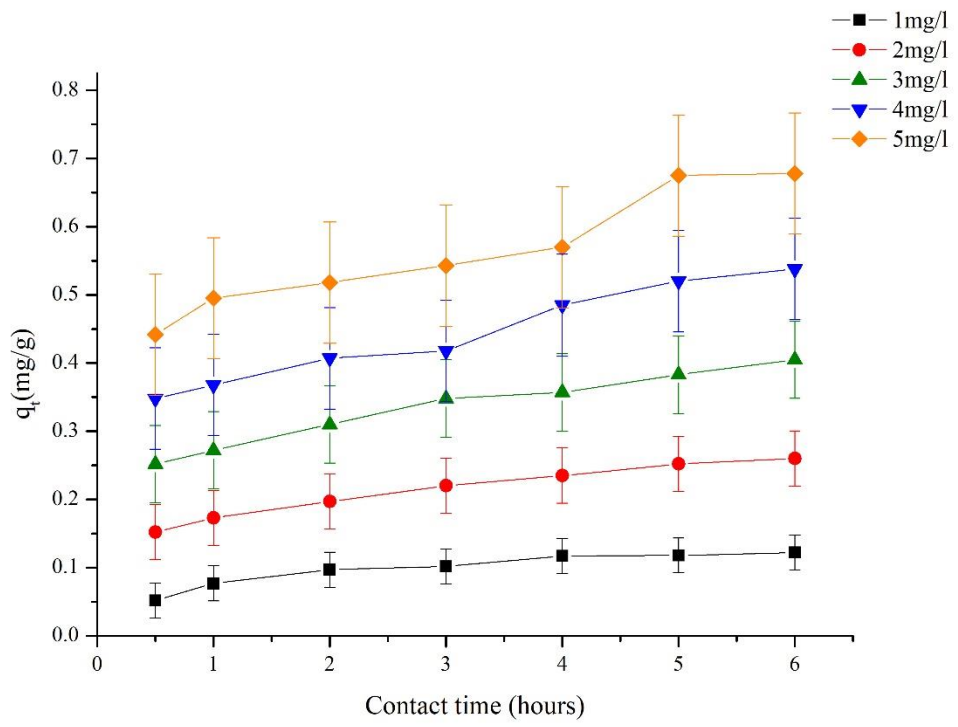
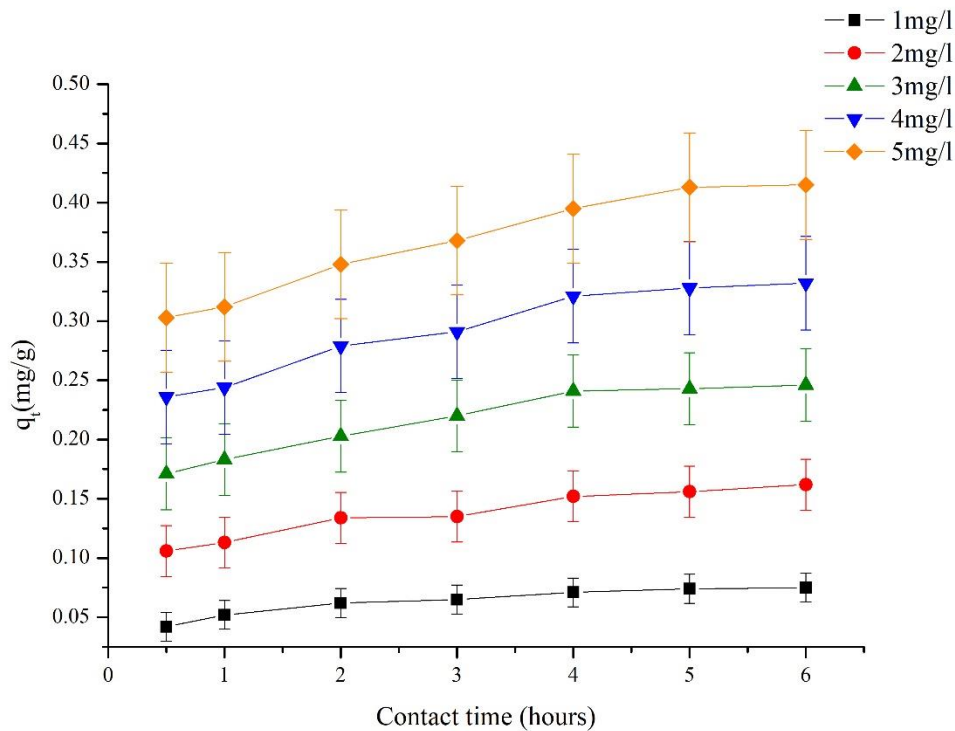


Figure 4.4 (a-e) shows the effect of initial concentration (1 to 5 mg/L) on adsorption of Iron on pyrolyzed arecanut husk at  $28 \pm 2$  °C. It is observed that the gradient of  $q_t$  versus contact time is steep for the first 30 to 60 minutes and then the gradient flattens. The rapid adsorption in the initial stage is due to the availability of many adsorption sites. The adsorption capacity of pyrolyzed Arecanut husk ( $w = 2$  g/L) for Iron removal by batch process increased from 0.05 to 1.8 mg/g with increase in initial concentration of Iron.







**Figure 4.4(a-e) Effect of initial concentration and contact time on Fe adsorption (W= 2,4,6,8 & 10 g; V = 1 L)**

### 4.3. ADSORPTION ISOTHERMS

Adsorbent Isotherms are important in understanding the performance of solutes. They are mathematical models that describe the behavior between solid and liquid phases for the adsorbate species. The equilibrium between the amount of contaminant adsorbed by carbonized arecanut husk and the concentration of the dissolved contaminant Iron is given by adsorption Isotherm. Langmuir, Freundlich, Temkin, and Dubinin-Radushkevich isotherm model is the most often used isotherms to describe the adsorption data for contaminant concentration.

According to Langmuir adsorption isotherm, there is only monolayer adsorption on the adsorbent. The equilibrium distribution of the contaminant Iron between the solid and liquid phases is given by a single layer. There is no adsorption occurring after this monolayer is formed on the surface of the adsorbent. This kind of single layer adsorption takes place on the adsorbent surface which has a restricted number of similar sites. This model used in bio-sorption processes is given by the equation:



$$q_e = \frac{q_m C_e}{1 + k_l C_e} \quad \dots (4.1)$$

The linearized form of the isotherm is

$$\frac{1}{q_e} = \frac{1}{q_m} + \frac{1}{(k_l q_m)} \frac{1}{C_e} \quad \dots (4.2)$$

where,  $C_e$  – equilibrium Iron ion concentration (mg/L) &  $q_e$  – amount of Iron adsorbed at equilibrium (mg/g).  $k_l$  (l/mg) and  $q_m$  (mg/g) are Langmuir constants related to energy of adsorption and adsorption capacity respectively.

The Freundlich isotherm model is based on the heterogeneous distribution of active sites accompanied by interactions between molecules adsorbed. The following equation expresses this model:

$$q_e = C_e^{1/n} k_f \quad \dots (4.3)$$

The linearized form of the isotherm is

$$\ln q_e = \ln k_f + \frac{1}{n} \ln C_e \quad \dots (4.4)$$

where,  $k_f$  (mg/g) and  $1/n$  are Freundlich constants related to relative adsorption capacity of carbonized arecanut husk and intensity of adsorption & indicate the tendency of the adsorbate to be adsorbed.

The Temkin isotherm assumes the heat of adsorption increases linearly with decreasing coverage. The following equation expresses this model:

$$Q_e = B \ln A + B \ln C_e \quad \dots (4.5)$$

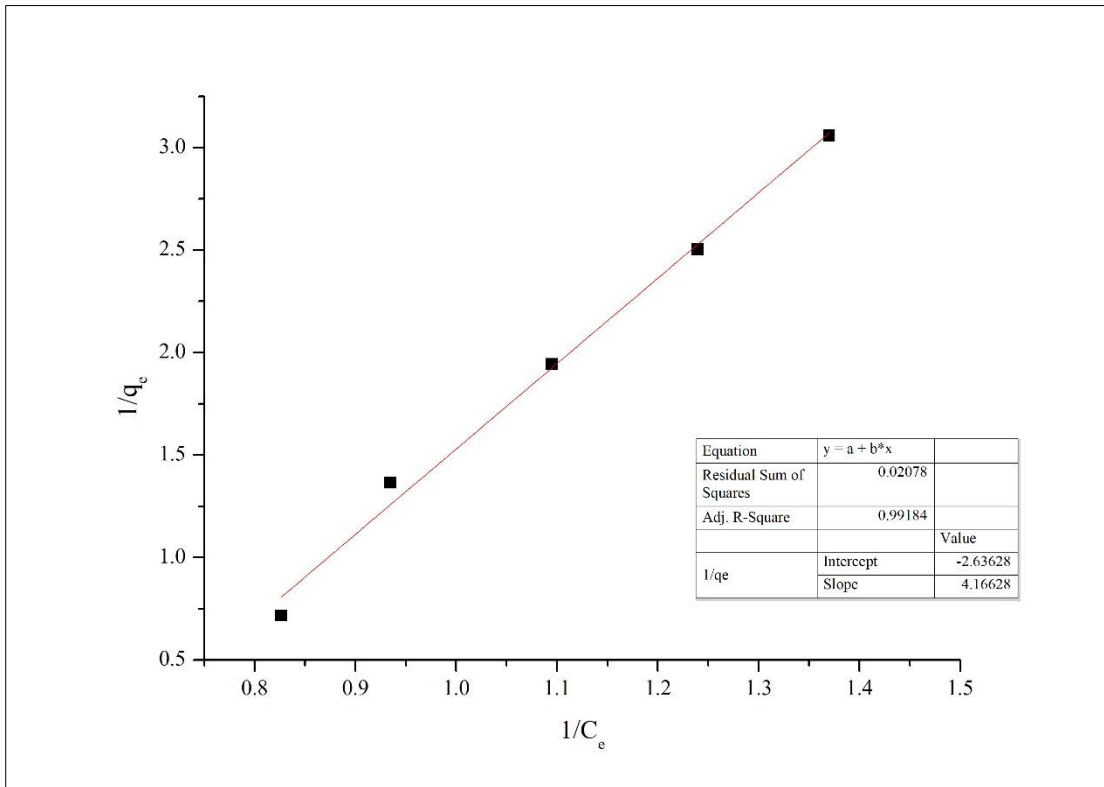
where,  $B = RT/b$ , is the Temkin constant related to heat of sorption (J/mol),  $A$  is the Temkin isotherm constant (l/g),  $R$  is the gas constant (8.314 J/mol K),  $b$  is Temkin isotherm constant, and  $T$  is the absolute temperature (K)

The Dubinin-Radushkevich (D-R) equation sheds detail on the type of adsorption as in whether it is physisorption or chemisorption and expressed as

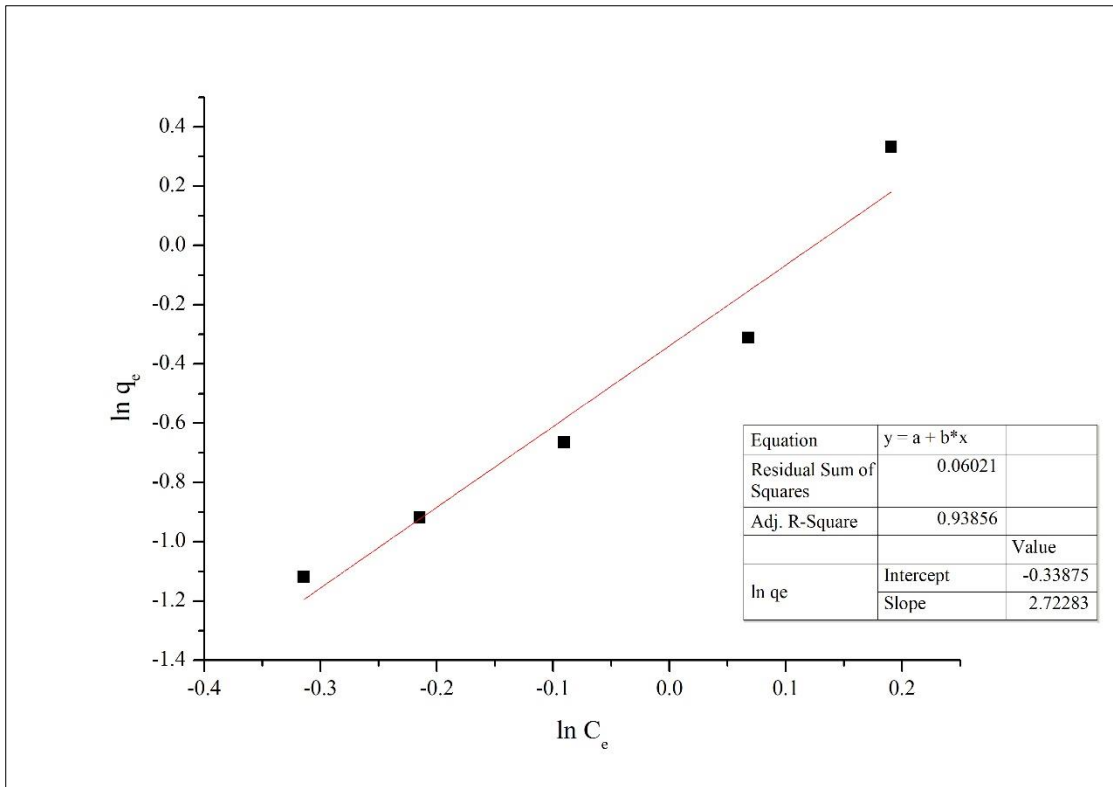
$$\ln q_e = X_m - \beta \varepsilon^2 \quad \dots (4.6)$$

where  $\varepsilon$  (Polanyi potential) =  $RT \ln(1+1/C_e)$ ,  $X_m = \ln q_m$ ,  $q_m$  is the maximum adsorption capacity (mg/g),  $\beta$  is related to mean free energy,  $E$  (E in kJ/mol) as:

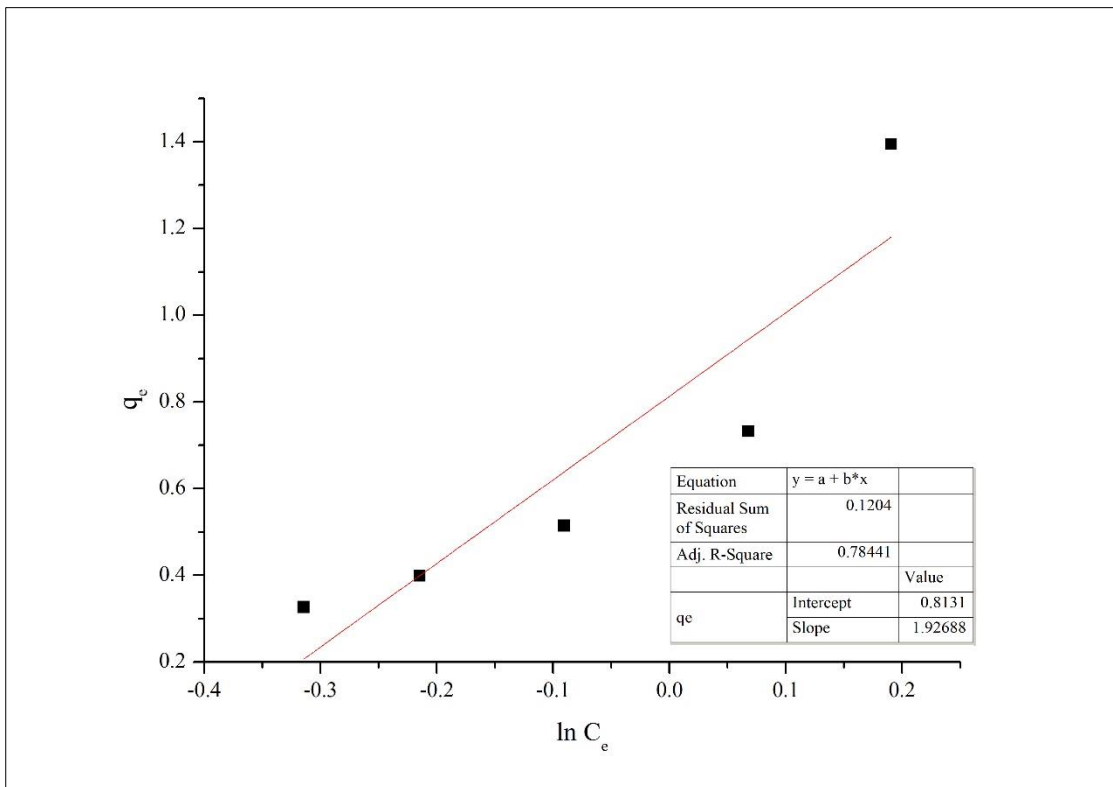
$$E = \frac{1}{\sqrt{-2\beta}} \quad \dots (4.7)$$



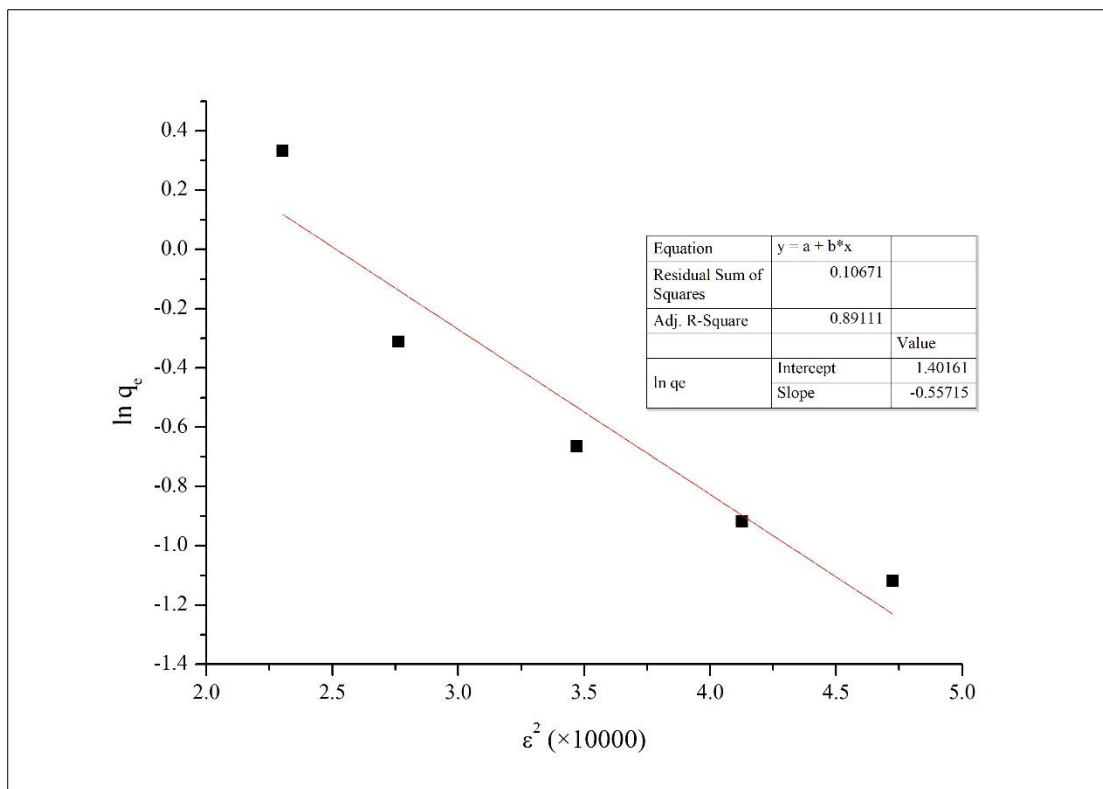
(a)



(b)



(c)



(d)

**Figure 4.5 Plots for Langmiur (a), Freundlich (b), Temkin (c) and Dubinin-Radushkevich (d) isotherms for Iron on pyrolyzed arecanut husk ( $C_0 = 4\text{mg/L}$ , Adsorbent = 2,4,6,8 & 10 mg/L)**

**Table 4.1 Langmuir, Freundlich, Temkin and Dubinin-Radushkevich Isotherm Parameters**

Langmuir isotherm			Freundlich isotherm				Temkin isotherm			Dubinin-Radushkevich isotherm			
$k_l$	$q_{max}$	$R^2$	$R_L$	$n$	$k_f$	$R^2$	A	B	$R^2$	$X_m$	$\beta$	E	$R^2$
1.579	0.379	0.993	0.136	0.367	0.713	0.954	1.525	1.926	0.838	0.65	0.208	1.55	0.99

Table 4.1 shows that Langmuir, Freundlich, Temkin and D-R isotherm model fitted well for Iron ions on Pyrolyzed areca husk with a high coefficient of correlation ( $R^2$ ) values. Langmuir adsorption isotherm presented a better fit for the experimental data. The value of  $k_1$  indicated the affinity of Iron ions with pyrolyzed areca husk. The maximum adsorption potential of pyrolyzed areca husk for Iron removal was 0.379 mg/g by Langmuir isotherm which was in accordance with the obtained experimental data. The  $R_L$  value indicated that the adsorption of Iron by pyrolyzed areca husk as a favorable process for iron adsorption.

Even though the coefficient of co-relation ( $R^2$ ) was high for Freundlich isotherm, the value of  $n$  was lesser than 1 which states an unfavorable tendency for the adsorbate to adsorb. This is attributed to the decrease in adsorption sites due to saturation. The correlation coefficient for Temkin Isotherm model is 0.838 indicating average linearity. The mean free energy,  $E$  calculated from D-R isotherm study is 1.55 kJ/mol which is less than 8kJ/mol suggesting that adsorption follows physisorption (Kundu and Gupta 2006).

From the results of Figure 4.5(a-e), it is evident that Langmuir and D-R isotherm model is the best predictor of the process of adsorption of Iron on Pyrolyzed Areca husk and also suggest carbonized areca offers monolayer adsorption surface and follows physisorption mechanism

#### **4.4. ADSORPTION KINETICS**

Adsorption kinetics are essential tools for evaluating the effectiveness of adsorption. Lagergren's pseudo-first order and pseudo-second-order models have been employed to clarify adsorption Kinetics of Iron ions onto pyrolyzed areca husk. For Kinetic studies, different concentrations of Iron ranging from 1 to 5 mg/L and contact time of 0.5, 1, 2, 3, 4, 5 and 6 hours is used at an optimum bio-sorbent concentration of 10 mg/L (Figure 4.6).

The Lagergren model is a pseudo-first-order rate equation and is as follows:

$$\log(q_e - q_t) = \log q_e - \frac{k_1 t}{2.303} \quad \dots (4.8)$$

where,  $q_e$  and  $q_t$  are the amounts of adsorbed metal ion (mg/g) at equilibrium and at time  $t$  (hours), respectively.  $k_1$  is the Lagergren rate constant relating to adsorption energy (l/min). The values of  $k_1$  and  $q_e$  is presented in Table 4.2

The pseudo-second-order kinetic model of McKay and Ho is expressed as follows:

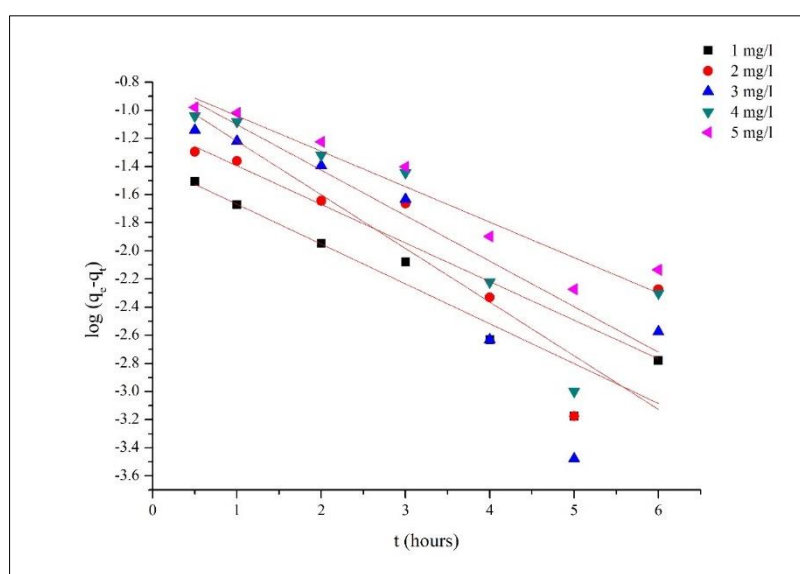
$$\frac{t}{q_t} = \frac{1}{k_s q_e^2} + \frac{1}{q_e} t \quad \dots (4.9)$$

where,  $q_e$  and  $q_t$  are the amounts of Iron adsorbed (mg/g) at equilibrium and at time  $t$  (hours), respectively.  $k_s$  (g/mg/hour) is the rate constant of pseudo-second-order kinetics.

The values of  $q_e$  and  $k_s$  that is presented in Table 4.2 are calculated from the slope and intercept of  $t/q_t$  versus  $t$ . From Table 4.2, it is evident that  $q_e$  values obtained from the pseudo-second-order kinetic model are in close agreement with experimental and best described the behaviour of Iron adsorption onto Pyrolyzed areca husk.

**Table 4.2 Lagergren's first-order and Pseudo-second-order kinetic parameters for the adsorption of Iron on Carbonised areca husk.**

Initial Concentration (mg/L)	$q_e$ (exp) (mg/g)	Pseudo-first-order kinetics			Pseudo-second-order kinetics		
		$k_1$ ( $\text{min}^{-1}$ )	$q_e$ (cal) (mg/g)	$R^2$	$q_e$ (cal) (mg/g)	$k_s$ ( $\text{g/mg}^{-1} \text{ hour}$ )	$R^2$
1	0.073	0.65	0.041	0.88	0.081	20.84	0.99
2	0.157	0.63	0.075	0.70	0.171	11.25	0.99
3	0.243	0.87	0.145	0.77	0.262	8.89	0.99
4	0.327	0.74	0.166	0.79	0.352	6.65	0.99
5	0.407	0.58	0.163	0.93	0.438	5.64	0.99





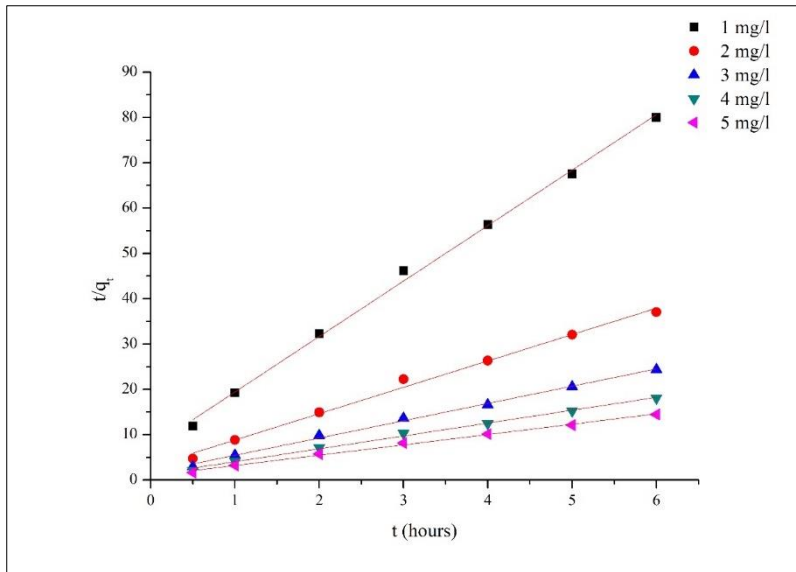


**Figure 4.6 Plots for Lagergren's pseudo-first order and pseudo-second-order models for Iron on carbonized arecanut husk**

The mechanism of the Iron adsorption onto pyrolyzed areca husk is studied by intra-particle diffusion also. According to the theory proposed by Weber and Morris:

$$q_t = k_{id}t^{1/2} + C_i \quad \dots (4.10)$$

where,  $k_{id}$  ( $\text{mg g}^{-1} \text{min}^{1/2}$ ), the rate parameter at stage  $i$ , is obtained from the slope of the straight line of  $q_t$  versus  $t^{1/2}$ . Weber and Morris plot ( $q_t$  versus  $t^{0.5}$ ) were used to inspect the intra-particle diffusion mechanism. The rate of adsorption is controlled by intra-particle diffusion for the entire adsorption period, if the value of  $C_i$  is zero (Table 4.3). However, the plot of  $q_t$  against  $t^{0.5}$  usually shows more than one linear portion. As seen from Figure 4.7, the plots were non-linear over the whole-time range, implying that the adsorption was affected by more than one process.

**Table 4.3 Intra-particle diffusion model parameters for the adsorption of Iron on Carbonised areca husk.**

Initial concentration (mg/L)	$k_{id}$ (mg g <sup>-1</sup> min <sup>1/2</sup> )	$C_i$	$R^2$
1	0.043	0.27	0.96
2	0.037	0.23	0.94
3	0.028	0.17	0.93
4	0.020	0.10	0.94
5	0.011	0.04	0.88

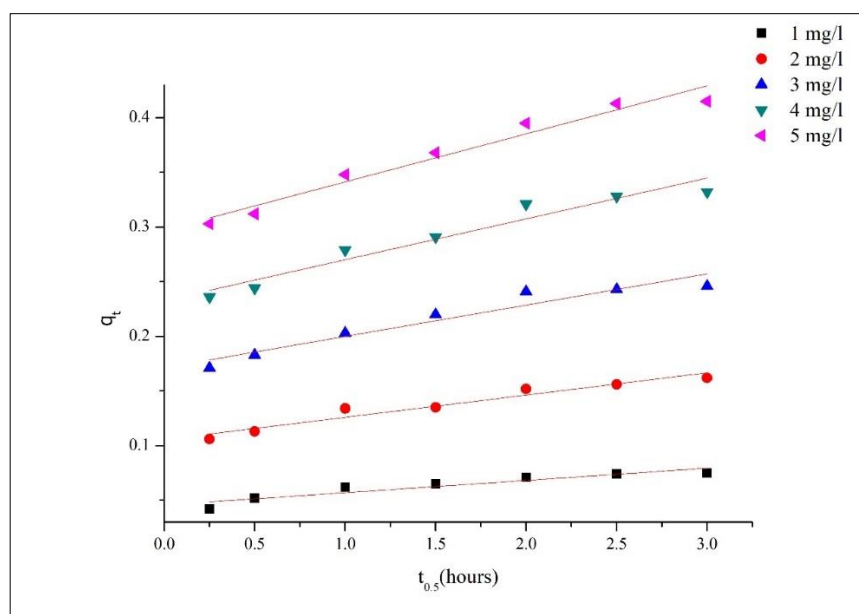


**Figure 4.7 Plot for intra-particle diffusion model for Iron on carbonized arecanut husk**

#### 4.5. DESORPTION STUDIES

It is essential to know the desorption behavior of Iron from carbonized areca husk to get an overall understanding of the adsorption mechanism. Carbonized areca husk can be used multiple times only if it can be regenerated using a suitable eluent. In the

present study 0.1M HCl, HNO<sub>3</sub>, H<sub>2</sub>SO<sub>4</sub> is explored for Iron desorption capability from Carbonised areca husk.

From the Figure 4.8, it is understood that 95% of the adsorbed ferrous ions is desorbed from carbonized areca husk with 0.1M HNO<sub>3</sub> giving optimum results. The acid environment lets the protonation on the surface of carbonized areca husk which allows the desorption of ferrous ions easily (Kołodynskaska et al. 2017). Acid containing waters precipitate a plethora of minerals on the carbonised areca husk. At lower pH, jarosite or amorphous ferric hydroxy sulphates may form. Formation of the well-crystalline ferric sulfate minerals may require prolonged time. The ferric compounds form a wide variety of complex metal precipitates (Majzlan and Myneni 2005). The contribution of ferrous salt precipitation with minerals can be explained with the quantitative analysis by XRD.

The adsorption-desorption cycle of ferrous ions on carbonized areca husk was repeated two times to check its reusability. There was no significant change in the adsorption potential of Carbonised areca husk during its operation, rendering it possible for repeated use.

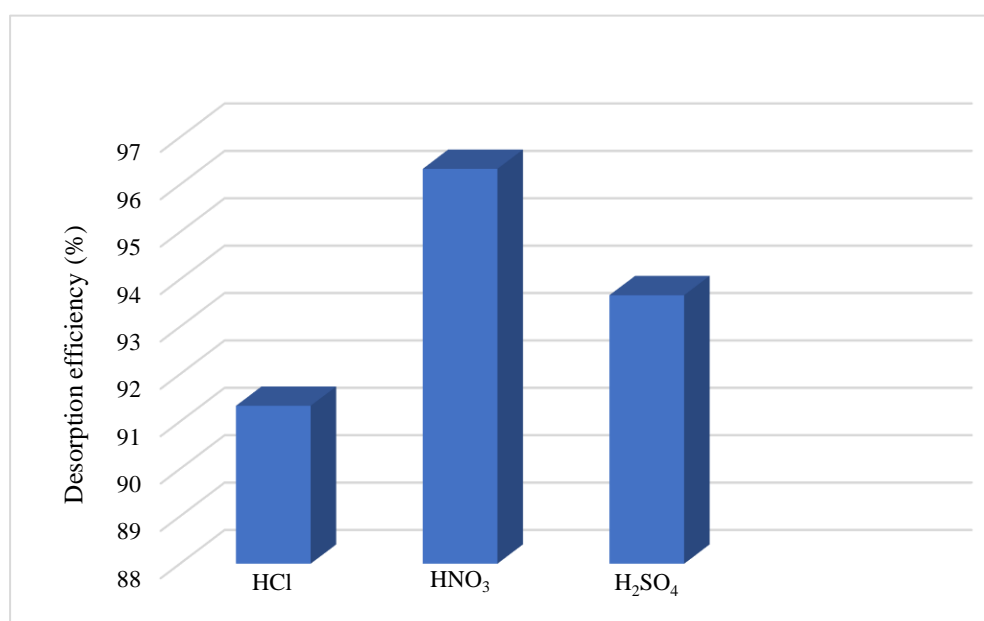


**Figure 4.8 Comparison of eluents at the concentration of 0.1 M on metal loaded pyrolyzed areca husk.**

## 4.6. ADSORPTION MECHANISM FOR THE ADSORPTION OF IRON ON CARBONISED ARECA HUSK

### 4.6.1. Thermodynamic studies

To investigate the adsorption feasibility of Iron on carbonized areca husk, thermodynamic studies are carried out at different temperatures ranging from 313K to 333K for the different initial Iron concentration of 2, 3 and 5 mg/L. From the plot of  $\ln K_c$  versus  $1/T$ , it is found that the adsorption capacity decreased with an increase in temperature. The calculated values of the thermodynamic parameters are given in Table 4.4.

The change in enthalpy ( $\Delta H^\circ$ ) values found for the adsorption of Iron were negative due to the exothermic nature of the adsorption process. The negative values of  $\Delta G^\circ$  indicate that the adsorption process is spontaneous. Also, the negative values of  $\Delta S^\circ$  point out the associative mechanism involved during the process of adsorption, and there is a decrease in the randomness at the stable/solution interface during the adsorption process.

The initial concentration of the adsorbate was varied to investigate its effect on the thermodynamic parameters. Similar phenomena were seen for all the various initial concentration as shown in Figure 4.9. The type of adsorption was investigated mainly using these parameters namely  $\Delta H^\circ$  - Enthalpy,  $\Delta S$  - Entropy,  $E$  - Mean free energy and the effect of temperature. A negative value of  $\Delta H^\circ$  indicates that the adsorption of Iron on areca husk is exothermic that is, energy is liberated during the process. This usually occurs when adsorbate molecules are adsorbed on the surface, freedom of movement of molecules become restricted, and this results in a decrease in entropy. At constant temperature and pressure, adsorption occurs spontaneously. Gorzin and Abadi (2018) states that if the enthalpy change value is lower than 20 kJ/mol, then the process is physisorption indicating weak electrostatic bonding of metal ions on the adsorbent surface. From the study, we can observe that  $\Delta H^\circ$  and also  $\Delta S^\circ$  values are lower, and hence it follows physisorption

**Table 4.4 Thermodynamic parameters for the adsorption of Iron on Carbonised areca husk**

T(K)	1/T (K)	C <sub>o</sub> (mg/L)	C <sub>e</sub> (mg/L)	C <sub>s</sub> = C <sub>o</sub> -C <sub>e</sub> (mg/L)	K <sub>c</sub> = C <sub>s</sub> /C <sub>e</sub>	ln K <sub>c</sub>	ΔG°	ΔH°	ΔS°
303	0.0033	5	0.79	4.21	5.329	1.673	-4.214		
313	0.0032	5	0.87	4.13	4.747	1.557	-4.053	-6.953	-0.0091
323	0.0031	5	0.91	4.09	4.494	1.502	-4.035		
303	0.0033	3	0.51	2.49	4.882	1.585	-3.994		
313	0.0032	3	0.56	2.44	4.357	1.471	-3.830	-7.275	-0.0108
323	0.0031	3	0.59	2.41	4.084	1.407	-3.779		
303	0.0033	2	0.39	1.61	4.128	1.417	-3.571		
313	0.0032	2	0.46	1.54	3.347	1.208	-3.144	-11.94	-0.0278
323	0.0031	2	0.49	1.51	3.081	1.125	-3.022		

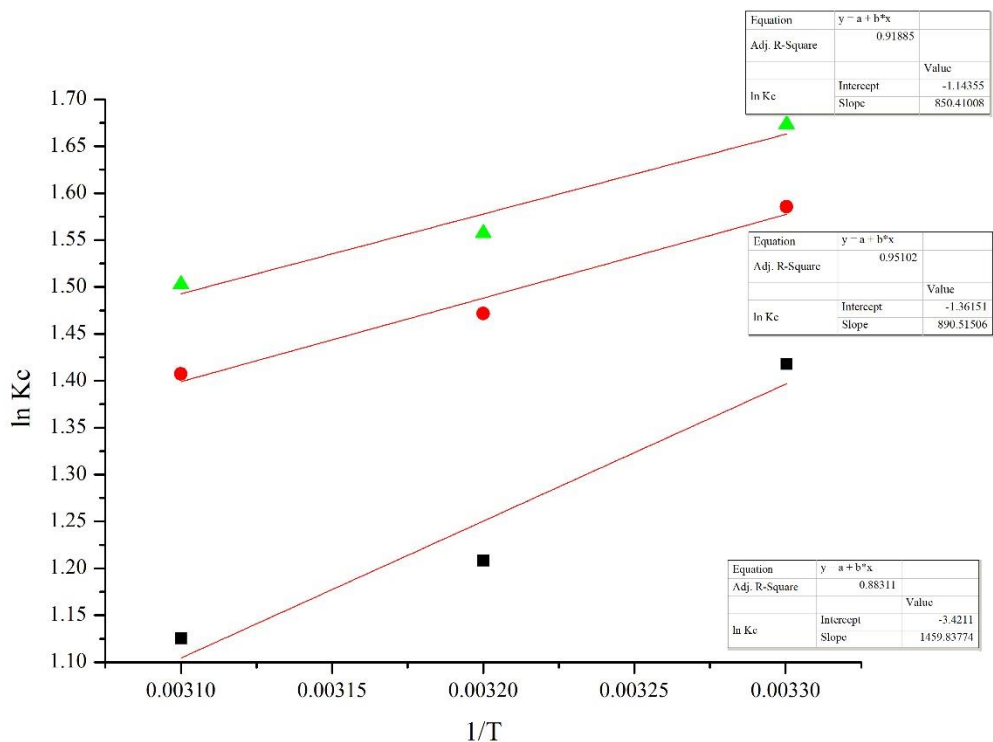
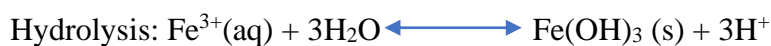
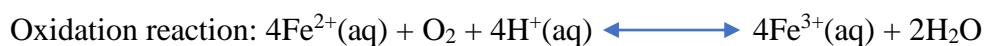


**Figure 4.9 Plot for ln Kc versus 1/T for the estimation of thermodynamic parameters for the adsorption of Iron on carbonized arecanut husk**

#### 4.6.2. Precipitation with minerals

Carbonized Areca husk was scanned by XRD (Figure 4.10) after Iron adsorption to check its role in the precipitation of minerals. In contrast to original pyrolyzed areca husk, the results after adsorption of Iron showed significant changes. This may be attributed to the precipitation of Iron as Goethite (FeO(OH)), Limonite FeO(OH)·nH<sub>2</sub>O, Jarosite (KFe<sup>3+</sup><sub>3</sub>(OH)<sub>6</sub>(SO<sub>4</sub>)<sub>2</sub>), ferric hydroxy sulfates or both and probably metal phosphates or silicates and these results are partly supported by FTIR. The combined oxidation and precipitation of is described by the following equations. The Fe<sup>2+</sup> can oxidize into Fe<sup>3+</sup>, which then hydrolyzes into “ferric hydroxides”



(Hove et al. 2007).

Similarly, Oxidation of Iron led to the formation of Two types of ferric hydroxy sulfate precipitates from acid ferrous sulfate solutions. Jarosites were also precipitated by oxidation in  $\text{FeSO}_4$  solutions containing suitable monovalent cations, such as  $\text{Na}^+$ ,  $\text{K}^+$  and an excess of sulfate anions at pH 2.5 (Lazaroff et al. 1982).

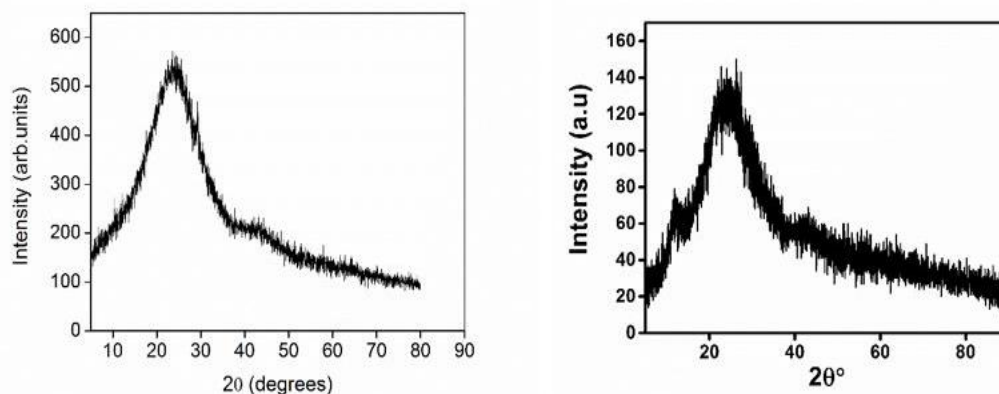


**Figure 4.10 XRD results of Pyrolyzed areca husk pre and post adsorption of  $\text{Fe}^{2+}$**

From SEM and EDS observations (Figure 4.11), complexation of  $\text{Fe}^{2+}$  ions have taken place on the surface with the Oxygen functional groups contributing to the adsorption capacity of pyrolyzed areca husk.

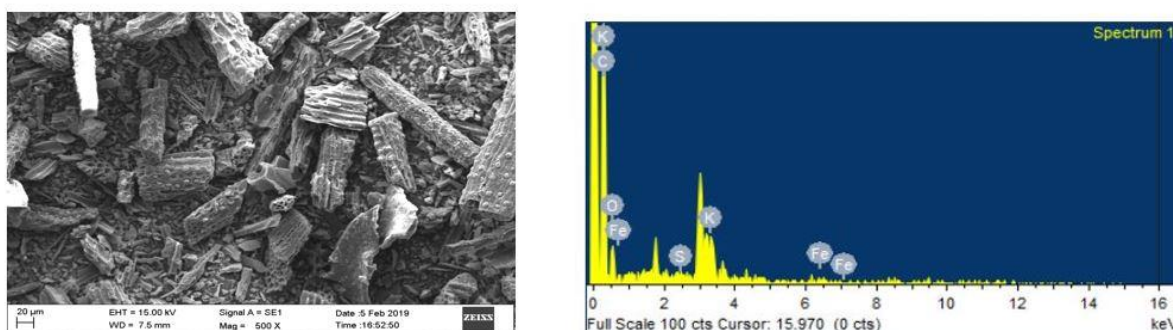


**Figure 4.11 SEM results of Pyrolyzed areca husk post adsorption of  $\text{Fe}^{2+}$**

#### 4.6.3. Complexation with functional groups

As shown in Figure 4.12, the functional group at  $3382\text{ cm}^{-1}$  representing the stretching vibration of the O-H group disappeared completely after interaction with the ferrous ions on the pyrolyzed areca husk. The bands at  $2920\text{ cm}^{-1}$  and  $2851\text{ cm}^{-1}$  corresponding to the Methyl C-H stretch also vanished indicating its participation in

the process of adsorption. The bands at  $1589\text{ cm}^{-1}$  assigned to Carboxylic acid salt weakened to C=O stretching vibrations of amides ( $1576\text{ cm}^{-1}$ ). Sulfate ions are deformed by ferrous complexation or hydrogen bonding and are distinguished from hydrogen sulfate by the stretching bands at  $880\text{ cm}^{-1}$ . Metal phosphates [ $\text{Fe}_3(\text{PO}_4)_2$  &  $\text{FePO}_4$ ] is precipitated at P-O stretching vibrations of  $\text{PO}_4^{3-}$  and was confirmed by the band at  $1110\text{ cm}^{-1}$ . The typical bending, symmetric and asymmetric stretching of Si-O-Si were observed at  $400$  to  $700\text{ cm}^{-1}$  which further confirmed the precipitation of Iron as  $\text{FeO}_4\text{Si}$  (Gao et al. 2019). On the whole, it suggested that the presence of many functional groups such as -OH, -CH<sub>3</sub> and -COOH are responsible for the adsorption of ferrous ions on pyrolyzed areca husk.

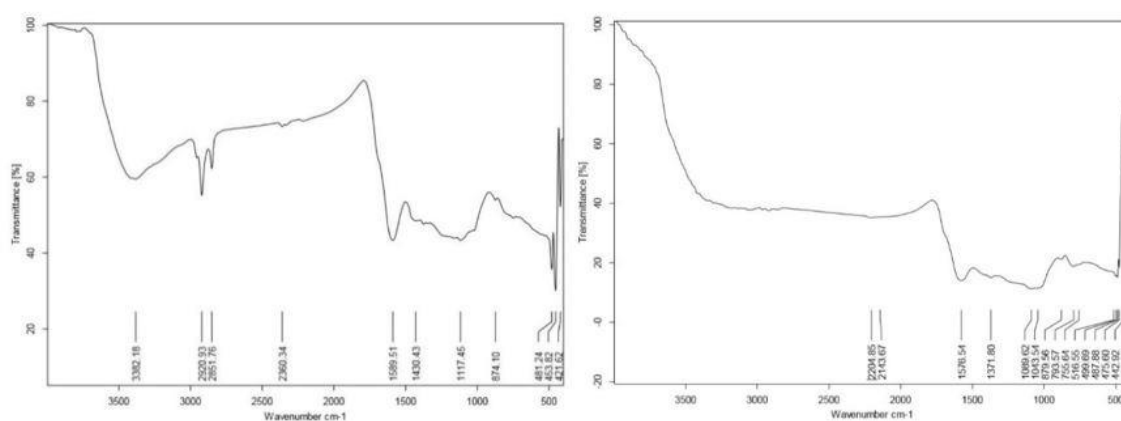


**Figure 4.12 FTIR results of Pyrolyzed areca husk before and after adsorption of  $\text{Fe}^{2+}$ .**

#### **4.7. PERFORMANCE APPRAISAL OF PYROLYZED ARECANUT HUSK FOR IRON REMOVAL IN CONTINUOUS MODE**

A continuous mode to treat contaminated water was envisaged as this processing involves less manpower, energy and time. In this mode, there will be continuous flow of treated water directly for customer consumption increasing productivity. So, for all practical approaches, continuous process is best for treating wastewater. The results from the batch studies were used to upscale into continuous mode. The bed height of pyrolyzed areca husk adsorbent, flowrate and initial concentration of Iron contaminated wastewater are considered as controllable factors and the values for each is decided from the analysis of batch process. The initial iron concentration investigated in batch process (2, 3 & 5mg/L) was used in this study so that it can be



analysed comparatively. Aside from that, flow rate of adsorbate (30, 60 & 120mL/hr) and bed height of adsorbent (3, 5 & 9cm) is determined based on time constraints and to ensure noteworthy results. Yu et al. (2015) conducted his experiments in this manner to remove phosphorus contamination from wastewater.

#### 4.7.1. Effect of initial concentration of adsorbate

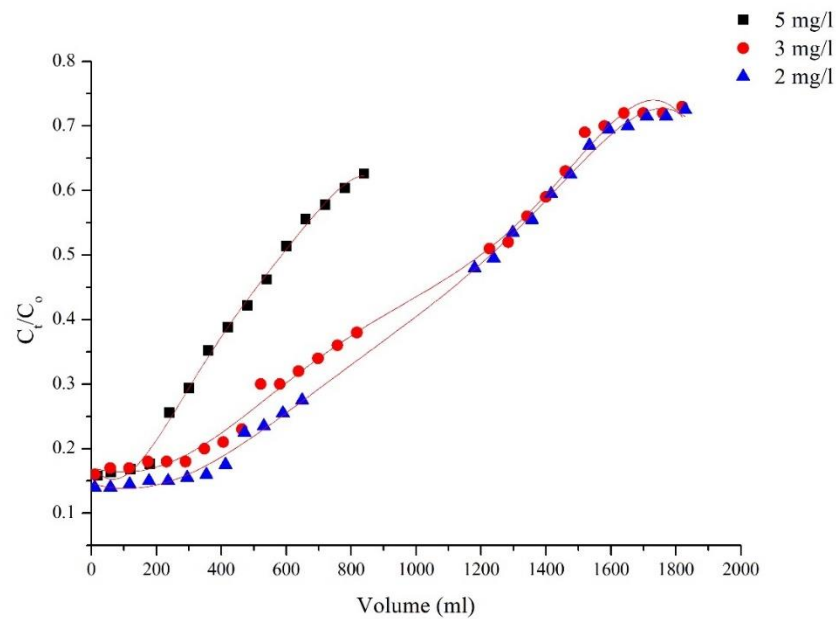


**Figure 4.13 Adsorption breakthrough curves of Fe<sup>2+</sup> ions at different concentrations (Bed ht - 3cm, Flowrate - 1mL/min)**

Figure 4.13. The breakthrough time was found to be 4, 6 and 8 hours for initial concentration of 5, 3 and 2mg/L respectively. As the concentration of Fe<sup>2+</sup> increased, the pyrolyzed areca bed got saturated resulting in the decrease of breakthrough and exhaustion time. The volume of treated effluent is 180, 290 and 413 mL for initial Fe<sup>2+</sup> concentration of 5, 3 and 2 mg/L respectively. At higher concentrations, the breakthrough time decreases and hence lower volume of the treated effluent at the breakthrough observed.

At higher concentration of  $\text{Fe}^{2+}$  ions, the rate of diffusion is higher because of higher difference in concentration between liquid and solid phases. However, the adsorption capacity decreases with decrease in initial concentration of ferrous ions. This decrease is attributed to the lower concentration gradient which improved the column performance. It is also observed that the breakthrough curves are more steeper and favourable at higher concentration of  $\text{Fe}^{2+}$  ions. (Padmesh et al. 2006)

#### 4.7.2. Effect of Flow Rate of adsorbate solution

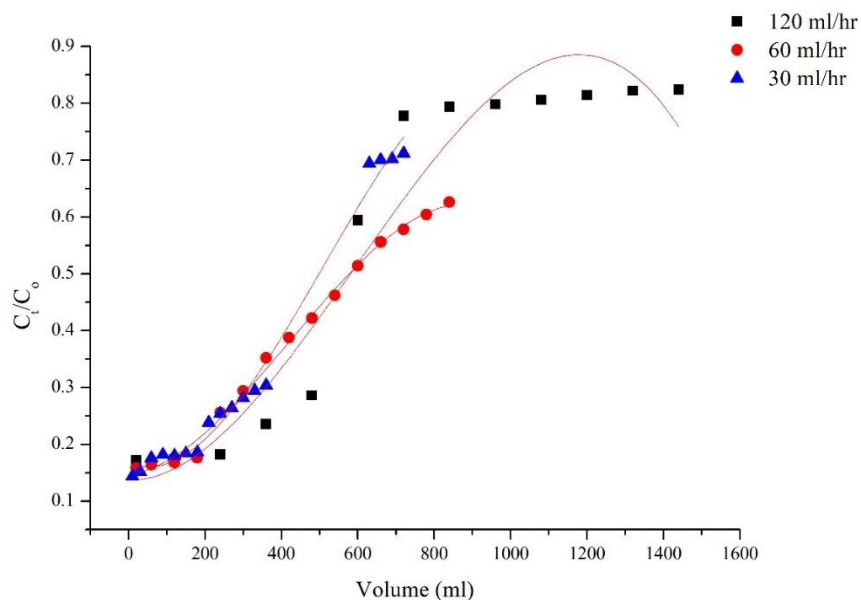


**Figure 4.14 Adsorption breakthrough curves of  $\text{Fe}^{2+}$  ions at different flowrate (Bed height – 3cm, Initial concentration – 5mg/L)**

The breakthrough curves for different flow rate of  $\text{Fe}^{2+}$  ions adsorption is projected in Figure 4.14. The breakthrough time for the removal of  $\text{Fe}^{2+}$  ions by pyrolyzed areca husk bed is found to be 2.5, 4 and 8.5 hours for flow rate of 120, 60 and 30 mL/hour respectively. The volume of treated effluent is 240, 180 and 180 mL for flow rate of 120, 60 and 30 mL/hour respectively. It can be observed that at lower flow rate, the efficacy of the column increased.

As the flow rate increases, pyrolyzed areca husk adsorbent gets saturated early because of reduced residence time, a larger amount of  $\text{Fe}^{2+}$  ions getting adsorbed on adsorbent and a weak distribution of the liquid into the column, which leads to lower diffusivity of the contaminant amidst the pyrolyzed areca bed. (Taty-Costodes et al. 2005)

#### 4.7.3. Effect of bed height of adsorbent on Iron adsorption

Figure 4.15 describes the breakthrough curves obtained at different bed heights. It can be perceived that the increase of adsorbent bed height increased both the breakthrough and exhaustion time, resulting in wider mass transfer zone. This can be ascribed to the metal ions having more contact time & numerous active adsorption sites to diffuse on, along with reduction in axial dispersion of ferrous ions. In order to obtain various bed heights, 10.8, 17.6 and 31.7g of pyrolyzed arecahusk adsorbent were added to produce 3, 5 and 9 cm respectively. It can be noted from Figure 4.15 that the time taken to reach breakthrough by the ferrous ions are 4, 6 and 10 hours and corresponding volume of effluent treated are 240, 360 and 600 mL for bed height 3, 5 and 9 cms respectively. Similar behaviour has been explained by Khalil et al. (2013).

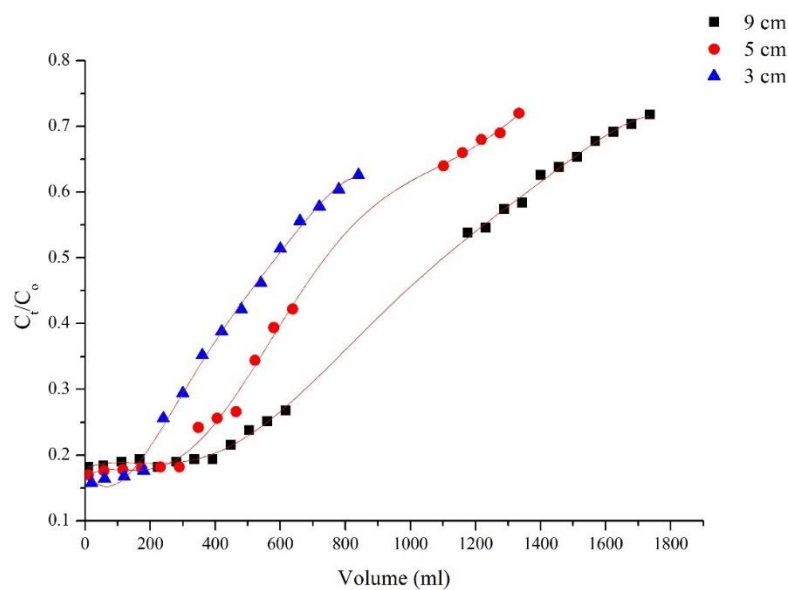


**Figure 4.15 Adsorption breakthrough curves of  $\text{Fe}^{2+}$  ions at different Bed height (initial concentration – 5mg/L, Flow rate –1mL/min)**

## 4.8. DYNAMIC ADSORPTION COLUMN MODELLING

Dynamic Adsorption Column modelling defines and forecasts the interactions across time connecting multiple components of a process that is regarded as a system. The basic mechanism involves on how the process components & the system progress over time (Matzopoulos 2011). Yoon Nelson Model, Thomas Model and Bohart Adam's Model has been envisaged to predict and understand in-depth the effect of bed height of adsorbent, flowrate and initial concentration of adsorbate on the removal efficiency of Iron from water. The experimental data was processed by employing Microsoft Excel 2010 program, and the linear regression method was used to determine the various models' parameters.

### 4.8.1. Yoon Nelson Model.

Based on an easy theoretical supposition, Yoon-Nelson model does not rely on the adsorbate characteristics nor adsorbent material & its bed features. According to this model the decrease in adsorption rate is directly proportional to breakthrough on the adsorbent and adsorbate adsorption. Yoon-Nelson equation for a single component system is expressed as

$$\frac{C_t}{C_0 - C_t} = \exp[k_{yN}t - \tau k_{yN}] \quad \dots (4.11)$$

where  $k_{yN}$  (1/min) is the rate constant and  $\tau$  is the time required for 50% adsorbate breakthrough.

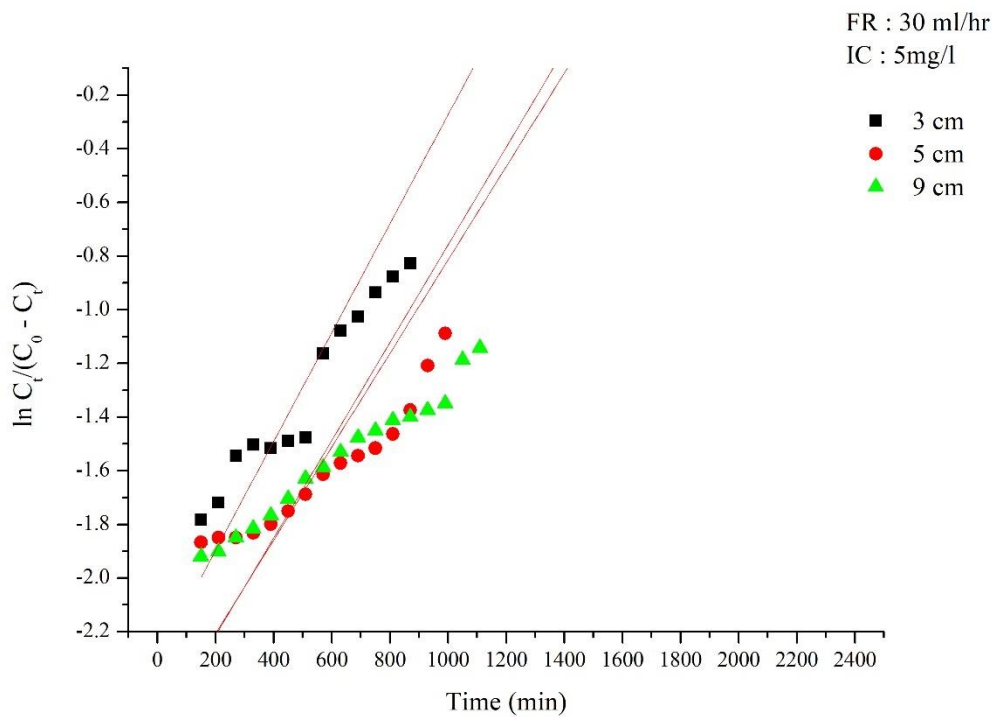
The linearized equation of Yoon-Nelson model is indicated as

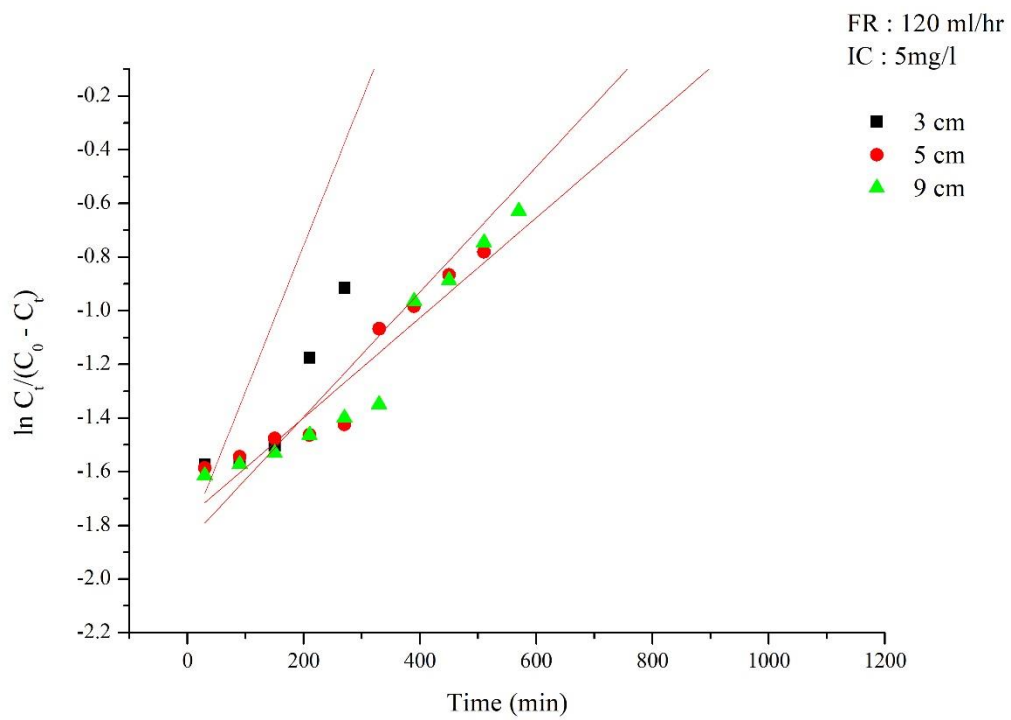
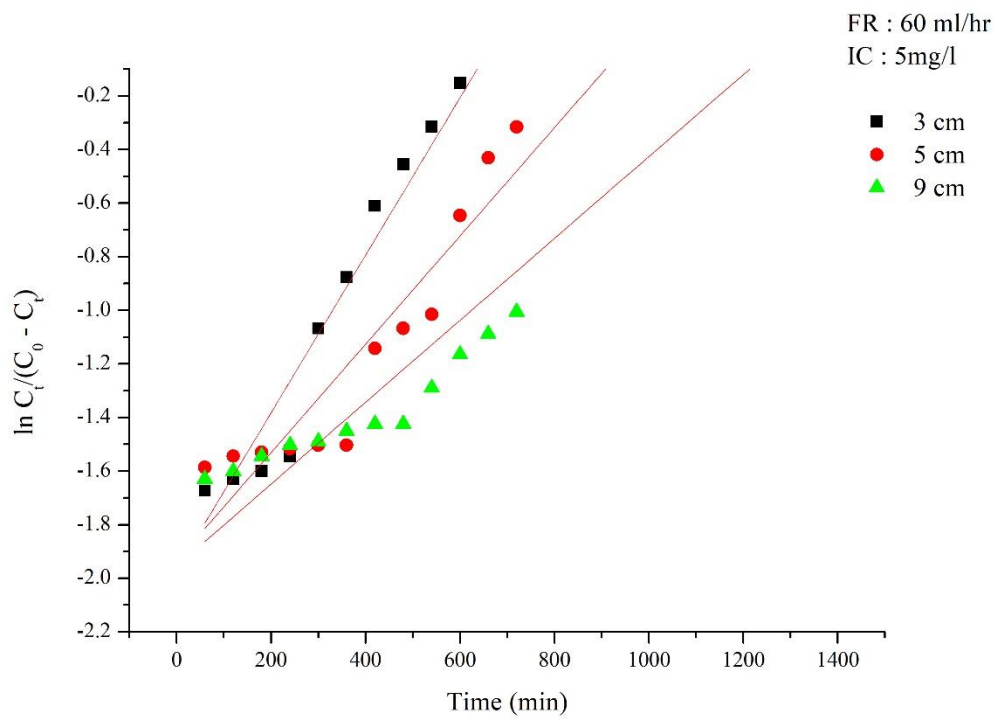
$$\ln \frac{C_t}{C_0 - C_t} = [k_{yN}t - \tau k_{yN}] \quad \dots (4.12)$$

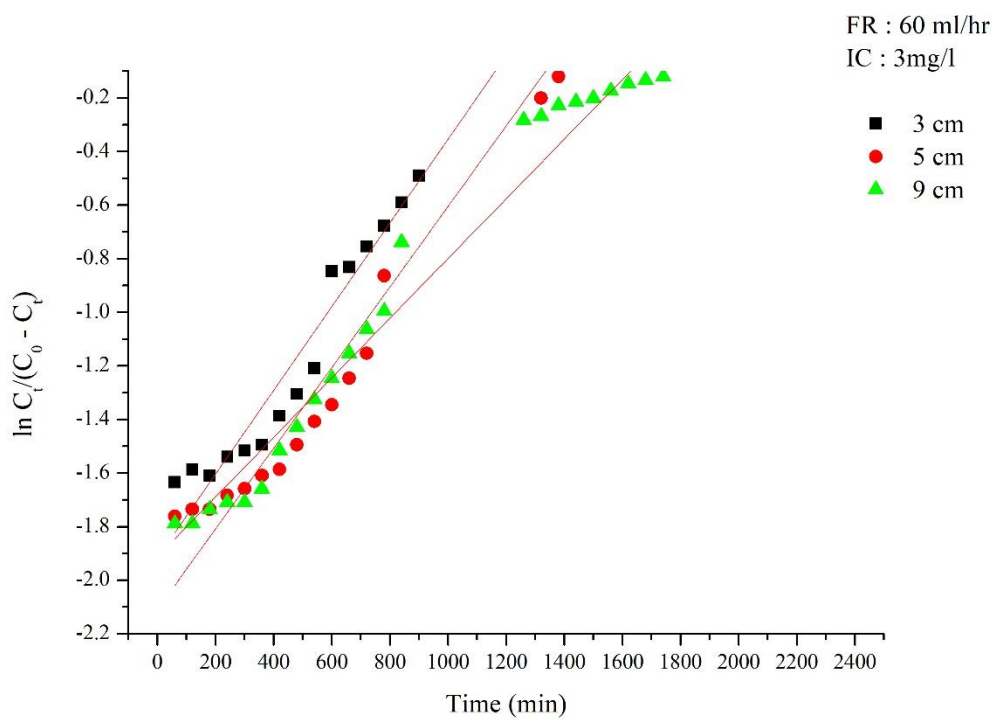
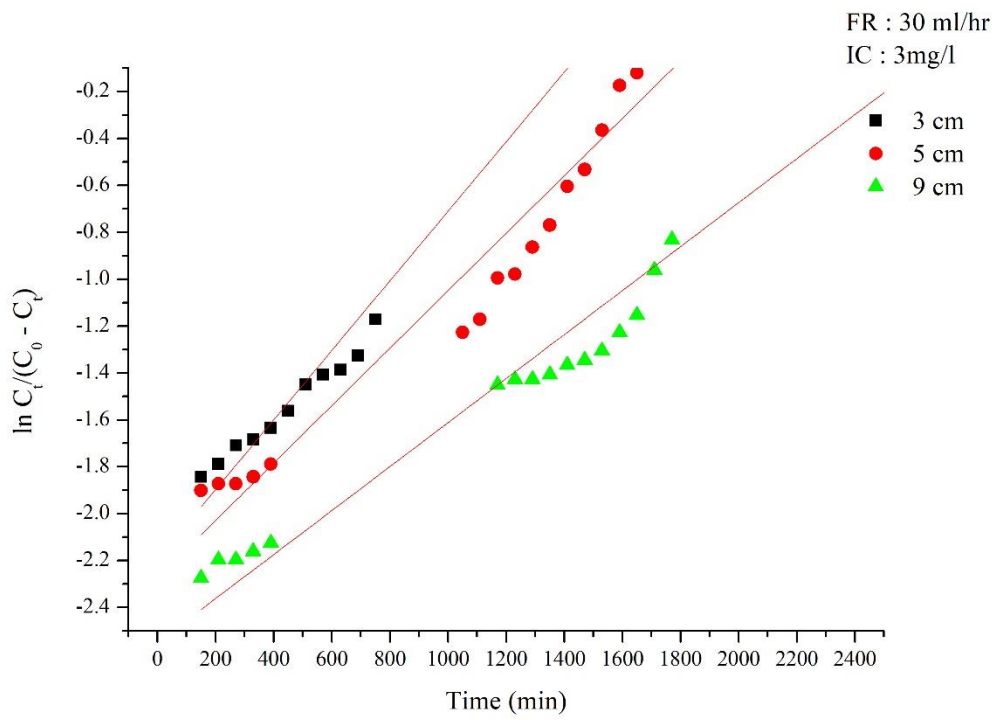
Graphs were plotted with the experimental data by varying operating conditions of initial concentration (2, 3 & 5 mg/L), flow rate (30, 60 & 120 mL/hr) and bed height (3, 5 & 9 cm) (see Figure 4.16 (a-i)) which resulted in 9 combination of graphs and

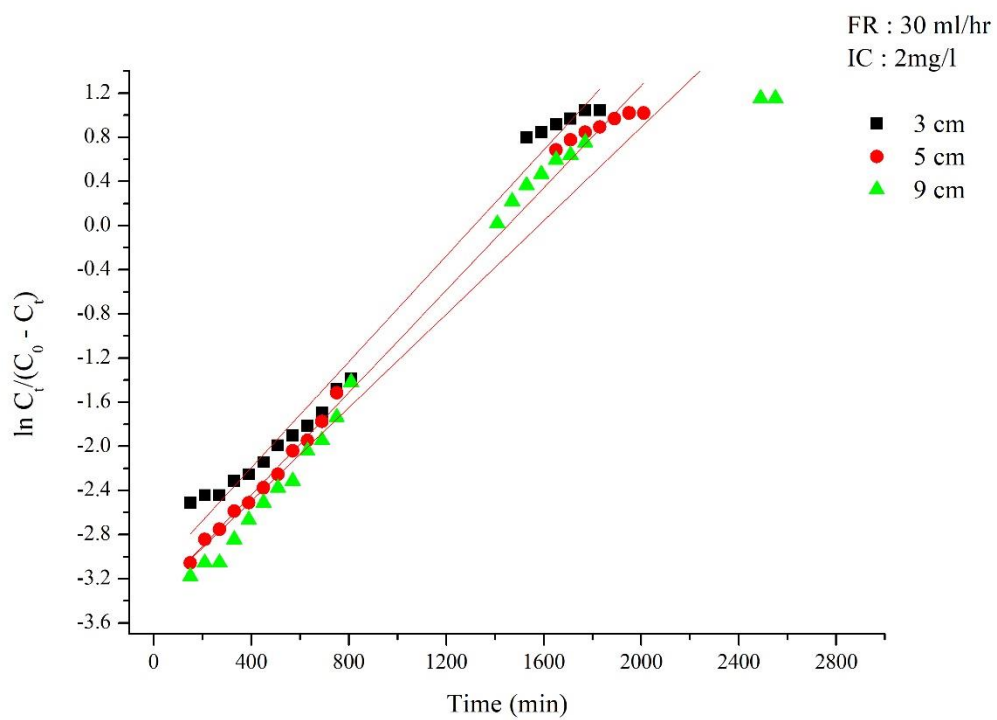
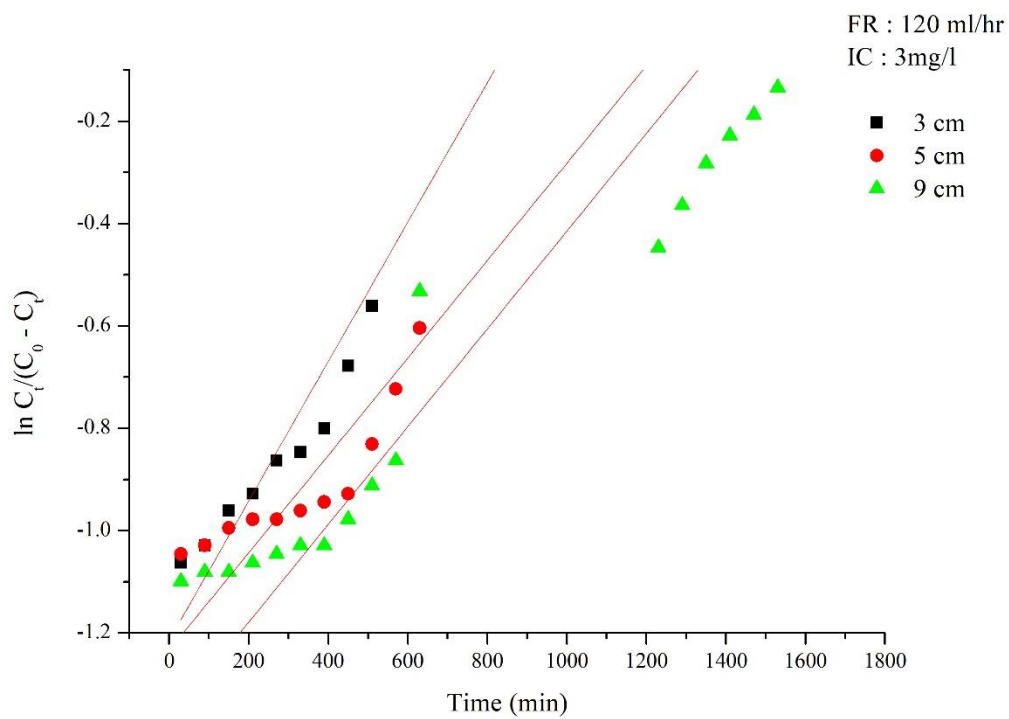
27 linear regression values (Table 4.5 ) along with Yoon- Nelson Rate constant and the time required to achieve 50% Iron contaminant wastewater breakthrough.

It can be observed from Table 4.5 that the Yoon-Nelson Model showed high  $R^2$  value for almost all combination indicating the experimental data fit well with the model. The union of minimum initial concentration of 2mg/L ferrous ions along with maximum flowrate of 120mL/hr & bed height of 9cm gave the best  $R^2$  value of 0.9962.











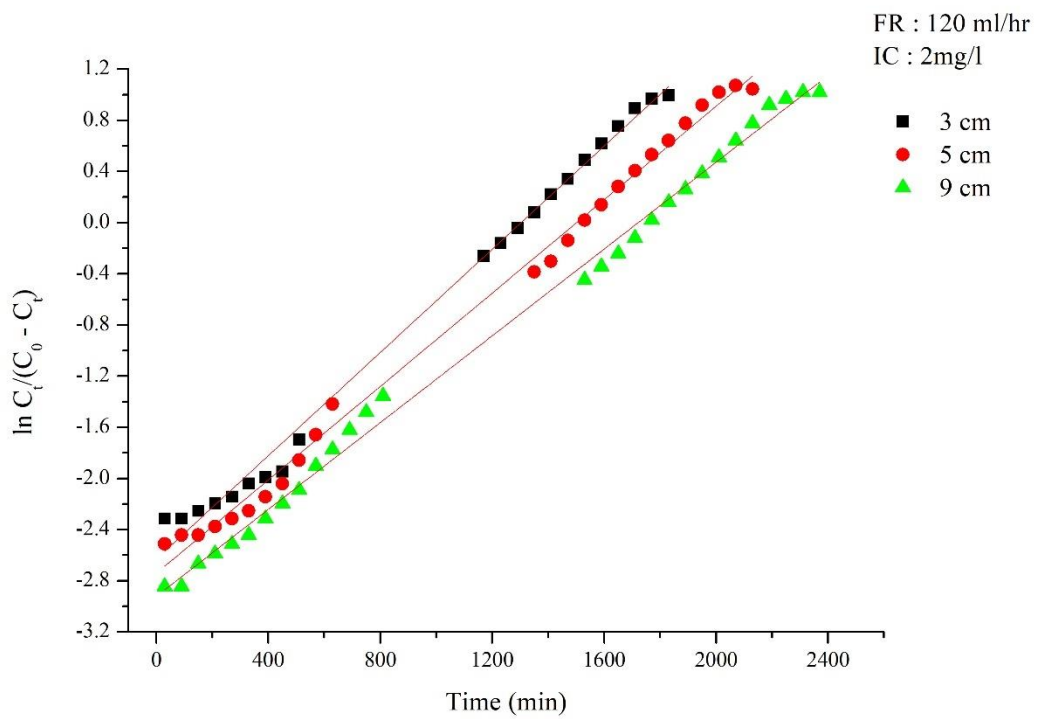
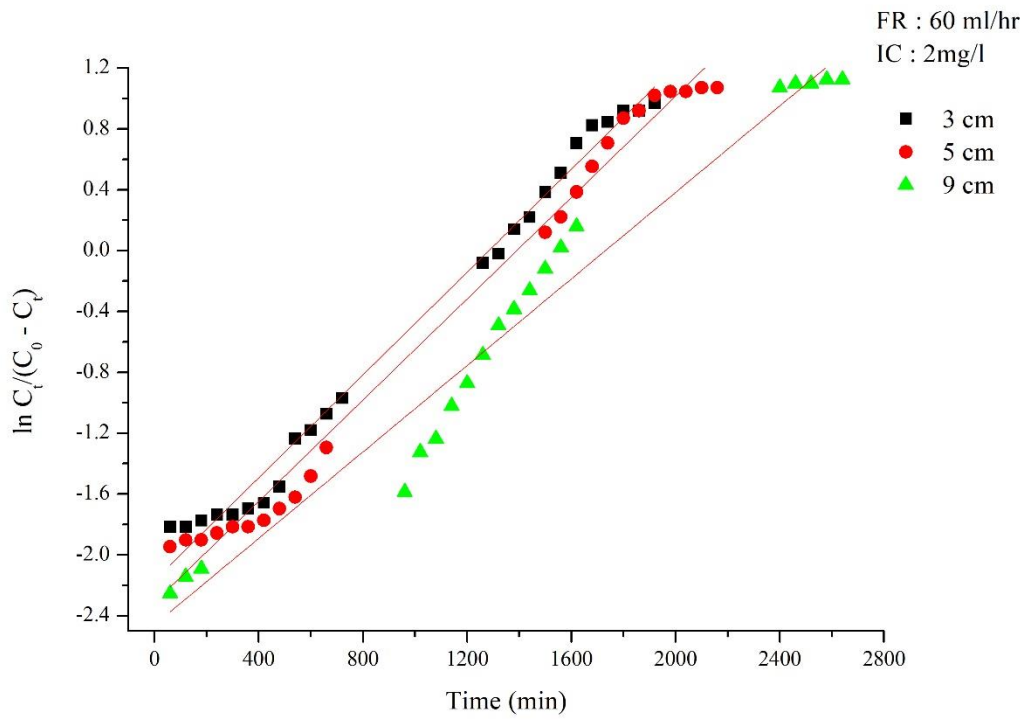


**Figure 4.16(a-i) Linear plot of Yoon-Nelson model with experimental data at different bed heights, flow rate and initial concentration**

**Table 4.5 Yoon-Nelson model parameters using linear regression analysis for Fe<sup>2+</sup> adsorption under various operating conditions**

<b>Concentration (mg/L)</b>	<b>Flow rate (mL/hr)</b>	<b>Bed Height (cm)</b>	<b>t<sub>b</sub> (EXP) (min)</b>	<b>R<sup>2</sup></b>	<b>k<sub>YN</sub></b>	<b>τ (min)</b>
5	120	3	300	0.8527	0.0054	341.3519
5	120	5	810	0.992	0.0023	809.1739
5	120	9	870	0.9945	0.0019	932
5	60	3	660	0.9777	0.0029	679.3448
5	60	5	900	0.9787	0.002	967.55
5	60	9	1260	0.9878	0.0015	1302.733
5	30	3	1170	0.9705	0.002	1151
5	30	5	1410	0.9585	0.0018	1432.111
5	30	9	1470	0.9418	0.0017	1502.941
3	120	3	910	0.9946	0.0014	867.5714
3	120	5	1230	0.973	0.001	1234
3	120	9	1350	0.9541	0.001	1370.2
3	60	3	1260	0.9875	0.0016	1197.5
3	60	5	1440	0.986	0.0015	1405.733
3	60	9	1800	0.9844	0.0011	1737.909
3	30	3	1410	0.9873	0.0015	1462.333
3	30	5	1890	0.9633	0.0012	1894.75
3	30	9	2790	0.9846	0.0009	2833
2	120	3	1290	0.9943	0.002	1314.95

2	120	5	1530	0.9954	0.0018	1523.056
2	120	9	1770	0.9962	0.0017	1718.294
2	60	3	1320	0.9901	0.0017	1276.118
2	60	5	1440	0.9881	0.0017	1361
2	60	9	1740	0.9961	0.0014	1757.357
2	30	3	1230	0.9882	0.0024	1314.042
2	30	5	1410	0.9953	0.0023	1464.826
2	30	9	1590	0.9433	0.0021	1592.238

For all combinations of flowrate and initial concentration of adsorbate considered, the values of rate constant ( $k_{YN}$ ) reduced or remained the same with increase in bed height of the adsorbent along with increase in time to reach  $\tau$  (50% adsorbate breakthrough time). It was noted that as the flowrate reduced from 120mL/hr to 30ml/hr for various combinations of bed height of adsorbent and initial concentration of ferrous ions the 50% adsorbate breakthrough time increased. This shows that there was sufficient residence time for ferrous ions to get adsorbed as the rate constant also decreased. The values showed varied trend when the initial ferrous concentration was 2mg/L with effect to 60mL/hr flowrate. The  $\tau$  value increased with decrease in initial concentration of ferrous ions (5, 3 & 2mg/L) for all amalgamations barring the combination of 30mL/hr flowrate, 2mg/L initial concentration. The rate constant values also showed a similar behaviour. Significant increase in  $\tau$  value with increase in adsorbent bed height, reduced flowrate as well as initial concentration of ferrous ions can be attributed to the swift saturation of the column. Sánchez-Machado et al. 2016 reported a similar behaviour for aqueous iron removal on chitosan-sodium tripolyphosphate beads. Both the experimental 50% adsorbate breakthrough time ( $t_{b0.5}$ ) and calculated breakthrough time ( $\tau$ ) were almost similar.

#### 4.8.2. Thomas Model.

Assuming plug flow behavior of adsorbent bed, Thomas model is based on equilibrium Langmuir Isotherm and second order kinetics. Often the process of Adsorption is controlled by interphase mass transfer and not restricted by chemical reaction kinetics. Hence this model is best suited for adsorption process where external and internal diffusion restraints are absent. Thomas model equation is expressed as

$$\frac{C}{C_0} = \frac{1}{1 + \exp[k_{Th}(q_0x - C_0V_{eff}) / Q]} \quad \dots (4.13)$$

where  $k_{Th}$  (L/min mg) is the Thomas rate constant and  $q_0$  is the maximum solid-phase concentration of the solute (mg/g),  $x$  is the mass of sorbent in the column (g),  $V_{eff}$  (mL) is the throughput volume, and  $Q$  (mL/hr) is the volumetric flow rate.

The linearized equation of Thomas model is indicated as

$$\ln \left[ \frac{C_0}{C} - 1 \right] = \frac{k_{Th}q_0x}{Q} - k_{Th}C_0t \quad \dots (4.14)$$

Graphs were plotted with the experimental data by varying operating conditions of initial concentration (2, 3 & 5 mg/L), flow rate (30, 60 & 120 mL/hr) and bed height (3, 5 & 9 cm) (see Figure 4.17 (a-i)) which resulted in 9 combination of graphs and 27 linear regression values along with Thomas rate constant and maximum solid-phase concentration of the solute (mg/g).

**Table 4.6 Thomas model parameters using linear regression analysis for Fe<sup>2+</sup> adsorption under various operating conditions**

Concentration [mg/L]	Flow rate [mL/hr]	Bed Height [cm]	Thomas [R <sup>2</sup> ]	k <sub>Th</sub> [L/min mg]	q <sub>exp</sub> [mg/g]	q <sub>o</sub> [mg/g]
5	120	3	0.853	0.0011	0.694	0.316
5	120	5	0.992	0.0005	0.869	0.460
5	120	9	0.995	0.0004	0.596	0.294
5	60	3	0.978	0.0006	0.417	0.315
5	60	5	0.979	0.0004	0.409	0.275
5	60	9	0.988	0.0003	0.303	0.205
5	30	3	0.971	0.0004	0.368	0.266
5	30	5	0.959	0.0004	0.286	0.203
5	30	9	0.942	0.0003	0.177	0.119
3	120	3	0.995	0.0005	0.917	0.482
3	120	5	0.973	0.0003	0.685	0.421
3	120	9	0.954	0.0003	0.517	0.259
3	60	3	0.988	0.0005	0.533	0.333
3	60	5	0.986	0.0005	0.327	0.240
3	60	9	0.984	0.0004	0.261	0.164
3	30	3	0.987	0.0005	0.229	0.203
3	30	5	0.963	0.0004	0.171	0.161
3	30	9	0.985	0.0003	0.141	0.134

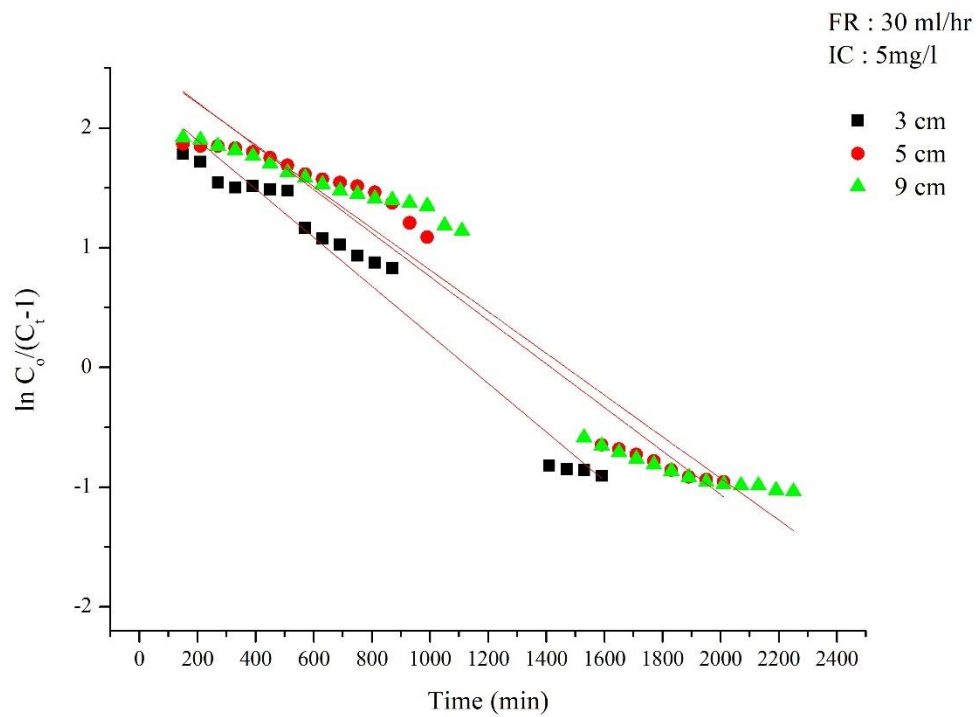
2	120	3	0.994	0.0010	0.678	0.487
2	120	5	0.995	0.0009	0.484	0.346
2	120	9	0.996	0.0009	0.299	0.217
2	60	3	0.990	0.0009	0.356	0.236
2	60	5	0.988	0.0009	0.245	0.155
2	60	9	0.996	0.0007	0.167	0.111
2	30	3	0.988	0.0012	0.169	0.122
2	30	5	0.995	0.0012	0.114	0.083
2	30	9	0.943	0.0011	0.080	0.050

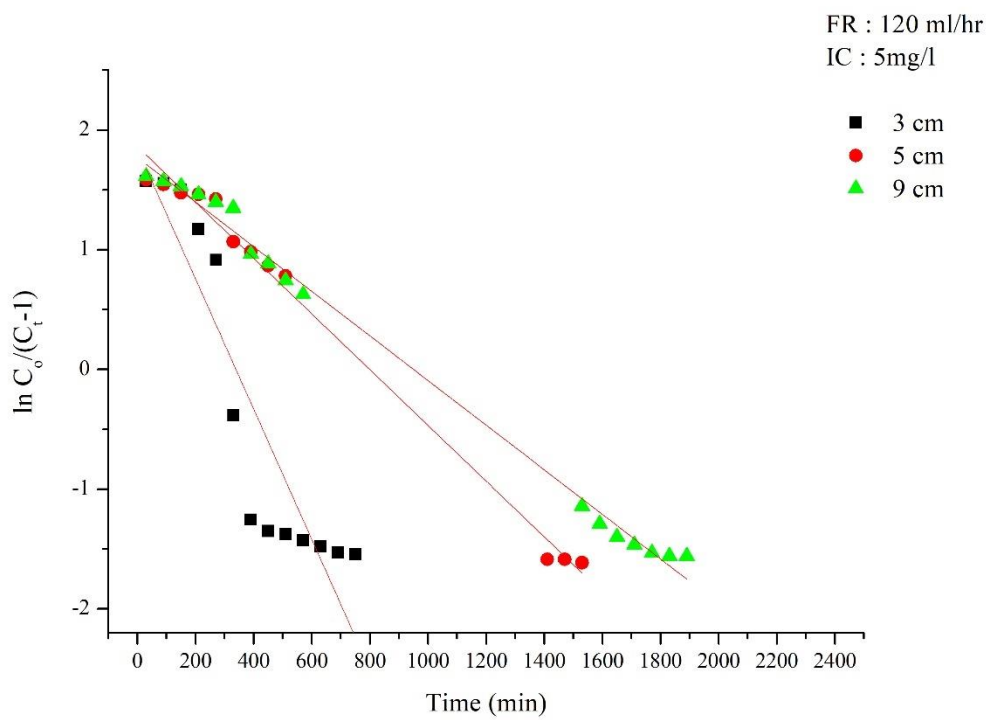
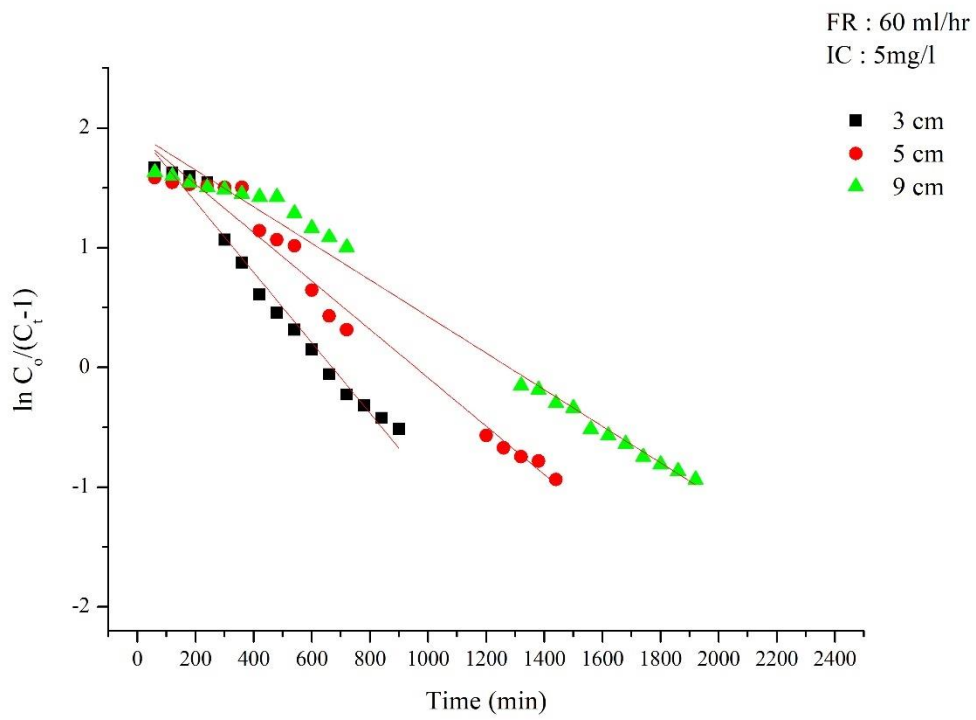
The  $R^2$  values from the linear regression using Thomas model are listed in Table 4.6 and it ranged from 0.853 to 0.996. The values are interpreted, with the experimental  $q_e$  almost similar to that calculated from Thomas model. This indicates that Thomas model is an appropriate predictor of the breakthrough curve.

It is observed from the Table 4.6 that the increase in initial concentration of ferrous ions and adsorbent bed height resulted in decrease of rate constant  $k_{Th}$ . But  $k_{Th}$  increased for increase in flowrate of effluent. This can be described as a mass transfer rate restriction; at a low ferrous ion concentration, there is less interaction between the adsorbent bed and ferrous ions; hence, the adsorption process requires more time to saturate the active sites and the breakthrough times tend to increase. The adsorption capacity of the adsorbent  $q_0$  increased with increase in both the initial concentration of ferrous ions and its flowrate which can be attributed to the large availability of reaction sites. Farrag et al. (2017) also reported a similar trend for removal of Iron from groundwater by ‘Abu Zenima’ synthetic zeolite in Egypt.

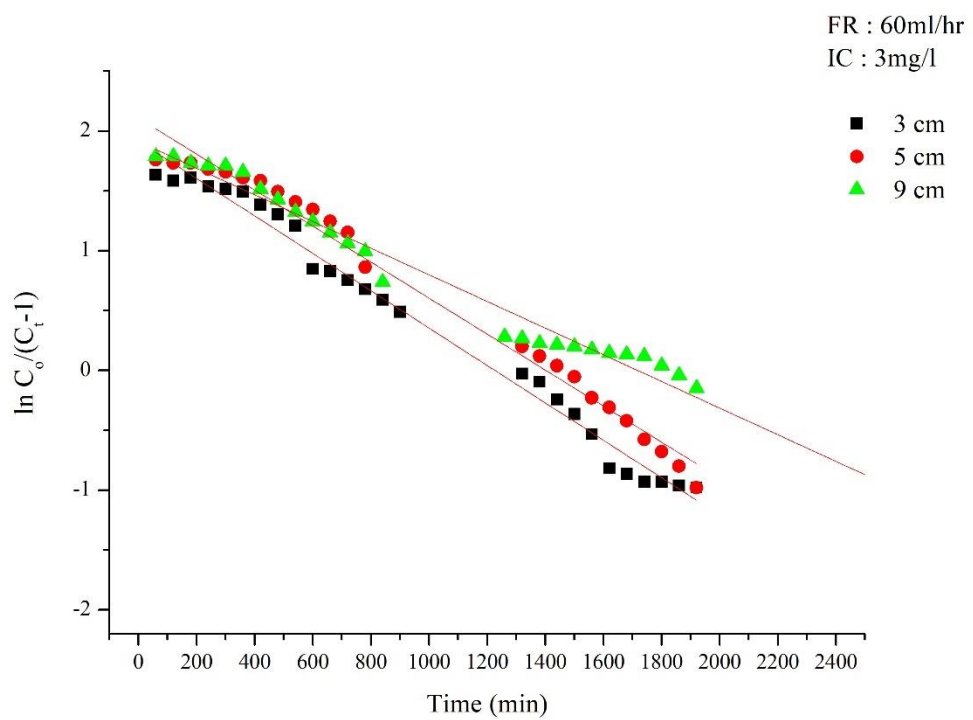
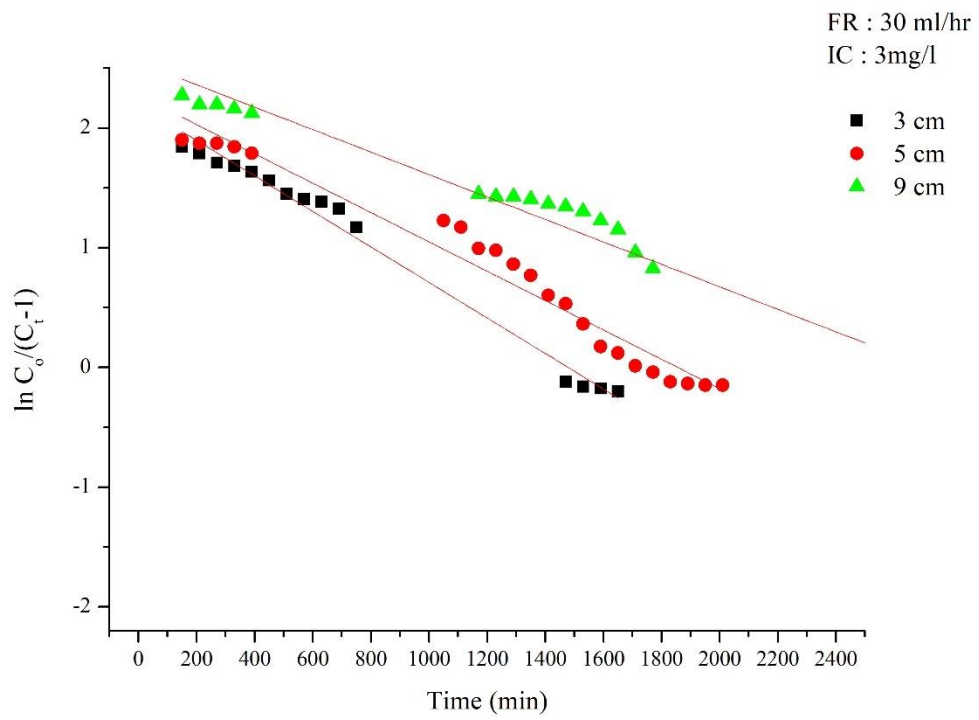
The increase in adsorbent weight that is increased bed height reduced the uptake capacity of the adsorbent. This may be because of other ions present in water competing to get adsorbed on the adsorbent surface, even though there are available binding sites. These competitions reduce the capacity of the adsorbent and it gets

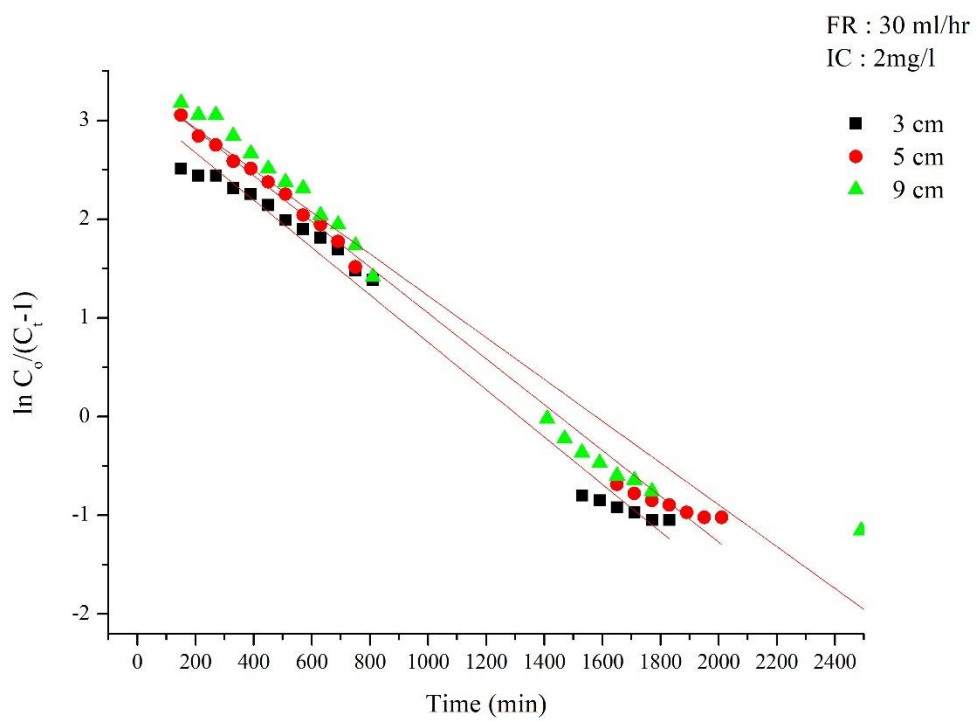
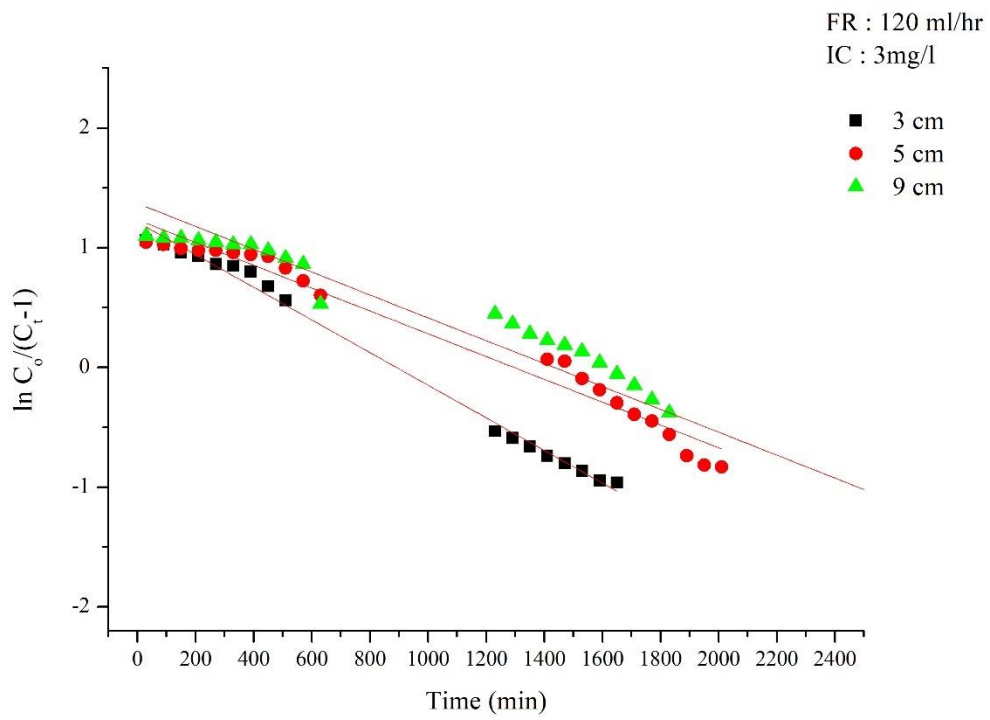
easily saturated. As the driving force for adsorption is the concentration gradient between the ferrous ions on the adsorbent and in the solution, the chances of reduced adsorption capacity may be because of low concentration of ferrous ions in the adsorbate as they cannot facilitate mass transfer. Higher flow rate can reduce contact time and also resist external film diffusion in turn reducing adsorbent capacity. (Kleinübing et al. 2011)











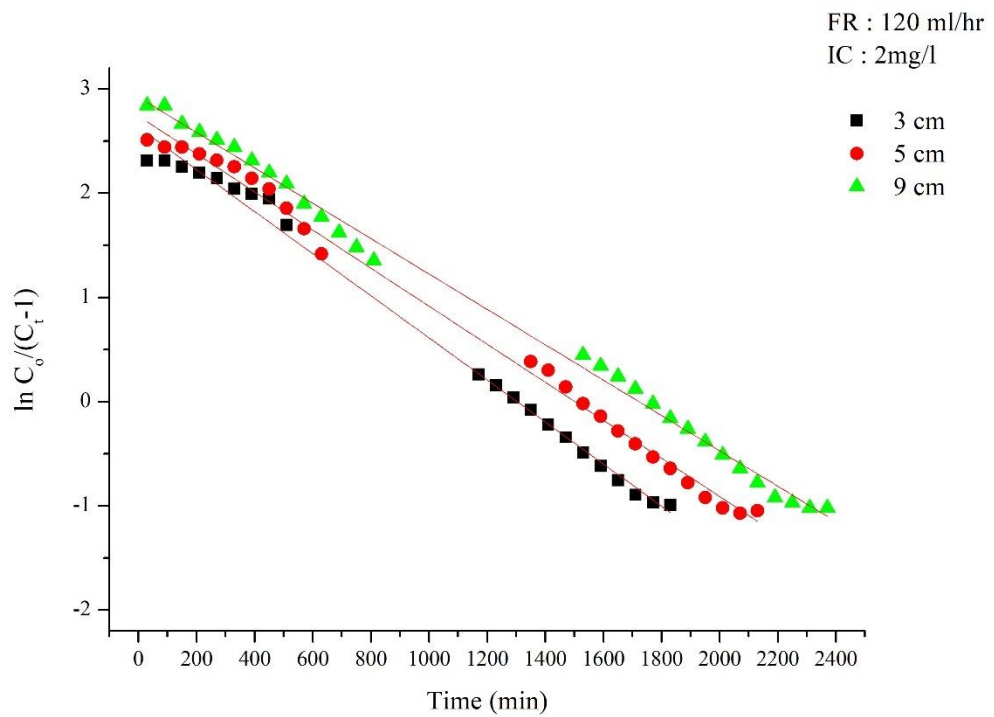
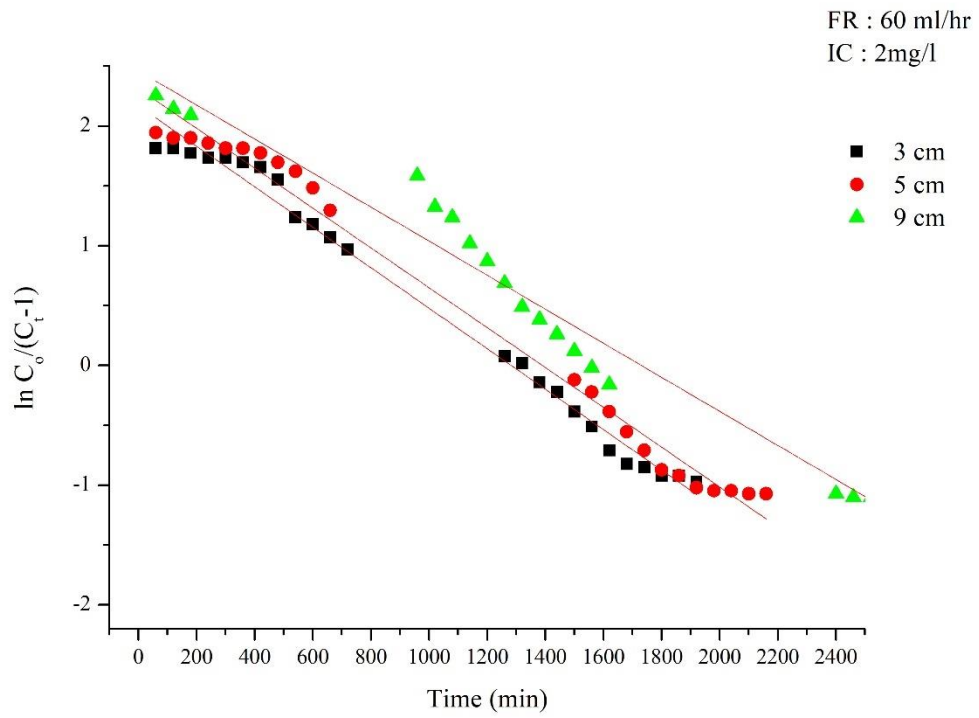


**Figure 4.17(a-i) Linear plot of Thomas model with experimental data at different bed heights, flow rate and initial concentration**

### 4.8.3. Bohart–Adam’s Model.

Bohart–Adam’s model is based on rectangular (irreversible) Isotherm and quasi-chemical rate expression. This model is similar to Thomas model, the difference being the assumption of the isotherm form. It can be observed that when the adsorption isotherm is highly favorable, the actual Thomas model reduces to the Bohart–Adam’s model.(Chu 2010). Both these models disregard the effect of axial dispersion and finite resistance to mass transfer. The Bohart–Adam’s model is regarded as a limiting form of the Thomas model, but many researchers have misunderstood and considered Thomas model as a separate and independent model. This model assumes that equilibrium is not spontaneous and is built on Surface Reaction Theory. Hence, the reaction rate is proportional to both the saturation capacity of the adsorbent and the concentration of the ferrous ions. As it predicts the initial part of the breakthrough curve, it helps in understanding the preliminary steps of the column process.

Bohart–Adam’s model equation is expressed as

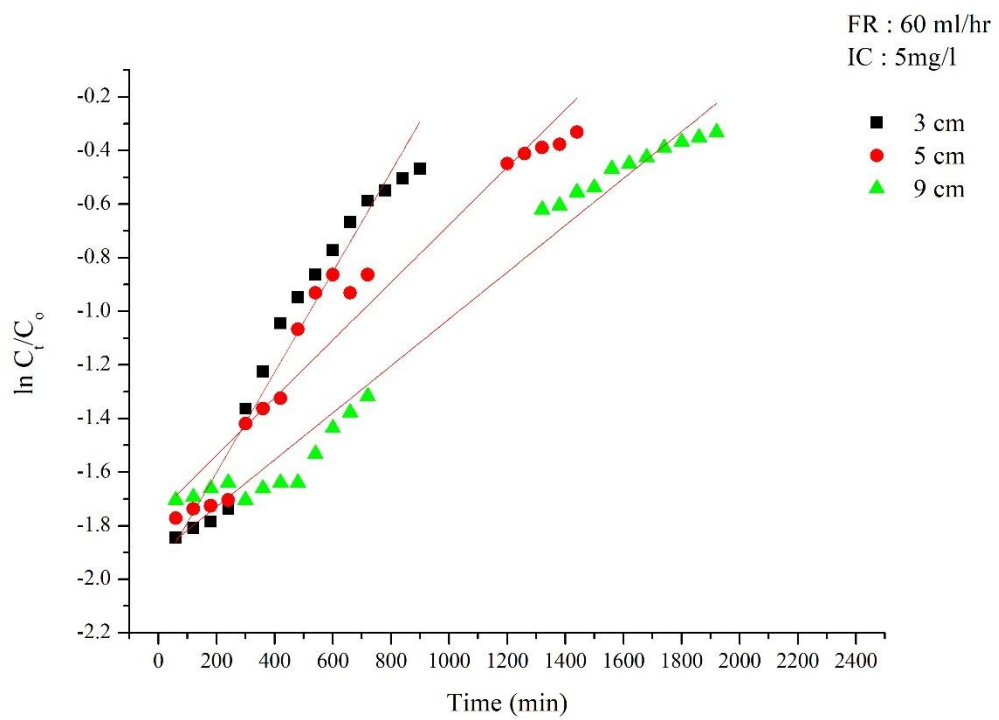
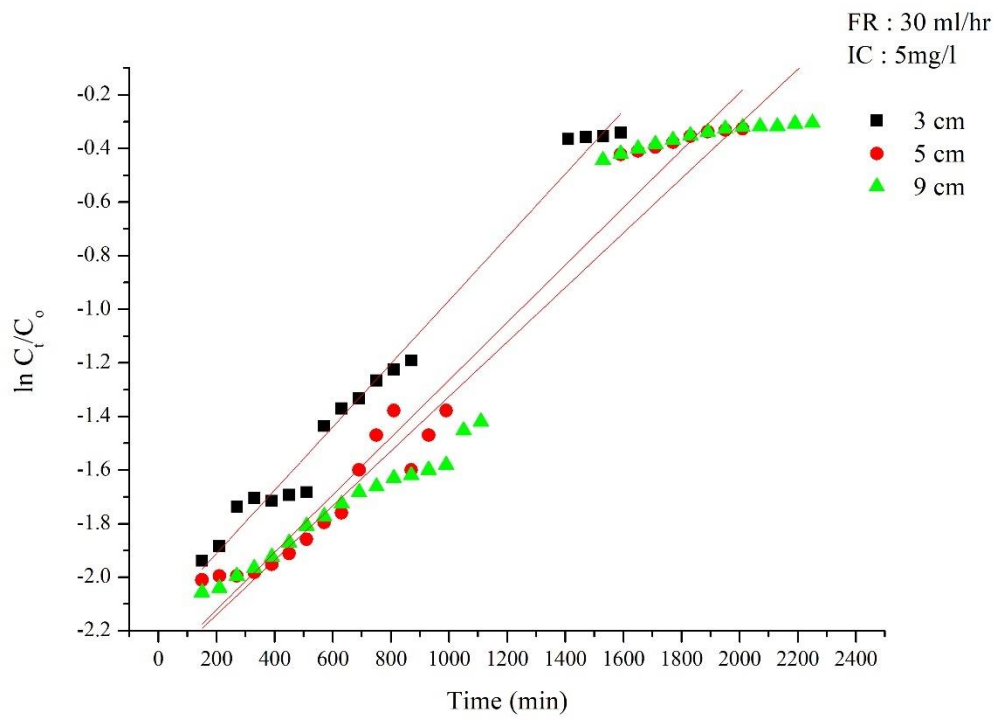
$$\frac{C_t}{C_0} = \exp\left(k_{AB}C_0t - k_{AB}N_0\frac{z}{U_0}\right) \quad \dots (4.15)$$

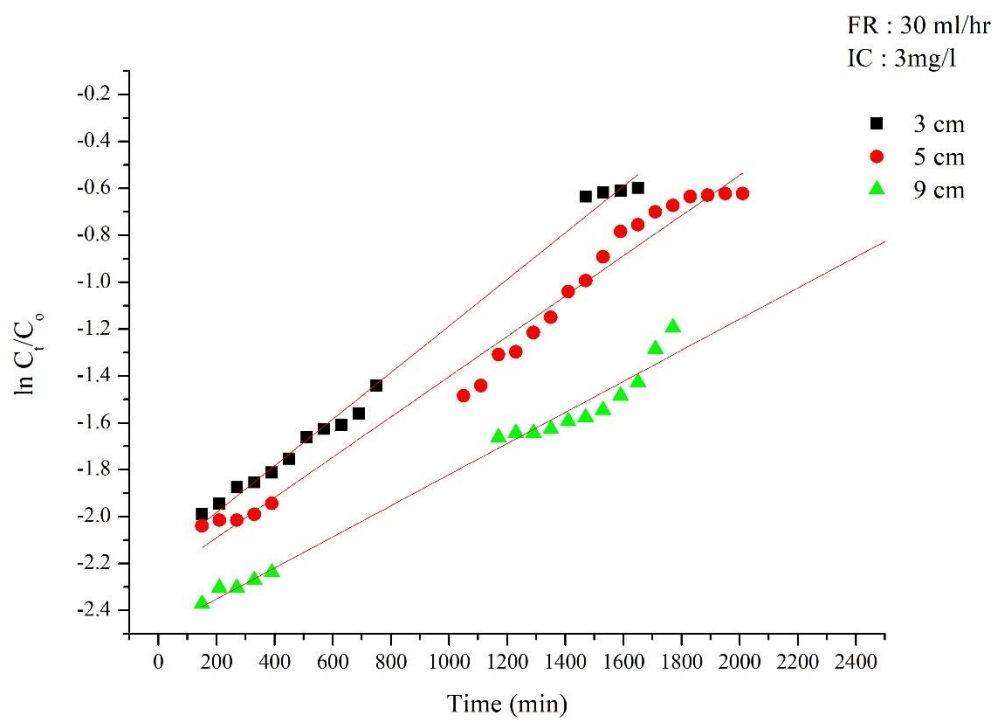
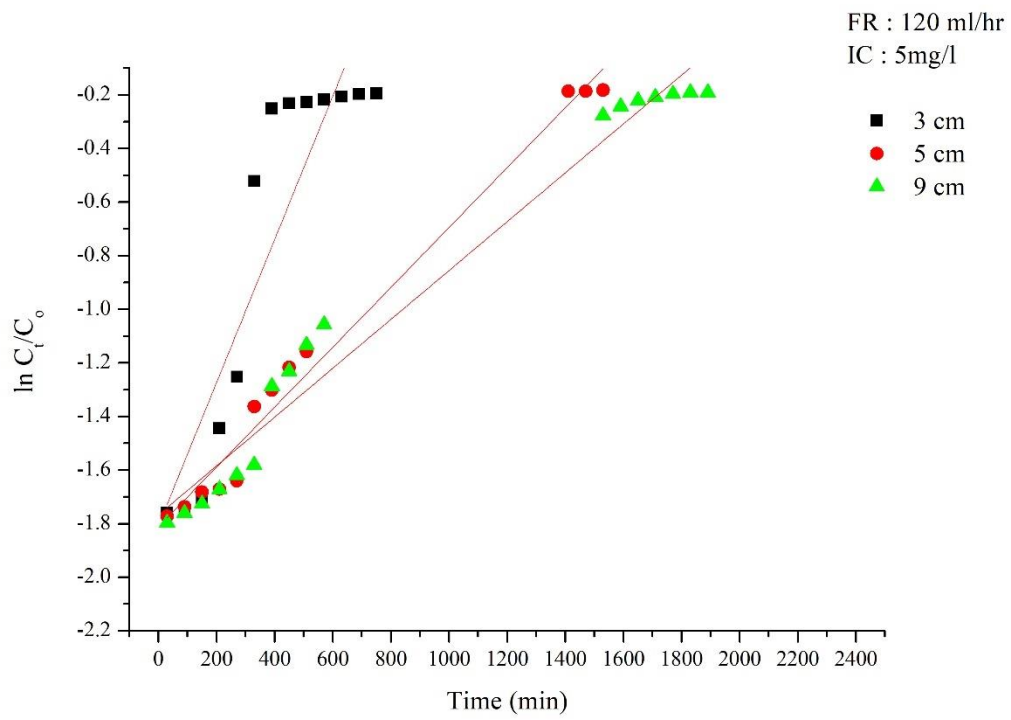
The linearized equation is given by

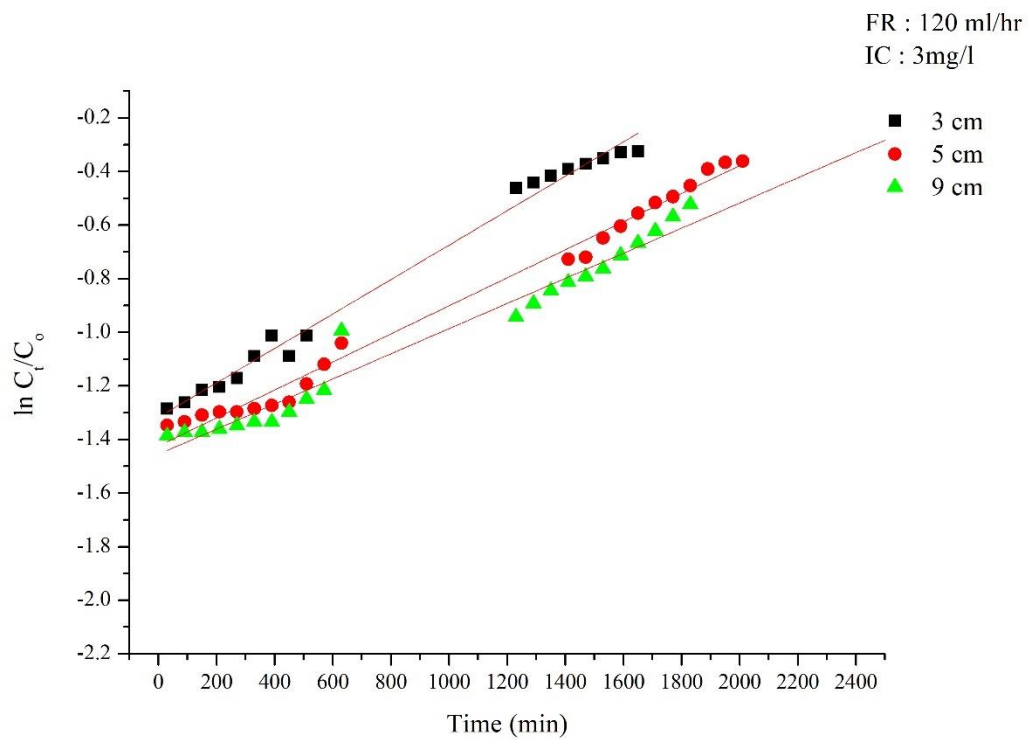
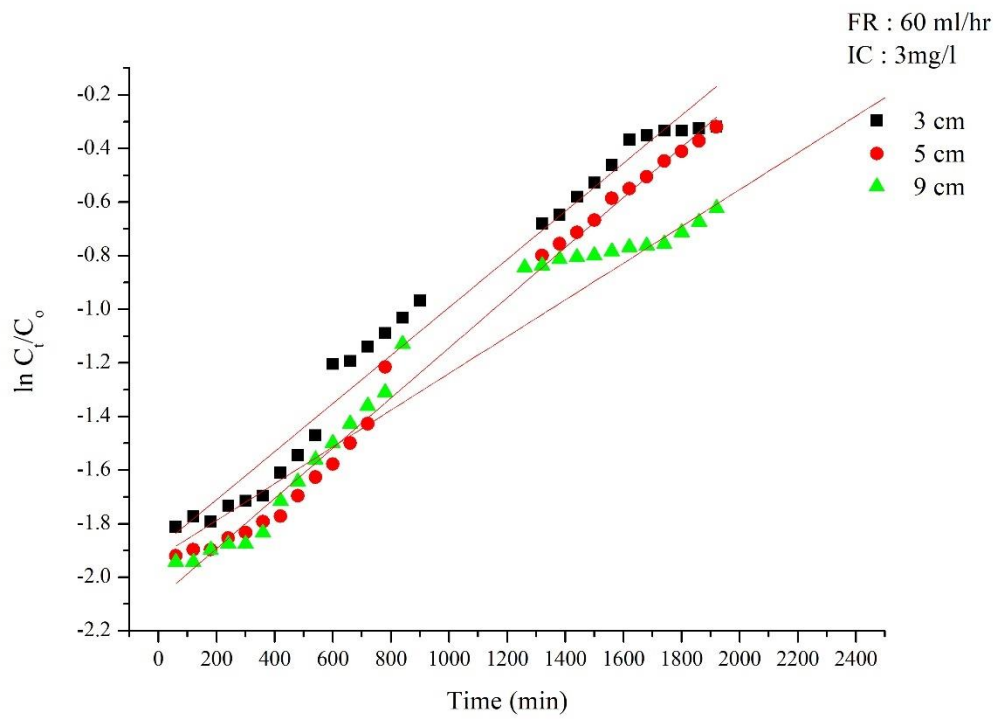
$$\ln\left(\frac{C_t}{C_0}\right) = \left(k_{AB}C_0t - k_{AB}N_0\frac{z}{U_0}\right) \quad \dots (4.16)$$

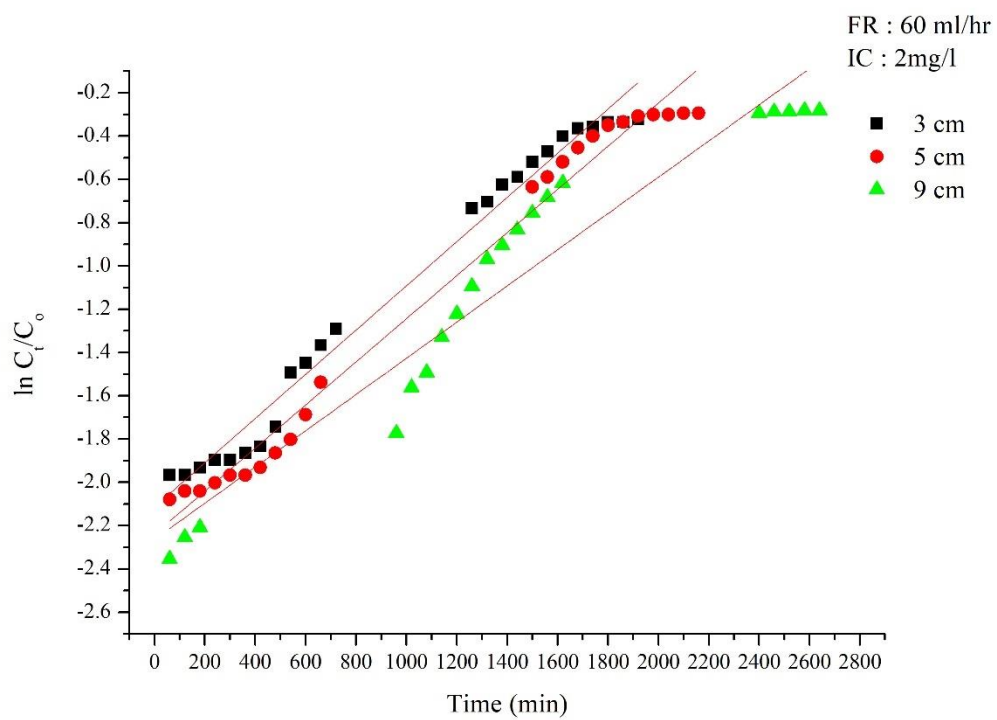
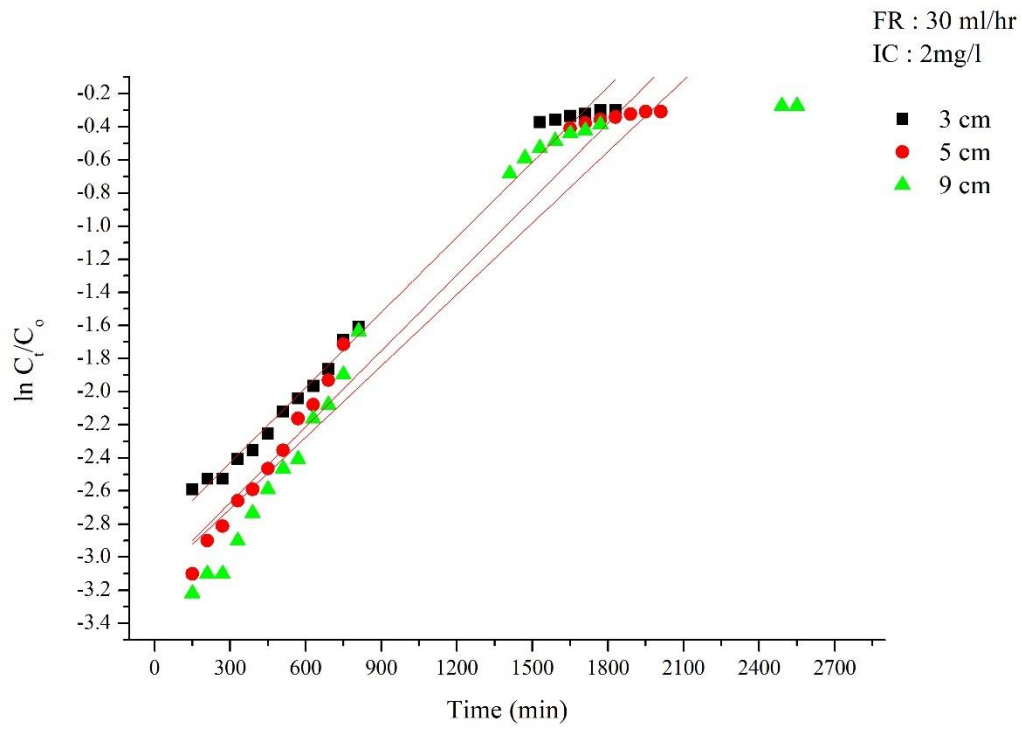
where  $k_{AB}$  (l/min.mg) is Bohart–Adam’s rate constant,  $z$  (cm) is the bed depth,  $N_0$  (mg/L) is maximum ferrous ion adsorption capacity per unit volume of adsorbent column, and  $U_0$  (cm/min) is the linear velocity of influent solution.

Graphs were plotted with the experimental data by varying operating conditions of initial concentration (2, 3 & 5 mg/L), flow rate (30, 60 & 120 ml/hr) and bed height (3, 5 & 9 cm) (see Figure 4.18 (a-i)) which resulted in 9 combination of graphs and 27 linear regression values (Table 4.7) along with Bohart–Adam’s rate constant and maximum solid-phase concentration of the solute (mg/g).











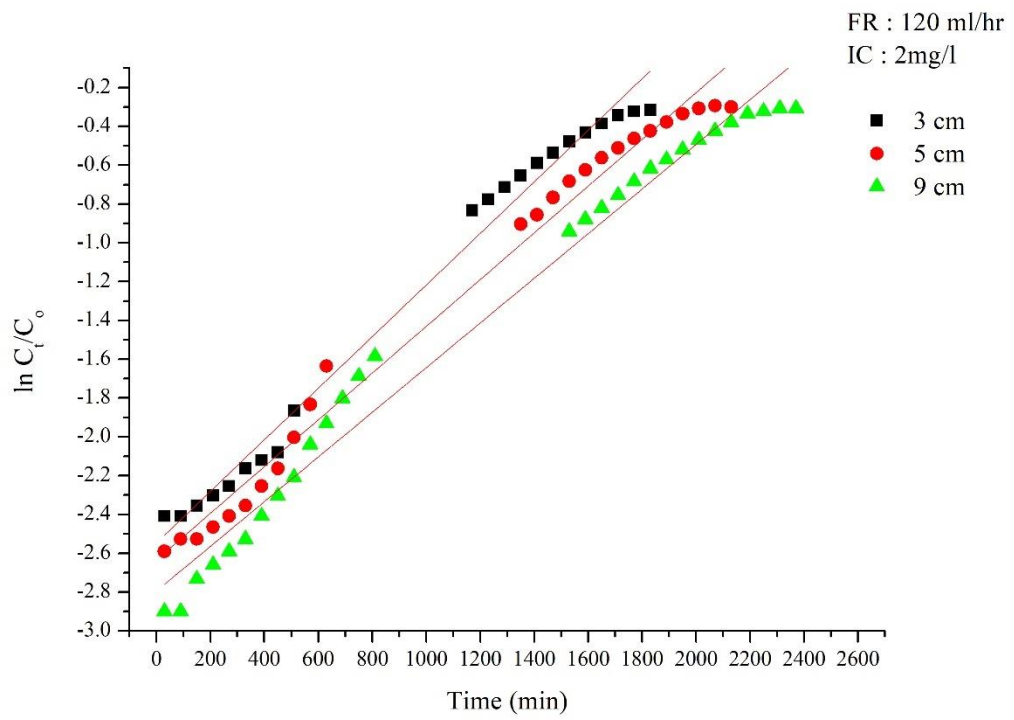


**Figure 4.18(a-i) Linear plot of Bohart Adam's Model with experimental data at different bed heights, flow rate and initial concentration**

**Table 4.7 Bohart-Adam's model parameters using linear regression analysis for Fe<sup>2+</sup> adsorption under various operating conditions**

Concentration [mg/L]	Flow rate [mL/hr]	Bed Height [cm]	R <sup>2</sup>	k <sub>AB</sub>	N <sub>0</sub> [mg/L]
5	120	3	0.8206	0.00054	710.62
5	120	5	0.9853	0.00022	1048.99
5	120	9	0.9734	0.00018	694.62
5	60	3	0.9507	0.00038	551.71
5	60	5	0.9336	0.00022	507.18
5	60	9	0.9779	0.00018	374.24
5	30	3	0.9868	0.00024	474.77
5	30	5	0.9757	0.00022	338.06
5	30	9	0.9491	0.0002	207.32
3	120	3	0.9911	0.0002	1397.98
3	120	5	0.9899	0.00167	108.88
3	120	9	0.9846	0.000167	617.96
3	60	3	0.9776	0.0003	668.68
3	60	5	0.9924	0.0003	441.59
3	60	9	0.9477	0.00023	291.92
3	30	3	0.9938	0.00033	347.18
3	30	5	0.9803	0.0003	240.02
3	30	9	0.9941	0.00023	188.32
2	120	3	0.9878	0.00065	832.04

2	120	5	0.9864	0.0006	559.41
2	120	9	0.9816	0.0006	329.69
2	60	3	0.9836	0.0005	448.60
2	60	5	0.9847	0.0005	285.31
2	60	9	0.9272	0.0004	200.19
2	30	3	0.9915	0.00075	204.08
2	30	5	0.9839	0.00075	132.89
2	30	9	0.897	0.0007	79.32

The saturation concentration  $[N_0]$  reduces with flowrate; but increases with bed height and initial concentration of the adsorbate. This indicates that the adsorption sites are not saturated. The rate constant  $k_{AB}$  decreases with the flow rate of the effluent. It is also noted that  $k_{AB}$  increases with decrease in the initial concentration of ferrous ions and adsorbent bed height. This behavior indicates that the overall kinetics of the system is influenced by external mass transfer during the initial part of the breakthrough curve (Vilvanathan and Shanthakumar 2017)

The  $R^2$  values from the linear regression using Bohart Adam's model are listed in Table 4.7 and it ranged from 0.8206 to 0.9941. As the values of  $R^2$  are relatively high, the model presented a good fit to the experimental column data of ferrous ions adsorption onto pyrolyzed areca husk. It can be inferred that the adsorption of ferrous ions on pyrolyzed areca husk adsorbent occurs by a complex mechanism involving more than one rate limiting step.

#### 4.9. PCA FOR COLUMN ADSORPTION DATA

Principal component analysis (PCA), is a statistical tool that uses an orthogonal conversion to transform a set of possible correlated variables into a set of linearly uncorrelated values of the variables called, principal components. PCA has been employed on the raw column adsorption data of the present investigation to understand the interplay among the variables under consideration and their influence

on Iron adsorption. The following units have been adopted for the variables. FR - lt/day, BH - Decimeter, Con - mg/100ml,  $T_b$  - Days and  $T_e$  - Days to have the range between 0.1 to 2.88. The data has been normalized before analysis to circumvent bias. The data set has dimension of  $27 \times 7$ , where 27 is the number of experiments and 7 is the number of variables.

The data decomposed has yielded, Eigenvalues 3.1424, 1.6354, 1.1443, 0.6955, 0.3155 0.0637 and 0.0030. Eigenvalues obtained indicate that the experimental data could be presented using two principal components (PC) which capture about 70% of the variance from the original adsorption data. The plot of first two principal axes is shown in Figure 4.19.

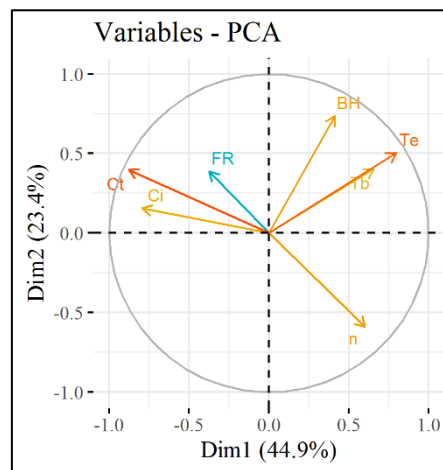


**Figure 4.19 Plot of first two principal axes**

Increase in bed height increases both the breakthrough and exhaustion time of the adsorbent bed. The variables namely the initial concentration ( $C_i$ ), flowrate (FR) and concentration at breakthrough time ( $C_t$ ) are clustered and have strong negative correlation with efficiency, indicating that the nature of the adsorbate and speed of effluent loading play an important role in the removal efficiency.

The main conclusion that can be drawn from the figure is that a favorable ferrous ion removal efficiency  $\eta$  can be obtained when the control variables namely initial concentration and flowrate are not very high for a given bed height.

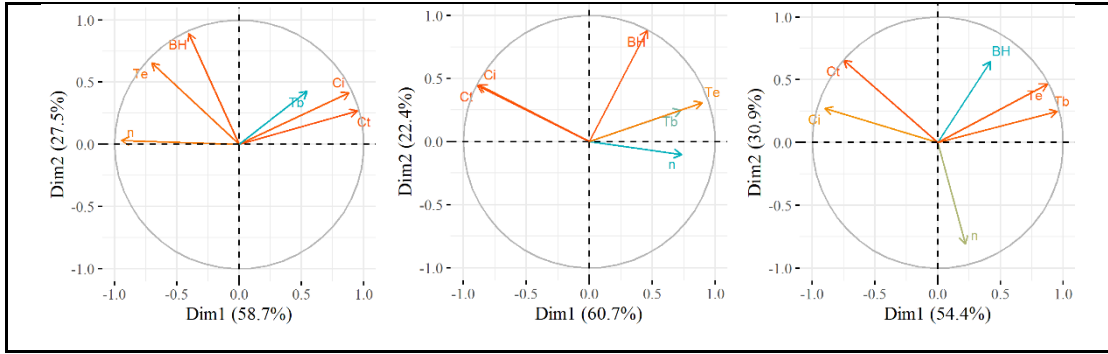


**Figure 4.20 PCA results for different flowrate (30, 60 & 120 mL/hr) datasets**

PCA results for different flowrate (30, 60 & 120 mL/hr) datasets are as in Figure 4.20. As is evident from the plots, at low flow rates there is slight increase in removal efficiency with increased bed heights but at higher flow rates this advantage is lost. It can be concluded that lower flow rate regimes are best in terms of removal efficiency.

#### 4.9.1. Prediction of $\eta$ from experimental variables using multi-variable linear regression

Multiple linear regression aims to model the relationship between two or more explanatory variables and a response variable by fitting a linear equation to observed data. Multi-variable linear regression (MVLRL) relationship for efficiency  $\eta$  in terms of  $C_i$ , FR, BH,  $T_b$ ,  $T_e$  is obtained as

$$\eta = a_0 + a_1 C_i + a_2 FR + a_3 BH + a_4 T_b + a_5 T_e \quad \dots (4.17)$$

The 5 coefficients in equation suggest the significance of the variables in influencing the efficiency.

$$\eta = 1.12 - 0.351 C_i - 0.039FR + 0.143BH - 0.163T_b - 0.105T_e \quad \dots (4.18)$$

It is evident that when all variables are set to zero,  $\eta=1$ .

Hence MVLRL for  $a_0=1$  has also been performed and results are presented and discussed. For  $a_0=1$  the equation for efficiency is as under.

$$\eta = 1 - 0.221C_i - 0.032FR + 0.082BH - 0.117T_b - 0.042T_e \quad \dots (4.19)$$

Lower regimes of flowrate and initial concentration are beneficial for attaining better removal efficiency. MVLRL equations for specified flow rates, bed heights and initial concentrations. Prediction equations for removal efficiency have also been obtained

from MVLr for specific flow rates, bed heights and initial concentration to check the veracity of results of PCA.

For flow rate – 30 mL/hr,

$$\eta = 1 - 0.273C_i + 0.084BH - 0.118T_b - 0.038T_e \quad \{R^2 = 0.996\}$$

For flow rate – 60 mL/hr

$$\eta = 1 - 0.288C_i + 0.128BH - 0.132T_b - 0.085T_e \quad \{R^2 = 0.999\}$$

For flow rate – 120 mL/hr

$$\eta = 1 - 0.321C_i + 0.163BH - 0.205T_b - 0.2005T_e \quad \{R^2 = 0.995\}$$

Similarly, for known bed heights (3, 5 & 9cm) efficiency can be estimated from equations below.

For BH – 3 cm

$$\eta = 1 - 0.224C_i - 0.021FR + 0.027T_b - 0.07T_e \quad \{R^2 = 0.997\}$$

For BH – 5 cm

$$\eta = 1 - 0.173C_i - 0.034FR - 0.199T_b + 0.002T_e \quad \{R^2 = 0.998\}$$

For BH – 9 cm

$$\eta = 1 - 0.191C_i - 0.037FR - 0.094T_b - 0.006T_e \quad \{R^2 = 0.998\}$$

If effluent concentrations are known in advance, removal efficiency can be computed from following equations.

For IC – 2 mg/L

$$\eta = 1 - 0.011FR + 0.123BH - 0.265T_b - 0.057T_e \quad \{R^2 = 0.999\}$$

For IC – 3 mg/L

$$\eta = 1 - 0.058FR + 0.072BH - 0.421T_b - 0.014T_e \quad \{R^2 = 0.999\}$$

for IC – 5 mg/L

$$\eta = 1 - 0.059FR + 0.009BH - 0.644T_b + 0.079T_e \quad \{R^2 = 0.999\}$$

These equations are valid for the following ranges of parameters.

Flow rate: 30 - 120 mL/hr

Bed height: 3 - 9cm

Concentration: 2 – 5mg/L

#### 4.9.2. Illustrative Example

To validate the model, a school located in Katipalla, near Surathkal was considered. The school has been pumping water from a bore well which has 2.05 mg/l as the initial iron concentration. The strength of the school was 300 students and 20 staff members. The working time was assumed for 6 hours and 3 liters drinking water per capita. Then the total flow rate for drinking water consumption is 5760 liters per day

As has been explained lower flow rate regimes yielded best performance, adopting flowrate of 30mL/hr

$$\begin{aligned}\text{Total water required} &= 5760 && \text{L/day} \\ &= 240 && \text{L/hr} \\ \text{dia of column} &= 20 && \text{mm} \\ \text{Surface area of the column, } \pi r^2 &= 314.2 && \text{mm}^2 \\ \text{Surface loading rate @ 30mL/hr} &= 0.095481 && \text{mm/hr} \\ \text{Area @30mL/hr} &= 2513600 && \text{mm}^2\end{aligned}$$

From the equations by MVLRL, the most appropriate for the data have been selected as  $\eta = 1 - 0.273C_i + 0.084BH - 0.118T_b - 0.038T_e$

$$\eta = 1 - 0.011FR + 0.123BH - 0.265T_b - 0.057T_e$$

Assuming  $\eta = 90\%$ , with known flow rate of 30mL/hr & initial ferrous ion concentration as 2.05mg/L for different bed height of 3, 5 & 9 cm, breakpoint time ( $T_b$ ) and exhaustion time ( $T_e$ ) can be determined.

From the values of  $T_b$  &  $T_e$ , the best bed height is identified for which the replacement time is the largest or rate of replacement [Bed height/  $T_e$ ] is least. In this case bed height of 5 cm was the best suitable.

## CHAPTER 5

### CONCLUSION

The utility of pyrolyzed arecanut husk as the adsorbent is experimentally investigated. The Batch Experimental results are compared and verified with available popular and recognized mathematical models. The study recommends that arecanut husk finds potential as an adsorbent with an indicated capacity of 0.38 mg/g for the kind of adsorbent developed and used in the study.

Langmuir & D-R Isotherm and pseudo-second-order kinetics are best suited for the performance appraisal of pyrolyzed arecanut husk as an adsorbent. Thermodynamic studies indicated the process of adsorption as spontaneous and exothermic. Adsorption mechanism indicated oxidation and precipitation of Iron complexes along with surface complexation with functional groups.

In addition, analysis of production cost of Pyrolysed Arecahusk resulted in it being cheaper in comparison with other commercially available activated charcoal.

The column studies yielded promising results, indicating that the adsorption process is cost effective and can be used to treat large quantities of wastewater in continuous mode. Ferrous ion adsorption through fixed-bed columns is dependent on the flow rate and bed depth. As the flowrate increased, the breakthrough curve became steeper, with reduced break point time and ferrous ion adsorption. It is found that treatment efficiency improved with reduced flow rate and an increase in the height of adsorbent bed of the column. Maximum adsorption capacity of ferrous ions was observed as 0.487mg/g at bed depth of 3 cm; flow rate of 2 ml/min and initial concentration of 2 mg/L.

Yoon–Nelson, Thomas and Bohart Adam’s model were used to analyse the performance of the column and the model parameters were evaluated. The



experimental data was in good agreement with the corresponding calculated breakthrough curves theoretical data.

PCA was also employed to predict the performance of the fixed bed column. This model successfully predicted that lower regimes of flowrate and initial concentration are best in achieving higher removal efficiency. The veracity of PCA was predicted with MVLR which also indicated the same. The  $R^2$  value of removal efficiency prediction equations is more than 0.99 in all cases indicating good reliability of PCA model.

## **SCOPE FOR FUTURE WORK**

On contemplating the research carried out on adsorption, there is more room for improvising the efficiency and looking out for novel adsorbents instead of depending on the traditional materials such as coal.

The present study deals with the adsorption potential of arecahusk and this extends its scope for further studies to deal with the other agricultural waste such as ricehusk, coffee husk, coconut husk etc.

Pyrolyzed arecahusk as an adsorbent has the potential to be utilized to remove various other dyes and heavy metals such as lead, nickel, chromium etc.

The pyrolytic gaseous fraction rising from pyrolysis of arecahusk can be studied as to understand its constituents and preventing the pollution of air.

The present study is a laboratory scale study which further gives a way for pilot plant studies for its industrial application or can be utilized in individual houses having ground water as their source of drinking water.

## REFERENCES

Acemioglu, B. (2004). "Removal of Fe ( II ) ions from aqueous solution by Calabrian pine bark wastes." *Bioresource Technology*, 93, 99–102.

Ahmad, A. A., and Hameed, B. H. (2010). "Fixed-bed adsorption of reactive azo dye onto granular activated carbon prepared from waste." *Journal of Hazardous Materials*, 175(1–3), 298–303.

Ahmad, M. F., and Haydar, S. (2016). "Evaluation of a newly developed biosorbent using packed bed column for possible application in the treatment of industrial effluents for removal of cadmium ions." *Journal of the Taiwan Institute of Chemical Engineers*, 62, 122–131.

Ahuja, S. C., and Ahuja, U. (2011). "Betel Leaf and Betel Nut in India : History and Uses." *Asian Agri-History*, 15(1), 13–35.

AL-Othman, Z. A., Ali, R., and Naushad, M. (2012). "Hexavalent chromium removal from aqueous medium by activated carbon prepared from peanut shell: Adsorption kinetics, equilibrium and thermodynamic studies." *Chemical Engineering Journal*, 184, 238–247.

Amuda, O. S., Giwa, A. A., and Bello, I. A. (2007). "Removal of heavy metal from industrial wastewater using modified activated coconut shell carbon." *Biochemical Engineering Journal*, 36, 174–181.

Anca-couce, A. (2020). "Reaction mechanisms and multi-scale modelling of lignocellulosic biomass pyrolysis." *Progress in Energy and Combustion Science*, 53(2016), 41–79.

Biswas, S., and Mishra, U. (2015). “Continuous Fixed-Bed Column Study and Adsorption Modeling : Removal of Lead Ion from Aqueous Solution by Charcoal Originated from Chemical Carbonization of Rubber Wood Sawdust.” *Journal of Chemistry*, 2015, 1–9.

Borba, C. E., Guirardello, R., Silva, E. A., Veit, M. T., and Tavares, C. R. G. (2006). “Removal of nickel ( II ) ions from aqueous solution by biosorption in a fixed bed column: Experimental and theoretical breakthrough curves.” *Biochemical Engineering Journal*, 30, 184–191.

Boukouvalas, C., Magoulas, K., and Tassios, D. (1998). “Application of Supercritical Fluid Extraction in Industrial Waste Treatment: Thermodynamic Modeling and Design.” *Separation Science and Technology*, 33(3), 387–410.

Braester, C., and Martinell, R. (1988). “The Vyredox and Nitredox Methods of In situ treatment of Groundwater.” *Water Science and Technology*, 20(3), 149–163.

Chakraborti, D., Das, B., and Murrill, M. T. (2011). “Examining India ’ s Groundwater.” *Environmental Science & Technology*, 45(1), 27–33.

Chu, K. H. (2010). “Fixed bed sorption : Setting the record straight on the Bohart – Adams and Thomas models.” *Journal of Hazardous Materials*, 177(1–3), 1006–1012.

Cullimore, D. ., and McCANN, A. E. (1977). “The Identification, Cultivation and Control of Iron Bacteria in Ground Water.” *Aquatic Microbiology*, 219–261.

Dabrowski, A. (2001). "Adsorption - from theory to practice." *Advances in Colloid and Interface Science*, 93, 135–224.

Desai, R. H., Krishnamurthy, L., and Shridhar, T. N. (2016). "Effectiveness of Areca ( Betel ) Fiber as a Reinforcing Material in Eco-friendly Composites: A Review." *Indian Journal of Advances in Chemical Science*, S(1), 27–33.

Dias, J. M., Alvim-Ferraz, M. C. M., Almeida, M. F., Rivera-Utrilla, J., and Saez-Polo, M. (2007). "Waste materials for activated carbon preparation and its use in aqueous-phase treatment: A review." *Journal of Environmental Management*, 85(4), 833–846.

Dichiara, A. B., Weinstein, S., and Rogers, R. E. (2015). "On the Choice of Batch or Fixed-Bed Adsorption Processes for Wastewater Treatment." *Industrial & Engineering Chemistry Research*, 54(34), 8579–8586.

Drag, E. B., Kulazynski, M., and Kaczmarczyk, J. (2002). "Porous Structure of multifunctional mineral - carbon and zeolite-carbon sorbents." *Studies in Surface Science and Catalysis*, 144, 499–506.

Duman, G., Onal, Y., Okutucu, C., Onenc, S., and Yanik, J. (2009). "Production of activated carbon from pine cone and evaluation of its physical, chemical, and adsorption properties." *Energy and Fuels*, 23(4), 2197–2204.

Ellis, D., Bouchard, C., and Lantagne, G. (2000). "Removal of iron and manganese from groundwater by oxidation and microfiltration." *Desalination*, 130(3), 255–264.

Elwakeel, K. Z., El-sayed, G. O., and El-nassr, S. M. A. (2014). “Removal of ferrous and manganous from water by activated carbon obtained from sugarcane bagasse.” *Desalination and Water Treatment*, 55(2), 471–483.

Farrag, A. E. H. A., Moghny, T. A., Mohamed, A. M. G., Saleem, S. S., and Fathy, M. (2017). “Abu Zenima synthetic zeolite for removing iron and manganese from Assiut governorate groundwater , Egypt.” *Applied Water Science*, 7(6), 3087–3094.

Gao, L. Y., Deng, J. H., Huang, G. F., Li, K., Cai, K. Z., Liu, Y., and Huang, F. (2019). “Relative distribution of Cd<sup>2+</sup> adsorption mechanisms on biochars derived from rice straw and sewage sludge.” *Bioresource Technology*, 272, 114–122.

Girods, P., Dufour, A., Fierro, V., Rogaume, Y., Rogaume, C., Zoulalian, A., and Celzard, A. (2009). “Activated carbons prepared from wood particleboard wastes: Characterisation and phenol adsorption capacities.” *Journal of Hazardous Materials*, 166(1), 491–501.

Gogoi, D., Bordoloi, N., Goswami, R., Narzari, R., Saikia, R., Sut, D., Gogoi, L., and Kataki, R. (2017). “Effect of torrefaction on yield and quality of pyrolytic products of arecanut husk: An agro-processing wastes.” *Bioresource Technology*, 242, 36–44.

Goher, M. E., Hassan, A. M., Abdel-Moniem, I. A., Fahmy, A. H., Abdo, M. H., and El-sayed, S. M. (2015). “Removal of aluminum, iron and manganese ions from industrial wastes using granular activated carbon and Amberlite IR-120H.” *The Egyptian Journal of Aquatic Research*,

41(2), 155–164.

Gokul, P. V, Singh, P., Singh, V. P., and Sawarkar, A. N. (2019). “Environmental Effects Thermal behavior and kinetics of pyrolysis of areca nut husk.” *Energy Sources, Part A: Recovery, Utilization, and Environmental Effects*, 41(23), 2906–2916.

Gorzin, F., and Bahri Rasht Abadi, M. M. (2018). “Adsorption of Cr(VI) from aqueous solution by adsorbent prepared from paper mill sludge: Kinetics and thermodynamics studies.” *Adsorption Science and Technology*, 36(1–2), 149–169.

Goud, V. V, Rao, M. S., Mohanty, K., and Jayakumar, N. S. (2005). “Phenol Removal from Aqueous Solutions by Tamarind Nutshell Activated Carbon : Batch and Column Studies.” *Chemical Engineering & Technology: Industrial Chemistry-Plant Equipment-Process Engineering-Biotechnology*, 28(7), 814–821.

Grazuleviciene, R., Nadisauskiene, R., Buinauskiene, J., and Grazulevicius, T. (2009). “Effects of Elevated Levels of Manganese and Iron in Drinking Water on Birth Outcomes.” *Polish Journal of Environmental Studies*, 18(5), 819–825.

Gregg, S. J., Sing, K. S. W., and Salzberg, H. W. (1967). “Adsorption, Surface Area and Porosity.” *Journal of The electrochemical society*, 114(11), 279C.

Hameed, B. H. (2009). “Evaluation of papaya seeds as a novel non-conventional low-cost adsorbent for removal of methylene blue.” *Journal of Hazardous Materials*, 162(2–3), 939–944.

Hana, R., Wanga, Y., Zhaoc, X., Wanga, Y., Xieb, F., Chengb, J., and Tanga, M. (2007). “Adsorption of methylene blue by phoenix tree leaf powder in a fixed-bed column: experiments and prediction of breakthrough curves.” *Desalination*, 238(1–3), 333–346.

Harvey, A. E., Smart, J. A., and Amis, E. S. (1955). “Simultaneous Spectrophotometric Determination of Iron(II) and Total Iron with 1,10-Phenanthroline.” *Analytical Chemistry*, 27(1), 26–29.

Hove, M., Hille, R. P. Van, and Lewis, A. E. (2007). “Iron solids formed from oxidation precipitation of ferrous sulfate solutions.” *AIChE Journal*, 53(10), 2569–2577.

<http://cwc.gov.in/publications>. (2018). *Status of Trace and Toxic Metals in Indian Rivers*.

Ibrahim, W., and Hassan, L. (2008). “Determination of Surface Diffusion Coefficient for Lead Removal Using Adsorption Model.” *Twelfth International Water Technology Conference, IWTC12 2008*, 1021.

Indhumathi, P., Syed Shabudeen, P. S., Shoba, U. S., and Saraswathy, C. P. (2014). “The removal of chromium from aqueous solution by using green micro algae.” *Journal of Chemical and Pharmaceutical Research*, 6(6), 799–808.

Ippolito, J. A., Laird, D. A., and Busscher, W. J. (2012). “Environmental benefits of biochar.” *Journal of Environmental Quality*, 41(4), 967–972.

Jimbo, Y., and Goto, K. (2001). “Iron and manganese removal by a membrane filtration system.” *Water Science and Technology: Water*



*Supply*, 1(5/6), 357–364.

Jusoh, A. bin, Cheng, W. H., Low, W. M., Nora'aini, A., and Noor, M. J. M. M. (2005). "Study on the removal of iron and manganese in groundwater by granular activated carbon." *Desalination*, 182(1–3), 347–353.

Kadirvelu, K., and Namasivayam, C. (2003). "Activated carbon from coconut coirpith as metal adsorbent: Adsorption of Cd(II) from aqueous solution." *Advances in Environmental Research*, 7(2), 471–478.

Kadirvelu, K., Senthilkumar, P., Thamaraiselvi, K., and Subburam, V. (2002). "Activated carbon prepared from biomass as adsorbent: Elimination of Ni(II) from aqueous solution." *Bioresource Technology*, 81(1), 87–90.

Kavitha, D., and Namasivayam, C. (2008). "Capacity of activated carbon in the removal of acid brilliant blue: Determination of equilibrium and kinetic model parameters." *Chemical Engineering Journal*, 139(3), 453–461.

Khalil, M. M. H., Al-wakeel, K. Z., Abd, S. S., Rehim, E., and El, H. A. (2013). "Journal of Environmental Chemical Engineering Efficient removal of ferric ions from aqueous medium by amine modified chitosan resins." *Biochemical Pharmacology*, 1(3), 566–573.

Khatri, N., Tyagi, S., and Rawtani, D. (2017). "Recent strategies for the removal of iron from water: A review." *Journal of Water Process Engineering*, 19(13), 291–304.

Kleinübing, S. J., Silva, E. A., Silva, M. G. C., and Guibal, E. (2011). “Equilibrium of Cu ( II ) and Ni ( II ) biosorption by marine alga *Sargassum filipendula* in a dynamic system: Competitiveness and selectivity.” *Bioresource Technology*, 102, 4610–4617.

Kołodynskaska, D., Krukowska, J., and Thomas, P. (2017). “Comparison of sorption and desorption studies of heavy metal ions from biochar and commercial active carbon.” *Chemical Engineering Journal*.

Korngold, E. (1994). “Iron removal from tap water by a cation exchanger.” *Desalination*, 94, 243–249.

Králik, M. (2014). “Adsorption , chemisorption , and catalysis.” *Chemical Papers*, 68(12), 1625–1638.

Kundu, S., and Gupta, A. K. (2006). “Arsenic adsorption onto iron oxide-coated cement (IOCC): Regression analysis of equilibrium data with several isotherm models and their optimization.” *Chemical Engineering Journal*, 122(1–2), 93–106.

Lazaroff, N., Sigal, W., and Wasserman, A. (1982). “Iron Oxidation and Precipitation of Ferric Hydroxysulfates by Resting *Thiobacillus ferrooxidans* Cells.” *Applied and environmental microbiology*, 43(4), 924–38.

Lesley, B., Daniel, H., and Paul, Y. (2015). “Iron and manganese removal in wetland treatment systems: Rates , processes and implications for management.” *Science of the Total Environment*, 394, 1–8.

Liang, S., Guo, X., Feng, N., and Tian, Q. (2010). “Isotherms, kinetics

and thermodynamic studies of adsorption of  $\text{Cu}^{2+}$  from aqueous solutions by  $\text{Mg}^{2+}/\text{K}^{+}$  type orange peel adsorbents.” *Journal of Hazardous Materials*, 174(1–3), 756–762.

Liew, R. K., Chai, C., Yek, P. N. Y., Phang, X. Y., Chong, M. Y., Nam, W. L., Su, M. H., Lam, W. H., Ma, N. L., and Lam, S. S. (2018). “Innovative production of highly porous carbon for industrial effluent remediation via microwave vacuum pyrolysis plus sodium-potassium hydroxide mixture activation.” *Journal of Cleaner Production*, 208, 1436–1445.

Liou, T. H., and Wu, S. J. (2009). “Characteristics of microporous/mesoporous carbons prepared from rice husk under base- and acid-treated conditions.” *Journal of Hazardous Materials*, 171(1–3), 693–703.

Majzlan, J., and Myneni, S. C. B. (2005). “Speciation of iron and sulfate in acid waters: Aqueous clusters to mineral precipitates.” *Environmental Science and Technology*, 39(1), 188–194.

Malkoc, E., and Nuhoglu, Y. (2006). “Cr ( VI ) adsorption by waste acorn of *Quercus ithaburensis* in fixed beds: Prediction of breakthrough curves.” *Chemical Engineering Journal*, 119(1), 61–68.

Matzopoulos, M. (2011). “Dynamic Process Modeling: Combining Models and Experimental Data to Solve Industrial Problems.” *Process systems engineering*, 7, 3–33.

Moghadam, M. R., Nasirizadeh, N., Dashti, Z., and Babanezhad, E. (2013). “Removal of Fe(II) from aqueous solution using pomegranate

peel carbon: equilibrium and kinetic studies.” *International Journal of Industrial Chemistry*, 4(1), 19.

Nwabanne, J. T., and Igbokwe, P. K. (2012). “Adsorption Performance of Packed Bed Column for the removal of Lead (ii) using oil Palm Fibre.” *International Journal of Applied Science and Technology*, 2(5), 106–115.

Padmesh, T. V. N., Vijayaraghavan, K., Sekaran, G., and Velan, M. (2006). “Biosorption of Acid Blue 15 using fresh water macroalga *Azolla filiculoides*: Batch and column studies.” *Dyes and Pigments*, 71(2), 77–82.

Papanikolaou, G., and Pantopoulos, K. (2005). “Iron metabolism and toxicity.” *Toxicology and applied pharmacology*, 202(2), 199–211.

Peng, W., Liu, Y. J., Wu, N., Sun, T., He, X. Y., Gao, Y. X., and Wu, C. J. (2015). “Areca catechu L. (Arecaceae): A review of its traditional uses, botany, phytochemistry, pharmacology and toxicology.” *Journal of Ethnopharmacology*, 164, 340–356.

Raghavan, V., & Baruah, H. K. (1958). “Areca nut: India’s Popular Masticatory - History , Chemistry and Utilization.” *Economic Botany*, 12(4), 315–345.

Rahman, M. M., Adil, M., Yusof, A. M., Kamaruzzaman, Y. B., and Ansary, R. H. (2014). “Removal of heavy metal ions with acid activated carbons derived from oil palm and coconut shells.” *Materials*, 7(5), 3634–3650.

Sánchez-Machado, D. I., López-Cervantes, J., Correa-Murrieta, M. A.,

and Sánchez-Duarte, R. G. (2016). “Modeling of breakthrough curves for aqueous iron (III) adsorption on chitosan-sodium tripolyphosphate.” *Water Science and Technology*, 74(10), 2297–2304.

Selvaraju, G., and Bakar, N. K. A. (2017). “Production of a new industrially viable green-activated carbon from *Artocarpus integer* fruit processing waste and evaluation of its chemical, morphological and adsorption properties.” *Journal of Cleaner Production*, 141, 989–999.

Sharma, S. K., Petrusovski, B., and Schippers, J. C. (2005). “Biological iron removal from groundwater : a review.” *Journal of Water Supply: Research and Technology—AQUA*, 54(4), 239-247.

Sudarsan, J. S., Annadurai, R., Subramani, S., and George, R. B. (2016). “Petrochemical wastewater treatment using constructed wetland technique.” *Pollution Research*, 35(4), 727–732.

Suksabye, P., Thiravetyan, P., and Nakbanpote, W. (2008). “Column study of chromium(VI) adsorption from electroplating industry by coconut coir pith.” *Journal of Hazardous Materials*, 160(1), 56–62.

Supriadi, C. P., Kartini, E., Honggowiranto, W., and Tri, K. (2017). “Synthesis and characterization of carbon material obtained from coconut coir dust by hydrothermal and pyrolytic processes.” *International Journal of Technology*, 2017(8), 1470–1478.

Taty-Costodes, V. C., Fauduet, H., Porte, C., and Ho, Y. S. (2005). “Removal of lead (II) ions from synthetic and real effluents using immobilized *Pinus sylvestris* sawdust: Adsorption on a fixed-bed column.” *Journal of Hazardous Materials*, 123(1–3), 135–144.

The CGWB, Ministry of Water Resources, RD & GR, G. of I. (2015). “Locations of Iron in ground water.”

Thomas, W. J., and Crittenden, B. (1998). *Adsorption Technology and Design*. Elsevier.

Tsai, W. T., Liu, S. C., and Hsieh, C. H. (2012). “Preparation and fuel properties of biochars from the pyrolysis of exhausted coffee residue.” *Journal of Analytical and Applied Pyrolysis*, 93, 63–67.

Verla, A. W., Horsfall, M., Verla, E. N., Spiff, A. I., and Ekpete, O. . (2012). “Preparation and Characterization of Activated Carbon From Fluted Pumpkin (*Telfairia Occidentalis* Hook. F) Seed Shell.” *Asian Journal of Natural & Applied Sciences.*, 1(3), 39–50.

Vijayaraghavan, K., Jegan, J., Palanivelu, K., and Velan, M. (2005). “Batch and column removal of copper from aqueous solution using a brown marine alga *Turbinaria ornata*.” *Chemical Engineering Journal*, 106(2), 177–184.

Vilvanathan, S., and Shanthakumar, S. (2017). “Column Adsorption Studies on Nickel and Cobalt Removal from Aqueous Solution Using Native and Biochar Form of *Tectona grandis*.” *Environmental Progress & Sustainable Energy*, 36(4), 1030–1038.

Volpe, D. (2012). *Assessment of Iron and Manganese Sequestration*.

Wasewar, K. L., Atif, M., Prasad, B., and Mishra, I. M. (2009). “Batch adsorption of zinc on tea factory waste.” *Desalination*, 244(1–3), 66–71.

Wei Zheng, Xiao-ming Li, Fei Wang, Qi Yang, Pin Deng, G. Z. (2008). “Adsorption removal of cadmium and copper from aqueous solution by areca—A food waste.” *Journal of Hazardous Materials*, 157(2–3), 490–495.

Wu, F. C., Tseng, R. L., and Juang, R. S. (2009). “Initial behavior of intraparticle diffusion model used in the description of adsorption kinetics.” *Chemical Engineering Journal*, 153(1–3), 1–8.

Yu, Y., Chen, N., Hu, W., and Feng, C. (2015). “Application of Taguchi experimental design methodology in optimization for adsorption of phosphorus onto Al / Ca-impregnated granular clay material.” *Desalination and Water Treatment*, 56(11), 2994–3004.

# APPENDIX I

## COST ESTIMATION

Item	Lab scale cost estimation
<u>Production Details</u>	
Operation hour	8 hours /day
Total Process time <sup>a</sup>	2 hours/ batch
Feedstock loading capacity	0.25 kg
Product yield	0.08 kg
Daily output of Product	$(8/2) \times 0.08 = 0.32 \text{ kg}$
Annual output of Product	$0.32 \times 260 = \mathbf{83.2 \text{ kg}}$
 (5d/week $\times$ 52 week/yr = 260 days)	
 <u>Operating Cost</u>	
Feedstock	1.5 INR
	$1.5 \times 3.125 \times 83.2 = \mathbf{390 \text{ INR/year}}$
Rental of Equipment (Muffle furnace, Oven, Ball mill, etc) <sup>b</sup>	<b>190 INR/ year</b>
Utilities (Power Consumption, Water, etc) <sup>c</sup>	<b>10 INR</b>
	$7.5 \times 4 \text{ batch/day} \times 260 = \mathbf{7800 \text{ INR/year}}$
Labour <sup>d</sup>	<b>375 INR/year</b>



Annual Operation Cost  $390 + 190 + 10 + 375 = 965$  **INR/year**

Production Cost of Carbonised Areca **0.09 INR/ kg**

Husk<sup>e</sup>

---

<sup>a</sup> Total process time include heating, cooling, feedstock reloading, product collection

<sup>b</sup> The rent was fixed by the lab authorities.

<sup>c</sup> Utilities include the electricity for oven and muffle furnace, water for washing and other necessary purpose. Price are based on rate charges in India.

<sup>d</sup> Estimated according to the price in India.

<sup>e</sup> Total annual operation cost (INR/year)/ Annual output of product (kg/year).

## APPENDIX II

### EXPERIMENTAL PHOTOGRAPHS



Cross section of the column used for adsorption studies in continuous flow mode with details of the plunger and SS sieve base

## **PUBLICATION**

- Subramani, B.S., Shrihari, S., Manu, B., Babunaryan, K.S., (2019) “Evaluation of pyrolyzed areca husk as a potential adsorbent for the removal of Fe<sup>2+</sup> ions from aqueous solutions.” *Journal of Environmental Management* 246, 345–354. <https://doi.org/10.1016/j.jenvman.2019.04.122>

## **CONFERENCE**

- Subramani, B.S., Shrihari, S., Manu, B., Babunaryan, K.S., (2020) “Usage Potential of Arecahusk as adsorbent in Water Treatment” *3<sup>rd</sup> International Conference on Waste Management – RECYCLE 2020, IIT Guwahati.*



#404, Aasara Apartments,

Brahmagiri

Udupi- 576101

9566049030

[Sheekasubramani5@gmail.com](mailto:Sheekasubramani5@gmail.com)

## SHEEKA CHINNAPPA A

### OBJECTIVE

I am looking for a faculty position in the area of Chemical engineering along with research opportunity, applying my acquired knowledge & utilizing my abilities to trend in the area of environmental engineering, while being resourceful and innovative.

### EDUCATIONAL QUALIFICATIONS

#### **Ph.D – NATIONAL INSTITUTE OF TECHNOLOGY, SURATHKAL**

Environmental Engineering [2015 – 2021]

**Thesis Title:** *Usage potential of Arecahusk as an adsorbent for the removal of ferrous ions from aqueous solution.*

#### **M.Tech – SRM INSTITUTE OF TECHNOLOGY, KATTANKULATHUR**

Environmental Engineering [2010-2012]

**Thesis Title:** *Low Cost Industrial waste water treatment (Primary treated Petroleum Effluent) using Constructed Wetland*

#### **B.E – SIDDAGANGA INSTITUTE OF TECHNOLOGY, TUMKUR**

Chemical Engineering [2005-2009]

**Thesis Title:** *Investigation into the degradation of Phenol using Phanerochaete Chrysosporium under acclimatized condition*

EXPERIENCE      **ASSISTANT PROFESSOR, MANIPAL INSTITUTE OF TECHNOLOGY, MANIPAL**

Sep 29<sup>th</sup> 2014 to July 9<sup>th</sup> 2015

Handled Environmental Chemistry Theory & lab for M.Tech in the Dept of Civil Engg

**SENIOR DESIGN ENGINEER, LARSEN & TOUBRO, CHENNAI**

July 15<sup>th</sup> 2012 to Aug 24<sup>th</sup> 2014

Process designing of Water, Sewage & Effluent Treatment plants including the list of Civil, Mechanical & Electrical load list.

Projects involved are 12.5 MLD & 25 MLD CETP of HSIIDC at Bahadurgarh & Manesar, Haryana, 6600m<sup>3</sup>/hr PWS for YTPS, RPCL, Raichur.

---

PUBLICATION

- **Subramani, B.S.**, Shrihari, S., Manu, B., Babunarayan, K.S., (2019) Evaluation of pyrolyzed areca husk as a potential adsorbent for the removal of Fe 2 + ions from aqueous solutions. Journal of Environmental Management 246, 345–354.  
<https://doi.org/10.1016/j.jenvman.2019.04.122>
- Sudarshan, J.S., **Subramani S.**, Rajan, RJ., Shah, I., Nithiyantham, S., (2018) Simulation of constructed wetland in treating wastewater using fuzzy logic technique. Journal of Physics: Conference Series 1000 (1), 12137.
- Sudarshan, J.S., Annadurai, R., **Subramani S.**, (2016) Petrochemical wastewater treatment using constructed wetland technique. Pollution Research 35 (4), 727-732.

---

ACHIVEMENTS

- Conducted lecture sessions for PWD – Karnataka and GEC, Jalawar at Dept of Civil Engg, NITK, Surathkal.
  - Worked extensively in achieving NBA accreditation for our branch Environmental Engg, Dept of Civil Engg, NITK, Surathkal
  - Held single point responsibility for approval of design & drawings for the project 6600m<sup>3</sup>/hr PWS for YTPS, RPCL, Raichur with L&T Construction.
  - First Rank Holder & Gold Medalist in M.Tech Environmental Engg (2010-12)
  - Worked as an intern at MRPL (ONGC), Mangalore on Process & design aspects and tracking of VOC emissions of the ETP.
-

## PERSONAL PROFILE

**Maiden Name: Sheeka Subramani B**

DOB: 14<sup>th</sup> January 1988

Sex/Status: Female/Married

Spouse: Dr Chinnappa A G

Consultant Ophthalmologist, Prasad Nethralaya,  
Udupi

Nationality/Passport No: Indian/ S3304502

Languages Known: English, Kannada, Hindi, Kodava

**Software Skills:** MS Word, Powerpoint, Excel,  
MATLAB (intermediate level)

---

## REFERENCES

**DR S SHRIHARI**

Professor, NITK, Surathkal

+91 9449087533; [s.shrihari@gmail.com](mailto:s.shrihari@gmail.com)

**DR K S BABUNARAYAN**

Professor, NITK, Surathkal

+91 9343342587; [shrilalisuta@gmail.com](mailto:shrilalisuta@gmail.com)

**DR B MANU**

Associate Professor, NITK, Surathkal

+91 8762569251; [bmanu8888@gmail.com](mailto:bmanu8888@gmail.com)

